

# Functional Mixed Membership Models

Nicholas Marco

*Department of Biostatistics, University of California, Los Angeles, USA.*

E-mail: ndmarco96@g.ucla.edu

Damla Şentürk

*Department of Biostatistics, University of California, Los Angeles, USA.*

E-mail: dsenturk@ucla.edu

Shafali Jeste

*Division of Neurology and Neurological Institute, Children's Hospital Los Angeles, Los Angeles, USA.*

E-mail: sjeste@chla.usc.edu

Charlotte DiStefano

*Division of Psychiatry, Children's Hospital Los Angeles, Los Angeles, USA*

E-mail: charlotte.distefano@gmail.com

Abigail Dickinson

*Department of Psychiatry and Biobehavioral Sciences, University of California, Los Angeles, USA.*

E-mail: abbydickinson317@gmail.com

Donatello Telesca

*Department of Biostatistics, University of California, Los Angeles, USA.*

E-mail: dtelesca@ucla.edu

**Summary.** Mixed membership models, or partial membership models, are a flexible unsupervised learning method that allows each observation to belong to multiple clusters. In this paper, we propose a Bayesian mixed membership model for functional data. By using the multivariate Karhunen-Lo  e theorem, we are able to derive a scalable representation of Gaussian processes that maintains data-driven learning of the covariance structure. Within this framework, we establish conditional posterior consistency given a known feature allocation matrix. Compared to previous work on mixed membership models, our proposal allows for increased modeling flexibility, with the benefit of a directly interpretable mean and covariance structure. Our work is motivated by studies in functional brain imaging through electroencephalography (EEG) of children with autism spectrum disorder (ASD). In this context, our work formalizes the clinical notion of “spectrum” in terms of feature membership proportions.

**Keywords:** Autism Spectrum Disorder, Bayesian, EEG, Functional Data Analysis, Mixed Membership Model, Neuroimaging

## 1. Introduction

Cluster analysis often aims to identify homogeneous subgroups of statistical units within a data-set (Hennig et al., 2015). A typical underlying assumption of both heuristic and model-based procedures posits the existence of a finite number of sub-populations, from which each sample is extracted with some probability, akin to the idea of *uncertain membership*. A natural extension of this framework allows each observation to belong to multiple clusters simultaneously; leading to the concept of mixed membership models, or partial membership models (Blei et al., 2003; Erosheva et al., 2004), akin to the idea of *mixed membership*. This manuscript aims to extend the class of mixed membership models to functional data.

Functional data analysis (FDA) is concerned with the statistical analysis of realizations of a random function. In the functional clustering framework, the random function is often conceptualized as a mixture of stochastic processes, so that each realization is assumed to be sampled from one of  $K < \infty$  cluster-specific sub-processes. The literature on functional clustering is well established and several analytical strategies have been proposed to handle different sampling designs and to ensure increasing levels of model flexibility. In the setting of sparsely observed functional data, James and Sugar (2003) proposed a mixed effects modeling framework for efficient dimension reduction after projection of the observed data onto a basis system characterized by natural cubic splines. Alternatively, Chiou and Li (2007) made use of functional principal component analysis to help reduce dimensionality by inferring cluster specific means and eigenfunctions. Jacques and Preda (2014) proposed a similar strategy for clustering multivariate functional data. Petrone et al. (2009) extended the previous work on functional mixture models by allowing hybrid species, where subintervals of the domain within each functional observation can belong to a different cluster. This type of clustering can be thought of as local clustering, where the cluster an observation belongs to changes depending on where you are in the domain of the function. Alternatively, mixed membership models can be thought of as a generalization of global clustering, where the membership allocation parameters do not change with respect to the domain of the random function.

Beyond clustering, the ability to model an observation's membership on a spectrum is particularly advantageous when we consider applications to biomedical data. For example, in diagnostic settings, the severity of symptoms may vary from person to person. It is therefore important to ask which symptomatic features characterize the sample, and whether subjects exhibit one or more of these traits. Within this general context, our work is motivated by functional brain imaging studies of neurodevelopmental disorders, such as the autism spectrum disorder (ASD). In this setting, typical patterns of neuronal activity are examined through the use of brain imaging technologies (e.g. electroencephalography (EEG) or functional magnetic resonance imaging (fMRI)), and result in observations which are naturally characterized as random functions on a specific evaluation domain. We are primarily interested in the discovery of distinct functional features characterizing the sample and in the explanation of how these features determine subject-level functional heterogeneity. To our knowledge, the literature on FDA is still silent on the concept mixed membership, defining both a methodological and scientific need for a rigorous statistical formulation of mixed membership models.

One of the earliest uses of these types of models appeared in the field of population genetics. [Pritchard et al. \(2000\)](#) used the idea of mixed membership to cluster individuals into sub-populations, while accounting for the presence of admixed cases, whose genetic makeup is drawn from more than one of  $K$  sub-populations. [Blei et al. \(2003\)](#) introduced the concept of latent Dirichlet allocation to model mixed membership in the context of information retrieval associated with text corpora and other discrete data. These ideas have been extended to sampling models in the exponential family of distributions by [Heller et al. \(2008\)](#), who illustrated the application of Bayesian mixed membership modeling to the characterization of political affiliation of US senators on a spectrum mixing liberal and conservative voting records. Prior distributions generalizing the concept of mixed membership to an arbitrary number of features have been discussed by [Heller et al. \(2008\)](#), who suggested leveraging the Indian buffet process ([Griffiths and Ghahramani, 2011](#)) to create a non-parametric mixed membership model. A comprehensive review and probabilistic generalizations of Bayesian clustering have been discussed by [Broderick et al. \(2013\)](#).

In this manuscript, we introduce the concept of mixed membership functions to the broader field of functional data analysis. Assuming a known number of latent functional features, we show how a functional mixed membership process is naturally defined through a simple extension of finite Gaussian process (GP) mixture models, by allowing mixing proportions to be indexed at the level of individual sample paths. Some sophistication is introduced through the multivariate treatment of the underlying functional features to ensure sampling models of adequate expressivity. Specifically, we represent a family of multivariate GPs through the multivariate Karhunen-Loève construction of [Happ and Greven \(2018\)](#). Using this idea, we jointly model the mean and covariance structures of the underlying functional features, and derive a sampling model through the ensuing finite dimensional marginal distributions. Since naïve GP mixture models assume that observations can only belong to one cluster, they only require the univariate treatment of the underlying GPs. However, when sample paths are allowed partial membership in multiple clusters, we need to either assume independence between clusters or estimate the cross-covariance functions. Since the assumption of independence does not often hold in practice, we propose a model that allows us to jointly model the covariance and cross-covariance functions through the eigenfunctions of the multivariate covariance operator. Typically, this representation would require sampling on a constrained space to ensure that the eigenfunctions are mutually orthogonal. However, in this context, we are able to relax these constraints and keep many of the desirable theoretical properties of our model by extending the multiplicative gamma process shrinkage prior proposed by [Bhattacharya and Dunson \(2011\)](#).

The remainder of the paper is organized as follows. Section 2 formalizes the concept of functional mixed membership as a natural extension of functional clustering. Section 3 discusses Bayesian inference through posterior simulation, and establishes conditions for weak posterior consistency. Section 4 carries out two simulation studies to assess operating characteristics on engineered data, and illustrates the application of the proposed model to a case study involving functional brain imaging through electroencephalography (EEG). Finally, we conclude our exposition with a critical discussion of methodological challenges and related literature in section 5.

## 2. Functional Mixed Membership

Functional data analysis (FDA) focuses on methods to analyze the sample paths of an underlying continuous stochastic process  $f : \mathcal{T} \rightarrow \mathbb{R}$ , where  $\mathcal{T}$  is a compact subset of  $\mathbb{R}^d$ . In the iid setting, a typical characterization of these stochastic processes relies on the definition of the mean function,  $\mu(t) = \mathbb{E}(f(t))$ , and the covariance function,  $C(s, t) = \text{Cov}(f(s), f(t))$ , where  $t, s \in \mathcal{T}$ . In this paper, we focus on jointly modeling  $K$  underlying stochastic processes, where each stochastic process represents one cluster. In this section, we will proceed under the assumption that the number of clusters,  $K$ , is known *a priori*. While  $K$  is fixed for the technical developments of the paper, section 4.2 discusses the use of various information criteria for selection of the optimal number of features.

Let  $f^{(k)} : \mathcal{T} \rightarrow \mathbb{R}$  denote the underlying stochastic process associated with the  $k^{th}$  cluster. Let  $\mu^{(k)}$  and  $C^{(k)}$  be, respectively, the mean and covariance function corresponding to the  $k^{th}$  stochastic process. To ensure desirable properties such as decompositions, FDA often makes the assumption that the random functions are elements in a Hilbert space. Specifically, we will assume  $f^{(k)} \in L^2(\mathcal{T})$  ( $\int_{\mathcal{T}} |f^{(k)}(t)|^2 dt < \infty$ ). Within this context, a typical model-based representation of functional clustering assumes that each underlying process is a latent Gaussian process,  $f^{(k)} \sim \mathcal{GP}(\mu^{(k)}, C^{(k)})$ , with sample paths  $f_i$  ( $i = 1, 2, \dots, N$ ), assumed to be independently drawn from a finite GP mixture

$$p(f_i | \rho^{(1:K)}, \mu^{(1:K)}, C^{(1:K)}) = \sum_{k=1}^K \rho^{(k)} \mathcal{GP}(f_i | \mu^{(k)}, C^{(k)});$$

where  $\rho^{(k)}$  is the mixing proportion (fraction of sample paths) for component  $k$ , s.t.  $\sum_{k=1}^K \rho^{(k)} = 1$ . Equivalently, by introducing latent variables  $\boldsymbol{\pi}_i = (\pi_{i1}, \dots, \pi_{iK})$ , s.t.  $\boldsymbol{\pi}_i \sim_{iid} \text{Multinomial}(1; \rho^{(1)}, \dots, \rho^{(K)})$ , it is easy to show that,

$$f_i | \boldsymbol{\pi}_1, \dots, \boldsymbol{\pi}_N, \mu^{(1:K)}, C^{(1:K)} \sim \mathcal{GP}\left(\sum_{k=1}^K \pi_{ik} \mu^{(k)}, \sum_{k=1}^K \pi_{ik} C^{(k)}\right). \quad (1)$$

Mixed membership is naturally defined by generalizing the finite mixture model to allow each sample path to belong to a finite positive number of mixture components, which we call *functional features* (Heller et al., 2008; Broderick et al., 2013). By introducing continuous latent variables  $\mathbf{z}_i = (Z_{i1}, \dots, Z_{iK})'$ , where  $Z_{ik} \in (0, 1)$  and  $\sum_{k=1}^K Z_{ik} = 1$ , the general form of the proposed mixed membership model follows the following convex combination:

$$f_i | \mathbf{z}_1, \dots, \mathbf{z}_N = \sum_{k=1}^K Z_{ik} f^{(k)}. \quad (2)$$

In equation 1, since each observation only belongs to one cluster, the Gaussian processes,  $f^{(k)}$ , are most commonly assumed to be mutually independent. The same assumption is, however, too restrictive for the model in equation 2. Thus, we will let  $C^{(k,k')}$  denote the cross-covariance function between  $f^{(k)}$  and  $f^{(k')}$ , and denote with  $\mathcal{C}$  the collection of covariance and cross-covariance functions. Therefore, the sampling model for the

proposed mixed membership scheme can be written as

$$f_i | \mathbf{z}_1, \dots, \mathbf{z}_N, \mu^{(1:K)}, \mathbf{C} \sim \mathcal{GP} \left( \sum_{k=1}^K Z_{ik} \mu^{(k)}, \sum_{k=1}^K Z_{ik}^2 C^{(k)} + \sum_{k=1}^K \sum_{k' \neq k} Z_{ik} Z_{ik'} C^{(k,k')} \right). \quad (3)$$

Given a finite evaluation grid  $\mathbf{t}_i = (t_{i1}, \dots, t_{in_i})'$ , the process' finite dimensional marginal distribution can be characterized s.t.

$$f_i(\mathbf{t}_i) | \mathbf{z}_1, \dots, \mathbf{z}_N, \mu^{(1:K)}, \mathbf{C} \sim \mathcal{N} \left( \sum_{k=1}^K Z_{ik} \mu^{(k)}(\mathbf{t}_i), C_i(\mathbf{t}_i, \mathbf{t}_i) \right), \quad (4)$$

where  $C_i(\mathbf{t}_i, \mathbf{t}_i) = \sum_{k=1}^K Z_{ik}^2 C^{(k)}(\mathbf{t}_i, \mathbf{t}_i) + \sum_{k=1}^K \sum_{k' \neq k} Z_{ik} Z_{ik'} C^{(k,k')}(\mathbf{t}_i, \mathbf{t}_i)$ . Since we do not assume that the functional features are independent, a concise characterization of the  $K$  stochastic processes is needed in order to ensure that our model is scalable and computationally tractable. In section 2.1, we review the multivariate Karhunen-Loëve theorem (Happ and Greven, 2018), which will provide a joint characterization of the latent functional features,  $(f^{(1)}, f^{(2)}, \dots, f^{(K)})$ . Using this joint characterization, we are able to specify a scalable sampling model for the finite-dimensional marginal distribution found in equation 4, which is described in full detail in section 2.2.

### 2.1. Multivariate Karhunen-Loëve Characterization

To aid computation, we will make the assumption that  $f^{(k)}$  is a smooth function and is in the  $P$ -dimensional subspace,  $\mathcal{S} \subset L^2(\mathcal{T})$ , spanned by a set of linearly independent square-integrable basis functions,  $\{b_1, \dots, b_P\}$  ( $b_p : \mathcal{T} \rightarrow \mathbb{R}$ ). While the choice of basis functions are user-defined, in practice B-splines (or the tensor product of B-splines for  $\mathcal{T} \subset \mathbb{R}^d$  for  $d \geq 2$ ) are a common choice due to their flexibility. Alternative basis systems can be selected in relation to application-specific considerations.

The multivariate Karhunen-Loëve (KL) theorem, proposed by Ramsay and Silverman (2005), can be used to jointly decompose our  $K$  stochastic processes. In order for our model to be able to handle higher dimensional functional data, such as images, we will use the extension of the multivariate KL theorem for different dimensional domains proposed by Happ and Greven (2018). While they state the theorem in full generality, we will only be considering the case when  $f^{(k)} \in \mathcal{S}$ . In this section, we will show that the multivariate KL theorem for different dimensional domains still holds under our assumption that  $f^{(k)} \in \mathcal{S}$ , given that the conditions in lemma 2.2 are satisfied.

We will start by defining the multivariate function  $\mathbf{f}(\mathbf{t})$  in the following way:

$$\mathbf{f}(\mathbf{t}) := \left( f^{(1)}(t^{(1)}), f^{(2)}(t^{(2)}), \dots, f^{(K)}(t^{(K)}) \right), \quad (5)$$

where  $\mathbf{t}$  is a  $K$ -tuple such that  $\mathbf{t} = (t^{(1)}, t^{(2)}, \dots, t^{(K)})$ , where  $t^{(1)}, t^{(2)}, \dots, t^{(K)} \in \mathcal{T}$ . This construction allows for the joint representation of  $K$  stochastic processes, each at different points in their domain. Since  $f^{(k)} \in \mathcal{S}$ , we have that  $\mathbf{f} \in \mathcal{H} := \mathcal{S} \times \mathcal{S} \times \dots \times \mathcal{S} := \mathcal{S}^K$ . We define the corresponding mean of  $\mathbf{f}(\mathbf{t})$ , such that  $\boldsymbol{\mu}(\mathbf{t}) := (\mu^{(1)}(t^{(1)}), \mu^{(2)}(t^{(2)}), \dots, \mu^{(K)}(t^{(K)}))$ , where  $\boldsymbol{\mu}(\mathbf{t}) \in \mathcal{H}$ , and the mean-centered cross-covariance functions as  $C^{(k,k')}(s, t) := \text{Cov}(f^{(k)}(s) - \mu^{(k)}(s), f^{(k')}(t) - \mu^{(k')}(t))$ , where  $s, t \in \mathcal{T}$ .

LEMMA 2.1.  $\mathcal{S}$  is a closed linear subspace of  $L^2(\mathcal{T})$ .

Proofs for all results are given in the appendix. From lemma 2.1, since  $\mathcal{S}$  is a closed linear subspace of  $L^2(\mathcal{T})$ , we have that  $\mathcal{S}$  is a Hilbert space with respect to the inner product  $\langle f, g \rangle_{\mathcal{S}} = \int_{\mathcal{T}} f(t)g(t)dt$  where  $f, g \in \mathcal{S}$ . By defining the inner product on  $\mathcal{H}$  as

$$\langle \mathbf{f}, \mathbf{g} \rangle_{\mathcal{H}} := \sum_{k=1}^K \int_{\mathcal{T}} f^{(k)}(t^{(k)}) g^{(k)}(t^{(k)}) dt^{(k)}, \quad (6)$$

where  $\mathbf{f}, \mathbf{g} \in \mathcal{H}$ , we have that  $\mathcal{H}$  is the direct sum of Hilbert spaces. Since  $\mathcal{H}$  is the direct sum of Hilbert spaces,  $\mathcal{H}$  is a Hilbert space (Reed and Simon, 1972). Thus we have constructed a subspace  $\mathcal{H}$  using our assumption that  $f^{(k)} \in \mathcal{S}$ , which satisfies proposition 1 in Happ and Greven (2018). With the inner product defined on  $\mathcal{H}$ , we can define the covariance operator  $\mathcal{K} : \mathcal{H} \rightarrow \mathcal{H}$  element-wise in the following way:

$$(\mathcal{K}\mathbf{f})^{(k)}(\mathbf{t}) := \left\langle C^{(\cdot, k)}(\cdot, t^{(k)}), \mathbf{f} \right\rangle_{\mathcal{H}} = \sum_{k'=1}^K \int_{\mathcal{T}} C^{(k', k)}(s, t^{(k)}) f^{(k')}(s) ds, \quad (7)$$

where  $\mathbf{f} \in \mathcal{H}$ . Since we made the assumption  $f^{(k)} \in \mathcal{S}$ , we can simplify equation 7. Since  $\mathcal{S}$  is the span of the basis functions, we have that

$$f^{(k)}(t) - \mu^{(k)}(t) = \sum_{p=1}^P \theta_{(k,p)} b_p(t) = \mathbf{B}'(t) \boldsymbol{\theta}_k, \quad (8)$$

for some  $\boldsymbol{\theta}_k \in \mathbb{R}^P$  and  $\mathbf{B}'(t) = [b_1(t) \cdots b_P(t)]$ . Thus we can see that

$$C^{(k, k')}(s, t) = \text{Cov}(\mathbf{B}'(s) \boldsymbol{\theta}_k, \mathbf{B}'(t) \boldsymbol{\theta}_{k'}) = \mathbf{B}'(s) \text{Cov}(\boldsymbol{\theta}_k, \boldsymbol{\theta}_{k'}) \mathbf{B}(t), \quad (9)$$

and we can rewrite equation 7 as:

$$(\mathcal{K}\mathbf{f})^{(k)}(\mathbf{t}) = \sum_{k'=1}^K \int_{\mathcal{T}} \mathbf{B}'(s) \text{Cov}(\boldsymbol{\theta}_{k'}, \boldsymbol{\theta}_k) \mathbf{B}(t^{(k)}) f^{(k')}(s) ds, \quad (10)$$

for some  $\mathbf{f} \in \mathcal{H}$ .

The following lemma establishes conditions under which  $\mathcal{K}$  is a bounded and compact operator, which is a necessary condition for the multivariate KL decomposition to exist.

LEMMA 2.2.  $\mathcal{K}$  is a bounded and compact operator under the following conditions:

- (a) The basis functions,  $b_1, \dots, b_P$ , are uniformly continuous,
- (b) There exists  $M \in \mathbb{R}$  such that  $|\text{Cov}(\theta_{(k,p)}, \theta_{(k',p')})| \leq M$ .

Assuming the conditions specified in lemma 2.2 hold, by the Hilbert-Schmidt theorem, since  $\mathcal{K}$  is a bounded, compact, and self-adjoint operator, we know that there exists real eigenvalues  $\lambda_1, \dots, \lambda_{KP}$  and a complete set of eigenfunctions  $\boldsymbol{\Psi}_1, \dots, \boldsymbol{\Psi}_{KP} \in \mathcal{H}$  such that

$$\mathcal{K}\boldsymbol{\Psi}_p = \lambda_p \boldsymbol{\Psi}_p, \quad p = 1, \dots, KP. \quad (11)$$

Since  $\mathcal{K}$  is a non-negative operator, we know that  $\lambda_p \geq 0$  for  $p = 1, \dots, KP$  (Happ and Greven (2018), proposition 2). From theorem VI.17 of Reed and Simon (1972), we have that the positive, bounded, self-adjoint, and compact operator  $\mathcal{K}$  can be written as

$$\mathcal{K}\mathbf{f} = \sum_{p=1}^{KP} \lambda_p \langle \Psi_p, \mathbf{f} \rangle_{\mathcal{H}} \Psi_p.$$

Thus from equation 7, we have that

$$\begin{aligned} \sum_{k'=1}^K \int_{\mathcal{T}} C^{(k',k)}(s, t^{(k)}) f^{(k')}(s) ds &= \sum_{p=1}^{KP} \lambda_p \langle \Psi_p, \mathbf{f} \rangle_{\mathcal{H}} \Psi_p^{(k)}(t^{(k)}) \\ &= \sum_{p=1}^{KP} \lambda_p \left( \sum_{k'=1}^K \int_{\mathcal{T}} \Psi_p^{(k')}(s) f^{(k')}(s) ds \right) \Psi_p^{(k)}(t^{(k)}) \\ &= \sum_{k'=1}^K \int_{\mathcal{T}} \left( \sum_{p=1}^{KP} \lambda_p \Psi_p^{(k')}(s) \Psi_p^{(k)}(t^{(k)}) \right) f^{(k')}(s) ds, \end{aligned}$$

where  $\Psi_p^{(k)}(t^{(k)})$  is the  $k^{th}$  element of  $\Psi_p(\mathbf{t})$ . Thus we can see that the covariance kernel can be written as the finite sum of eigenfunctions and eigenvalues,

$$C^{(k,k')}(s, t) = \sum_{p=1}^{KP} \lambda_p \Psi_p^{(k)}(s) \Psi_p^{(k')}(t). \quad (12)$$

Since we are working under the assumption that the random function,  $\mathbf{f} \in \mathcal{H}$ , we can use a modified version of the Multivariate KL theorem. Considering that  $\{\Psi_1, \dots, \Psi_{KP}\}$  form a complete basis for  $\mathcal{H}$  and  $\mathbf{f}(\mathbf{t}) - \boldsymbol{\mu}(\mathbf{t}) \in \mathcal{H}$ , we have

$$\mathbf{f}(\mathbf{t}) - \boldsymbol{\mu}(\mathbf{t}) = \mathbf{P}_{\mathcal{H}} \circ (\mathbf{f} - \boldsymbol{\mu})(\mathbf{t}) = \sum_{p=1}^{KP} \langle \Psi_p, \mathbf{f} - \boldsymbol{\mu} \rangle_{\mathcal{H}} \Psi_p(\mathbf{t}),$$

where  $\mathbf{P}_{\mathcal{H}}$  is the projection operator onto  $\mathcal{H}$ . Letting  $\rho_p = \langle \Psi_p, \mathbf{f} - \boldsymbol{\mu} \rangle_{\mathcal{H}}$ , we have that  $\mathbf{f}(\mathbf{t}) - \boldsymbol{\mu}(\mathbf{t}) = \sum_{p=1}^{KP} \rho_p \Psi_p(\mathbf{t})$ , where  $\mathbb{E}(\rho_p) = 0$  and  $\text{Cov}(\rho_p, \rho_{p'}) = \lambda_p \delta_{pp'}$  (Happ and Greven (2018), proposition 4).

Since  $\Psi_p \in \mathcal{H}$  and  $\boldsymbol{\mu} \in \mathcal{H}$ , there exists  $\boldsymbol{\nu}_k \in \mathbb{R}^P$  and  $\boldsymbol{\phi}_{kp} \in \mathbb{R}^P$  such that  $\boldsymbol{\mu}^{(k)}(\mathbf{t}) = \boldsymbol{\nu}'_k \mathbf{B}(t^{(k)})$  and  $\sqrt{\lambda_p} \Psi_p^{(k)}(\mathbf{t}) = \boldsymbol{\phi}'_{kp} \mathbf{B}(t^{(k)}) := \boldsymbol{\Phi}_p^{(k)}(\mathbf{t})$ . These scaled eigenfunctions,  $\boldsymbol{\Phi}_p^{(k)}(\mathbf{t})$ , are used over  $\Psi_p^{(k)}(\mathbf{t})$  because they fully specify the covariance structure of the latent features, as described in section 2.2. From a modeling prospective, the scaled eigenfunction parameterization is advantageous as it admits a prior model based on the multiplicative gamma process shrinkage prior proposed by Bhattacharya and Dunson (2011), allowing for adaptive regularized estimation (Shamshoian et al., 2022). Thus we have that

$$\mathbf{f}^{(k)}(\mathbf{t}) = \boldsymbol{\mu}^{(k)}(\mathbf{t}) + \sum_{p=1}^{KP} \chi_p \boldsymbol{\Phi}_p^{(k)}(\mathbf{t}) = \boldsymbol{\nu}'_k \mathbf{B}(t^{(k)}) + \sum_{p=1}^{KP} \chi_p \boldsymbol{\phi}'_{kp} \mathbf{B}(t^{(k)}), \quad (13)$$

where  $\chi_p = \langle (\lambda_p)^{-1/2} \Psi_p, \mathbf{f} - \boldsymbol{\mu} \rangle_{\mathcal{H}}$ ,  $\mathbb{E}(\chi_p) = 0$ , and  $\text{Cov}(\chi_p, \chi_{p'}) = \delta_{pp'}$ . Equation 13 gives us a way to jointly decompose any realization of the  $K$  stochastic processes,  $\mathbf{f} \in \mathcal{H}$ , as a finite weighted sum of basis functions.

**COROLLARY 2.3.** *If  $\chi_p \sim_{iid} \mathcal{N}(0, 1)$ , then the random function  $\mathbf{f}(\mathbf{t})$  follows a multivariate  $\mathcal{GP}$  with means  $\boldsymbol{\mu}^{(k)}(\mathbf{t}) = \boldsymbol{\nu}'_k \mathbf{B}(t^{(k)})$ , and cross-covariance functions  $C^{(k,k')}(s, t) = \mathbf{B}'(s) \sum_{p=1}^{KP} (\phi_{kp} \phi'_{k'p}) \mathbf{B}(t)$ .*

## 2.2. Functional Mixed Membership Process

In this section, we will describe a Bayesian additive model that allows for the constructive representation of mixed memberships for functional data. Our model allows for direct inference on the mean and covariance structures of the  $K$  stochastic processes, which are often of scientific interest. To aid computational tractability, we will use the joint decomposition described in section 2.1. In this section, we will make the assumption that  $f^{(k)} \in \mathcal{S}$ , and that the conditions from lemma 2.2 hold.

We aim to model the mixed membership of  $N$  observed sample paths,  $\{\mathbf{Y}_i(\cdot)\}_{i=1}^N$ , to  $K$  latent functional features  $\mathbf{f} = (f^{(1)}, f^{(2)}, \dots, f^{(K)})$ . Assuming each path is observed over  $n_i$  evaluation points  $\mathbf{t}_i = [t_{i1} \cdots t_{in_i}]'$ , without loss of generality we define a sampling model for the finite dimensional marginals of  $\mathbf{Y}_i(\mathbf{t}_i)$ . To allow for path-specific partial membership, we extend the finite mixture model in equation 1 and introduce path-specific mixing proportions  $Z_{ik} \in (0, 1)$ , s.t.  $\sum_{k=1}^K Z_{ik} = 1$ , for  $i = 1, 2, \dots, N$ .

Let  $\mathbf{S}(\mathbf{t}_i) = [\mathbf{B}(t_1) \cdots \mathbf{B}(t_{n_i})] \in \mathbb{R}^{P \times n_i}$ ,  $\chi_{im} \sim \mathcal{N}(0, 1)$ , and  $\boldsymbol{\Theta}$  denote a collection of model parameters. Let  $M \leq KP$  be the number of eigenfunctions used to approximate the covariance structure of the  $K$  stochastic processes. Using the decomposition of  $f^{(k)}(t)$  in equation 13 and assuming a normal distribution on  $\mathbf{Y}_i(\mathbf{t}_i)$ , we obtain:

$$\mathbf{Y}_i(\mathbf{t}_i) | \boldsymbol{\Theta} \sim \mathcal{N} \left\{ \sum_{k=1}^K Z_{ik} \left( \mathbf{S}'(\mathbf{t}_i) \boldsymbol{\nu}_k + \sum_{m=1}^M \chi_{im} \mathbf{S}'(\mathbf{t}_i) \boldsymbol{\phi}_{km} \right), \sigma^2 \mathbf{I}_{n_i} \right\}. \quad (14)$$

If we integrate out the latent  $\chi_{im}$  variables, we obtain a more transparent form for the proposed functional mixed membership process. Specifically, we have

$$\mathbf{Y}_i(\mathbf{t}_i) | \boldsymbol{\Theta}_{-\chi} \sim \mathcal{N} \left\{ \sum_{k=1}^K Z_{ik} \mathbf{S}'(\mathbf{t}_i) \boldsymbol{\nu}_k, \mathbf{V}_i + \sigma^2 \mathbf{I}_{n_i} \right\}, \quad (15)$$

where  $\boldsymbol{\Theta}_{-\chi}$  is the collection of our model parameters excluding the  $\chi_{im}$  variables, and the error-free mixed membership covariance is

$$\mathbf{V}_i = \sum_{k=1}^K \sum_{k'=1}^K Z_{ik} Z_{ik'} \left\{ \mathbf{S}'(\mathbf{t}_i) \sum_{m=1}^M (\boldsymbol{\phi}_{km} \boldsymbol{\phi}'_{k'm}) \mathbf{S}(\mathbf{t}_i) \right\}. \quad (16)$$

Thus, for a sample path, we have that the mixed membership mean is a convex combination of the functional feature means, and the mixed membership covariance, is a weighted sum of the covariance and cross-covariance functions between different functional features, following from the multivariate KL characterization in 2.1. Furthermore,

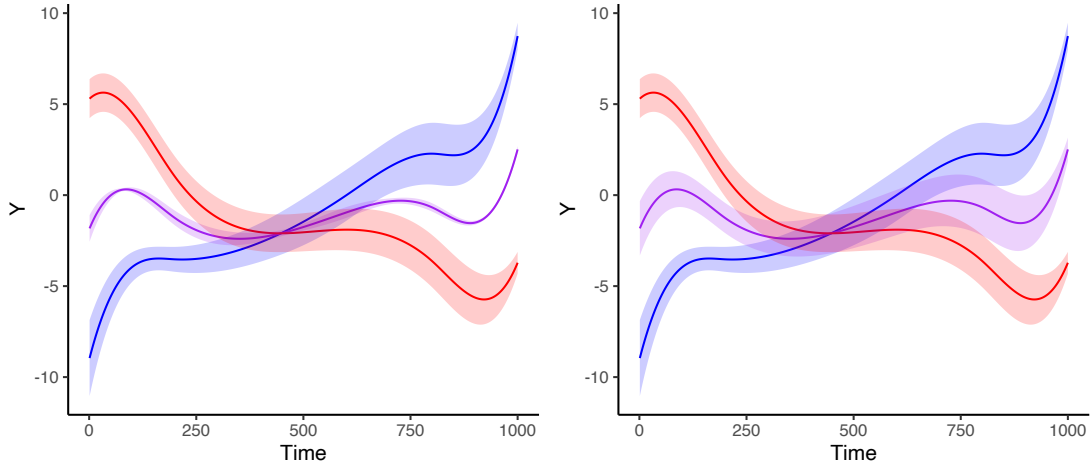


**Fig. 1.** Visualizations of data generated from the proposed model with various cross-covariance functions. The red and blue functions represent the distribution of functions belonging in only one functional feature, while the purple function represents the distribution of functions belonging equally to both functional features.

from equation 12 it is easy to show that, for large enough  $M$ , we have

$$\mathbf{S}'(\mathbf{t}_i) \sum_{m=1}^M (\phi_{kp} \phi'_{k'p}) \mathbf{S}(\mathbf{t}_i) \approx C^{(k,k')}(\mathbf{t}_i, \mathbf{t}_i),$$

with equality when  $M = KP$ .

In a mixed membership model, we may want to infer the distribution of observations that belong partially to multiple functional features. Figure 1 shows two examples of data generated from a two feature mixed membership model, with no measurement error ( $\sigma^2 = 0$ ). The function in blue represents the mean of observations that belong entirely to one functional feature, while the function in red represents the mean of observations that belong to the other functional feature. The function in purple depicts the mean function of observations that equally belong to both functional features. The two examples were generated with the same mean and covariance functions, however they have different cross-covariance functions. The graph on the left allows us to visualize what observed functions would look like when data is generated from the proposed mixed membership model with negative cross-covariance between the two functional features. In contrast, the graph on the right illustrates the case when there is positive cross-covariance between the two functional features. In this case, a negative cross-covariance function refers to the eigenvalues of the symmetric part of the cross-covariance operator being negative. Therefore, as illustrated in figure 1, the cross-covariance functions are crucial to ensuring a flexible model, as it controls the variation of observations that belong to more than one functional feature.

Mixed membership models can be thought of as a generalization of clustering. As such, these stochastic schemes are characterized by an inherent lack of likelihood identifiability.

A typical source of non-identifiability is the common *label switching* problem. To deal with the *label switching* problem, a relabelling algorithm can be derived for this model directly from the work of [Stephens \(2000\)](#). A second source of non-identifiability stems from allowing  $Z_{ik}$  to be continuous random variables. Specifically, consider a model with 2 features, and let  $\Theta_0$  be the set of “true” parameters. Let  $Z_{i1}^* = 0.5(Z_{i1})_0$  and  $Z_{i2}^* = (Z_{i2})_0 + 0.5(Z_{i1})_0$  (transformation preserves the constraint that  $Z_{i1}^* + Z_{i2}^* = 1$ ). If we let  $\nu_1^* = 2(\nu_1)_0 - (\nu_2)_0$ ,  $\nu_2^* = (\nu_2)_0$ ,  $\phi_{1m}^* = 2(\phi_{1m})_0 - (\phi_{2m})_0$ ,  $\phi_{2m}^* = (\phi_{2m})_0$ ,  $\chi_{im}^* = (\chi_{im})_0$ , and  $(\sigma^2)^* = \sigma_0^2$ , we have that  $P(Y_i(t)|\Theta_0) = P(Y_i(t)|\Theta^*)$  (equation 14). Thus we can see that our model is not identifiable, and we will refer to this problem as the *rescaling problem*. To address the *rescaling problem*, we developed the Membership Rescale Algorithm (Algorithm 2 in the appendix). This algorithm will rescale the allocation parameters so that at least one observation will completely belong to each of the two functional features. Section C.4 in the appendix also briefly reviews the work of [Chen et al. \(2022\)](#) which focuses on identifiability when we have more than two functional features. A third non-identifiability problem may arise numerically as a form of concurrency, i.e. when  $\nu_{k'} \propto \phi_{km}$  in equation 14. Typically, overestimation of the magnitude of  $\phi_{km}$ , may result in small variance estimates for the allocation parameters (smaller credible intervals). This phenomenon does need to be considered when studying how well we can recover the model parameters, as in section 4.1, but it is typically of little practical relevance in applications.

### 2.3. Prior Distributions and Model Specification

The sampling model in section 2.2, allows a practitioner to select how many eigenfunctions are to be used in the approximation of the covariance function. In the case where of  $M = KP$ , we have a fully saturated model and can represent any realization  $\mathbf{f} \in \mathcal{H}$ . In equation 13,  $\Phi$  parameters are mutually orthogonal (where orthogonality is defined by the inner product defined in equation 6), and have a magnitude proportional to the square root of the corresponding eigenvalue,  $\lambda_p$ . Thus, a modified version of the multiplicative gamma process shrinkage prior proposed by [Bhattacharya and Dunson \(2011\)](#) will be used as our prior for  $\phi_{km}$ . By using this prior, we promote shrinkage across the  $\phi_{km}$  coefficient vectors, with increasing prior shrinkage towards zero as  $m$  increases.

To facilitate MCMC sampling from the posterior target we will remove the assumption that  $\Phi$  parameters are mutually orthogonal. Even though  $\Phi$  parameters can no longer be thought of as scaled eigenfunctions, posterior inference can still be conducted on the eigenfunctions by post-processing posterior samples of  $\phi_{km}$  (given that we can recover the true covariance operator). Specifically, given posterior samples from  $\phi_{km}$ , we obtain posterior realizations for the covariance function, and then calculate the eigenpairs of the posterior samples of the covariance operator using the method described in [Happ and Greven \(2018\)](#).

Thus, letting  $\phi_{kpm}$  be the  $p^{th}$  element of  $\phi_{km}$ , we have

$$\phi_{kpm} | \gamma_{kpm}, \tilde{\tau}_{mk} \sim \mathcal{N} \left( 0, \gamma_{kpm}^{-1} \tilde{\tau}_{mk}^{-1} \right), \quad \gamma_{kpm} \sim \Gamma(\nu_\gamma/2, \nu_\gamma/2), \quad \tilde{\tau}_{mk} = \prod_{n=1}^m \delta_{nk},$$

$$\delta_{1k} | a_{1k} \sim \Gamma(a_{1k}, 1), \quad \delta_{jk} | a_{2k} \sim \Gamma(a_{2k}, 1), \quad a_{1k} \sim \Gamma(\alpha_1, \beta_1), \quad a_{2k} \sim \Gamma(\alpha_2, \beta_2),$$

where  $1 \leq k \leq K$ ,  $1 \leq p \leq P$ ,  $1 \leq m \leq M$ , and  $2 \leq j \leq M$ . In order for us to promote shrinkage across the  $M$  matrices, we need that  $\delta_{jk} > 1$ . Thus letting  $\alpha_2 > \beta_2$ , we have that  $\mathbb{E}(\delta_{jk}) > 1$ , which will promote shrinkage. In this construction, we allow for different rates of shrinkage across different functional features, which is particularly important in cases where the covariance functions of different features have different magnitudes. In cases where the magnitudes of the covariance functions are different, we would expect the  $\delta_{mk}$  to be relatively smaller in the  $k$  associated with the functional feature with a large covariance function.

To promote adaptive smoothing in the mean function, we will use a first order random walk penalty proposed by [Lang and Brezger \(2004\)](#). The first order random walk penalty penalizes differences in adjacent B-spline coefficients. In the case where  $\mathcal{T} \subset \mathbb{R}$ , we have that

$$P(\boldsymbol{\nu}_k | \tau_k) \propto \exp \left( -\frac{\tau_k}{2} \sum_{p=1}^{P-1} (\nu'_{pk} - \nu'_{(p+1)k})^2 \right),$$

for  $k = 1, \dots, K$ , where  $\tau_k \sim \Gamma(\alpha, \beta)$  and  $\nu_{pk}$  is the  $p^{\text{th}}$  element of  $\boldsymbol{\nu}_k$ . Since we have that  $Z_{ik} \in (0, 1)$  and  $\sum_{k=1}^K Z_{ik} = 1$ , it is natural to consider prior Dirichlet sampling for  $\mathbf{z}_i = [Z_{i1} \dots Z_{iK}]$ . Therefore, following [Heller et al. \(2008\)](#), we have

$$\mathbf{z}_i | \boldsymbol{\pi}, \alpha_3 \sim_{\text{iid}} \text{Dir}(\alpha_3 \boldsymbol{\pi}), \quad \boldsymbol{\pi} \sim \text{Dir}(\mathbf{c}), \quad \alpha_3 \sim \text{Exp}(b)$$

for  $i = 1, \dots, N$ . Lastly, we will use a conjugate prior for our random error component of the model, such that  $\sigma^2 \sim \text{IG}(\alpha_0, \beta_0)$ . While we relax the assumption of orthogonality, [Kowal et al. \(2017\)](#) describes a framework to sample from the posterior when linear constraints are imposed. In section C.1 of the appendix, we outline an alternative sampling scheme where we impose the condition that the  $\Phi$  parameters form orthogonal eigenfunctions.

### 3. Posterior Inference

#### 3.1. Weak Posterior Consistency

In the previous section we saw that the  $\Phi$  parameters are not assumed to be mutually orthogonal. By removing this constraint, we facilitate MCMC sampling from the posterior target and perform inference on the eigenpairs of the covariance operator, as long as we can recover the covariance structure. In this section, we will show that under certain conditions, we can recover the mean structure and the covariance structures of the  $K$  underlying stochastic processes from equation 15. Let  $\boldsymbol{\Pi}$  be the prior distribution on  $\boldsymbol{\omega} := \{\boldsymbol{\nu}_1, \dots, \boldsymbol{\nu}_K, \boldsymbol{\Sigma}_{11}, \dots, \boldsymbol{\Sigma}_{1K}, \dots, \boldsymbol{\Sigma}_{KK}, \sigma^2\}$ , where  $\boldsymbol{\Sigma}_{kk'} := \sum_{p=1}^{KP} (\phi_{kp} \phi'_{k'p})$ . We will be proving weak posterior consistency with respect to the parameters  $\boldsymbol{\Sigma}_{kk'}$  because the parameters  $\phi_{kp}$  are non-identifiable. Since the covariance and cross-covariance structure are completely specified by the  $\boldsymbol{\Sigma}_{kk'}$  parameters, the lack of identifiability of the  $\phi_{kp}$  parameters bears no importance on inferential considerations. We will denote the true set of parameter values as

$$\boldsymbol{\omega}_0 = \{(\boldsymbol{\nu}_1)_0, \dots, (\boldsymbol{\nu}_K)_0, (\boldsymbol{\Sigma}_{11})_0, \dots, (\boldsymbol{\Sigma}_{1K})_0, \dots, (\boldsymbol{\Sigma}_{KK})_0, \sigma_0^2\}.$$

In order to prove weak posterior consistency, will make the following assumptions:

ASSUMPTION 1. *The observed realizations  $\mathbf{Y}_1, \dots, \mathbf{Y}_N$  are observed on the same grid of  $R > KP$  points in the domain, say  $\{t_1, \dots, t_R\}$ .*

ASSUMPTION 2. *The variables  $Z_{ik}$  are known a-priori for  $i = 1, \dots, N$  and  $k = 1, \dots, K$ .*

ASSUMPTION 3. *The true parameter modeling the random noise is positive ( $\sigma_0^2 > 0$ ).*

Under assumptions 1, 2, and 3, we would like to show that the posterior distribution  $\Pi_N(\cdot | \mathbf{Y}_1, \dots, \mathbf{Y}_N)$ , is weakly consistent at  $\omega_0 \in \Omega$ . In order to do that, we will first specify the following quantities related to the Kullback–Leibler (KL) divergence. Following the notation of Choi and Schervish (2007), we will define the following quantities

$$\Lambda_i(\omega_0, \omega) = \log \left( \frac{f_i(\mathbf{Y}_i; \omega_0)}{f_i(\mathbf{Y}_i; \omega)} \right), \quad K_i(\omega_0, \omega) = \mathbb{E}_{\omega_0}(\Lambda_i(\omega_0, \omega)), \quad V_i(\omega_0, \omega) = \text{Var}_{\omega_0}(\Lambda_i(\omega_0, \omega)),$$

where  $f_i(\mathbf{Y}_i; \omega_0)$  is the likelihood under  $\omega_0$ . To simplify the notation, we will define the following two quantities

$$\begin{aligned} \mu_i &= \sum_{k=1}^K Z_{ik} \mathbf{S}'(\mathbf{t}) \nu_k, \\ \Sigma_i &= \sum_{k=1}^K \sum_{k'=1}^K Z_{ik} Z_{ik'} \left( \mathbf{S}'(\mathbf{t}) \sum_{p=1}^{KP} (\phi_{kp} \phi'_{k'p}) \mathbf{S}(\mathbf{t}) \right) + \sigma^2 \mathbf{I}_R = \mathbf{U}'_i \mathbf{D}_i \mathbf{U}_i + \sigma^2 \mathbf{I}_R, \end{aligned}$$

where  $\mathbf{U}'_i \mathbf{D}_i \mathbf{U}_i$  is the corresponding spectral decomposition. Let  $d_{il}$  be the  $l^{th}$  diagonal element of  $\mathbf{D}_i$ . Let  $\Omega_\epsilon(\omega_0)$  be the set of parameters such that the KL divergence is less than some  $\epsilon > 0$  ( $\Omega_\epsilon(\omega_0) := \{\omega : K_i(\omega_0, \omega) < \epsilon \text{ for all } i\}$ ). Let  $a, b \in \mathbb{R}$  be such that  $a > 1$  and  $b > 0$ , and define

$$\mathcal{B}(\omega_0) := \left\{ \omega : \frac{1}{a} ((d_{il})_0 + \sigma_0^2) \leq d_{il} + \sigma^2 \leq a ((d_{il})_0 + \sigma_0^2), \|\mu_i)_0 - \mu_i\| \leq b \right\}.$$

LEMMA 3.1. *Let  $\mathcal{C}(\omega_0, \epsilon) := \mathcal{B}(\omega_0) \cap \Omega_\epsilon(\omega_0)$ . Thus for  $\omega_0 \in \Omega$  and  $\epsilon > 0$ , there exists  $a > 1$  and  $b > 0$  such that*

- (a)  $\sum_{i=1}^{\infty} \frac{V_i(\omega_0, \omega)}{i^2} < \infty$ , for any  $\omega \in \mathcal{C}(\omega_0, \epsilon)$ ,
- (b)  $\Pi(\omega \in \mathcal{C}(\omega_0, \epsilon)) > 0$ .

Lemma 3.1 shows that the prior probability of our parameters being arbitrarily close (where the measure of closeness is defined by the KL divergence) to the true parameters is positive. Since  $\mathbf{Y}_1, \dots, \mathbf{Y}_N$  are not identically distributed, condition (a) in lemma 3.1 is need in order to prove lemma 3.2.

LEMMA 3.2. *Under assumptions 1-3, the posterior distribution,  $\Pi_N(\cdot | \mathbf{Y}_1, \dots, \mathbf{Y}_N)$ , is weakly consistent at  $\omega_0 \in \Omega$ .*

All proofs are provided in the supplemental appendix. Lemma 3.2 shows us that we are able to recover the covariance structure of the  $K$  stochastic processes. Relaxing the orthogonality constraint on the  $\phi_{km}$  parameters does not affect our ability to perform posterior inference on the main functions of scientific interest. Inference on the eigen-structure can still be performed by calculating the eigenvalues and eigenfunctions of the covariance operator using the MCMC samples of the  $\phi_{km}$  parameter. Finally, we point out that, in most cases, the parameters  $Z_{ik}$  are unknown. While theoretical guarantees for consistent estimation of the latent mixed allocation parameters is still elusive, we provide some empirical evidence of convergence in Section 4.1.

### 3.2. Simulation-Based Posterior Inference

Statistical inference is based on Markov chain Monte Carlo samples from the posterior distribution. To achieve this we used the Metropolis-within-Gibbs algorithm. By introducing the latent  $\chi_{im}$  variables, many of the posterior distributions related to the covariance process were easily sampled through Gibbs updates. More details on the sampling scheme can be found in section C.1 of the appendix. The sampling scheme is relatively simple, and was implemented using the RcppArmadillo package created by [Eddelbuettel and Sanderson \(2014\)](#) to speed up computation.

While the naïve sampling scheme is relatively simple, ensuring good exploration of the posterior target can be challenging due to the potentially multimodal nature of the posterior distribution. Specifically, some sensitivity of results to the starting values of the chain can be observed for some data. Section C.2 of the appendix outlines an algorithm for the selection of informed starting values. Furthermore, to mitigate sensitivity to chain initialization, we also implemented a tempered transition scheme, which improves the mixing of the Markov chain by allowing for transitions between modal configuration of the target. Implementation details for the proposed tempered transition scheme are reported in section C.3 of the appendix.

Given Monte Carlo samples from the posterior distribution of all parameters of interest, posterior inference is implemented descriptively; either directly on the Monte Carlo samples for parameters of interest, such as the mixed membership proportions  $\mathbf{z}_i$ , or indirectly through the evaluation of relevant functions of the parameters of interest, e.g. the mean and cross-covariance functions of the latent features.

In this setting, to calculate the simultaneous credible intervals, we will use the simultaneous credible intervals proposed by [Crainiceanu et al. \(2007\)](#). Let  $\mathbf{g}_n$  be simulated realizations using the MCMC samples of the function of interest, and let  $\{t_1, \dots, t_R\}$  be a fine grid of time points in  $\mathcal{T}$ . Let  $\mathbb{E}(\mathbf{g}(t_i))$  be the expected value of the function evaluated at time point  $t_i \in \mathcal{T}$ , and  $\text{SD}(\mathbf{g}(t_i))$  be the standard deviation of the function evaluated at time point  $t_i \in \mathcal{T}$ . Let  $M_\alpha$  be the  $(1 - \alpha)$  quantile of  $\max_{1 \leq i \leq R} \left| \frac{\mathbf{g}_n(t_i) - \mathbb{E}(\mathbf{g}(t_i))}{\text{SD}(\mathbf{g}(t_i))} \right|$ , for  $1 \leq n \leq N_{MC}$ , where  $N_{MC}$  are the number of MCMC samples of the converged MCMC chain. Thus the simultaneous credible intervals can be constructed as

$$\mathcal{I}(t_i) = [\mathbb{E}(\mathbf{g}(t_i)) - M_\alpha \text{SD}(\mathbf{g}(t_i)), \mathbb{E}(\mathbf{g}(t_i)) + M_\alpha \text{SD}(\mathbf{g}(t_i))].$$

Thus we estimate simultaneous credible intervals for all mean functions,  $\mu^{(k)}$ , and similarly generalize this procedure to define simultaneous credible intervals for the cross-

covariance functions,  $C^{(k,k')}$ . Figure 5, illustrates the difference between a simultaneous credible interval and a pointwise credible interval for one of the EEG case studies.

## 4. Case Studies and Experiments on Simulated Data

### 4.1. *Simulation Study 1*

In this simulation study, we examine how well our model can recover the mean and covariance functions when we vary the number of observed functions. The model used in this section will be a mixed membership model with 2 functional features ( $K = 2$ ), that can be represented by a basis constructed of 8 b-splines ( $P = 8$ ), and uses 3 eigenfunctions ( $M = 3$ ). Since the goal of this simulation is to test how well the model can recover the true mean and covariance functions, we must address the fact that that mean and covariance functions may not be identifiable (the third form of non-identifiability discussed in section 2.2). To mitigate the effects of this, we ensured that the eigenfunctions of the covariance operators were orthogonal to the mean functions when simulating the data. We consider the case when we have 40, 80, and 160 observed functional observations, where each observation is uniformly observed at 100 time points. We then simulated 50 datasets for each of the three cases ( $N = 40, 80, 160$ ). Section B.1 of the appendix goes into further detail of how the model parameters were drawn and how estimates of all quantities of interest were calculated in this simulation. To measure how well we recovered the functions of interest, we estimated the relative mean integrated square error (R-MISE) of the mean, covariance, and cross-covariance functions, where

$$\text{R-MISE} = \frac{\int \{f(t) - \hat{f}(t)\}^2 dt}{\int f(t)^2 dt} \times 100\%.$$

In this case, the  $\hat{f}$  used to estimate the R-MISE is the estimated posterior median of the function  $f$ . To measure how well we recovered the allocation parameters,  $Z_{ik}$ , we calculated the root-mean-square error (RMSE).

From figure 2, we can see that we have good recovery of the mean structure with as little as 40 functional observations. While the R-MISE of the mean functions improve as we increase the number of functional observations ( $N$ ), this improvement will likely have little practical impact. However, when looking at the recovery of the covariance and cross-covariance functions, we can see that the R-MISE noticeably decreases as more functional observations are added. As the recovery of the mean and covariance structures improve, the recovery of the allocation structure ( $Z$ ) improves. Visualizations of the recovered covariance structures for one of the datasets can be found in section B.1 of the appendix.

### 4.2. *Simulation Study 2*

Choosing the number of latent features can be challenging, especially when no prior knowledge is available for this quantity. Information criteria, such as the AIC, BIC, or DIC, are often used to aid practitioners in the selection of a data-supported value for  $K$ . In this simulation, we evaluate how various types of information criteria perform in recovering the true number of latent features. To do this, we simulate 10 different

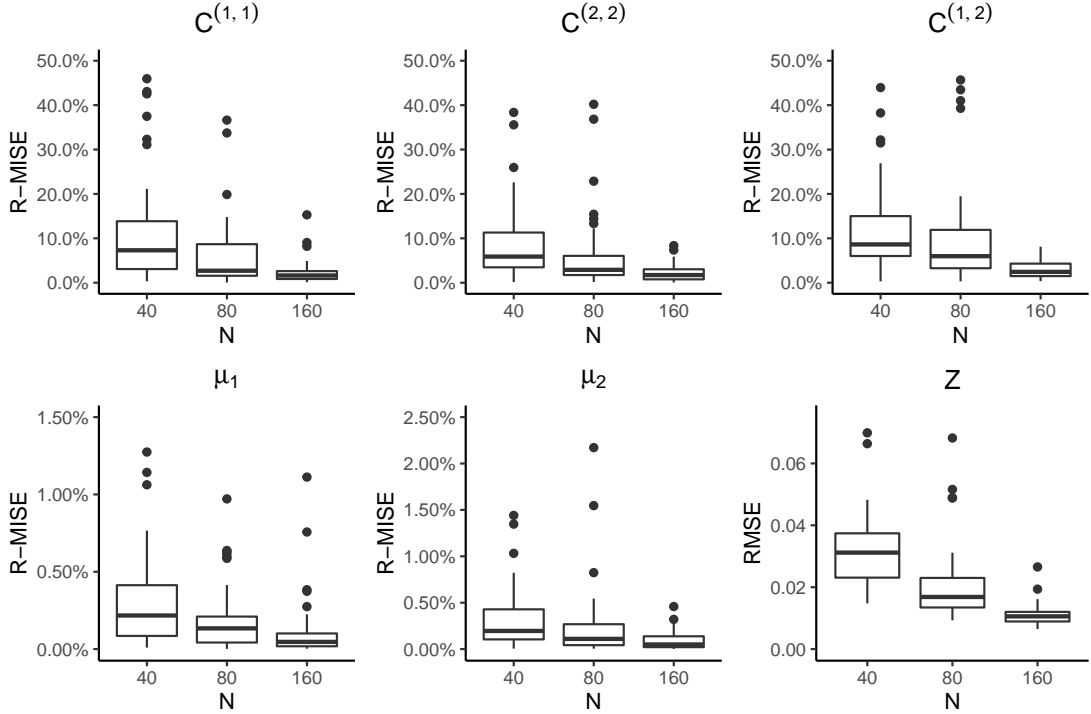


**Fig. 2.** R-MISE values for the latent feature means and cross-covariances, as well as RMSE values for the allocation parameters, evaluated as we increase sample size (number of functional observations).

data-sets, each with 200 functional observations, from a mixed membership model with three functional features. We then calculate these information criteria on the 10 data-sets for mixed membership models where  $K = 2, 3, 4, 5$ . In addition to examining how AIC, BIC, and DIC perform, we will also look at the performance of simple heuristics such as the “elbow-method”. Additional information on how the simulation study was conducted can be found in section B.2 of the appendix.

The BIC, proposed by [Schwarz \(1978\)](#), is defined as:

$$\text{BIC} = 2\log P(\mathbf{Y}|\hat{\Theta}) - d\log(n)$$

where  $d$  is the number of parameters and  $\hat{\Theta}$  are the maximum likelihood estimators (MLE) of our parameters. In the case of our proposed model, we have that

$$\text{BIC} = 2\log P(\mathbf{Y}|\hat{\nu}, \hat{\Phi}, \hat{\sigma}^2, \hat{\mathbf{Z}}, \hat{\chi}) - d\log(\tilde{N}) \quad (17)$$

where  $\tilde{N} = \sum_i n_i$  (where  $n_i$  is the number of observed time points observed for the  $i^{th}$  function), and  $d = (N + P)K + 2MKP + 4K + (N + K)M + 2$ .

Similarly, the AIC, proposed by [Akaike \(1974\)](#), can be written as

$$\text{AIC} = -2\log P(\mathbf{Y}|\hat{\nu}, \hat{\Phi}, \hat{\sigma}^2, \hat{\mathbf{Z}}, \hat{\chi}) + 2d. \quad (18)$$

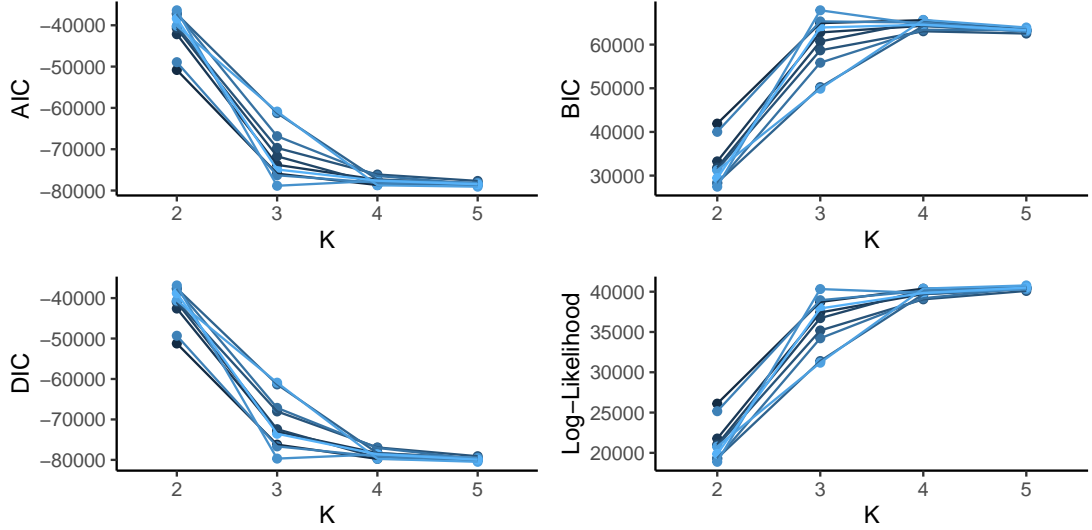


**Fig. 3.** AIC, BIC, DIC, and the average log-likelihood evaluated for each of the 10 simulated data-sets.

Following the work of [Roeder and Wasserman \(1997\)](#), we will use the posterior mean instead of the MLE for our estimates of BIC and AIC. In particular, we will use the posterior mean of the mean function in equation 14 for each functional observation, as well as the posterior mean of  $\sigma^2$ , to estimate the BIC and AIC.

The modified DIC, proposed by [Celeux et al. \(2006\)](#), is advantageous to the original DIC proposed by [Spiegelhalter et al. \(2002\)](#) when we have a posterior distribution with multiple modes, and when identifiability may be a problem. The modified DIC (referred to as  $\text{DIC}_3$  in [Celeux et al. \(2006\)](#)) is specified as:

$$\text{DIC} = -4\mathbb{E}_{\Theta}[\log f(\mathbf{Y}|\Theta)|\mathbf{Y}] + 2\log \hat{f}(\mathbf{Y}) \quad (19)$$

where  $\hat{f}(y_{ij}) = \frac{1}{N_{MC}} \sum_{l=1}^{N_{MC}} P(y_{ij}|\boldsymbol{\nu}^{(l)}, \boldsymbol{\Phi}^{(l)}, (\sigma^2)^{(l)}, \mathbf{Z}^{(l)})$ ,  $\hat{f}(\mathbf{Y}) = \prod_{i=1}^N \prod_{j=1}^{n_i} \hat{f}(y_{ij})$ , and  $N_{MC}$  is the number of MCMC samples used for estimating  $\hat{f}(y_{ij})$ . We can approximate  $\mathbb{E}_{\Theta}[\log f(\mathbf{Y}|\Theta)|\mathbf{Y}]$  by using the MCMC samples, such that

$$\mathbb{E}_{\Theta}[\log f(\mathbf{Y}|\Theta)|\mathbf{Y}] \approx \frac{1}{N_{MC}} \sum_{l=1}^{N_{MC}} \sum_{i=1}^N \sum_{j=1}^{n_i} \log \left[ P(y_{ij}|\boldsymbol{\nu}^{(l)}, \boldsymbol{\Phi}^{(l)}, (\sigma^2)^{(l)}, \mathbf{Z}^{(l)}) \right].$$

As specified above, the optimal model should have the largest BIC, smallest AIC, and smallest DIC.

From the simulation results presented in figure 3, we can see that on average, each information criterion overestimated the number of functional features in the model. While the three information criteria seem to greatly penalize models that do not have enough features, they do not seem punish overfit models to a great enough extent. Figure 3 also shows the average log-likelihood of the models. As expected, the log-likelihood

increases as we add more features, however, we can see that there is an elbow at  $K = 3$  for most of the models. Using the “elbow-method” led to selecting the correct number of latent functional features 8 times out of 10, while BIC picked the correct number of latent functional features twice. DIC and AIC were found to be the least reliable information criteria, only choosing the correct number of functional features once. Thus, through empirical consideration, we suggest using the “elbow-method” along with the information criteria discussed in this section to aid a final selection for the number of latent features to be interpreted in analyses. While formal considerations of model-selection consistency are out of scope for the current contribution, we maintain that some of these techniques are best interpreted in the context of data exploration, with a potential for great improvement in interpretation if semi-supervised considerations allow for an *a-priori* informed choice of  $K$ .

### 4.3. A Case Study of EEG in ASD

Autism spectrum disorder (ASD) is a term used to describe individuals with a collection of social communication deficits and restricted or repetitive sensory-motor behaviors (Lord et al., 2018). While once considered a very rare disorder with very specific symptoms, today the definition is more broad and is now thought of as a spectrum. Some individuals with ASD may have minor symptoms, while others may have very severe symptoms and require lifelong support. To diagnose a child with ASD, pediatricians and psychiatrists often administer a variety of tests and come to a diagnosis based off of the test results and reports from the parents or caregivers. In this case study, we will be using electroencephalogram (EEG) data that was previously analyzed by Scheffler et al. (2019) in the context of regression. The data-set consists of 39 typically developing (TD) children and 58 children with ASD between the ages of 2 and 12 years old. Each child was instructed to look at a computer monitor displaying bubbles for two minutes in a dark, sound-attenuated room (Dickinson et al., 2018). While the children were watching the screen, the EEG data were being recorded using a 128-channel HydroCel Geodesic Sensor Net. The data were then filtered to remove signals outside of the 0.1 - 100 Hz band, and then interpolated to match the international 10-20 system 25 channel montage. The data were also transformed into the frequency domain using a fast Fourier transform (FFT).

Scheffler et al. (2019) found that the T8 electrode, corresponding to the right temporal region, had the highest average contribution to the log-odds of ASD diagnosis, so we will specifically be using data from the T8 electrode in our mixed membership model. We focus our analysis to the alpha band of frequencies (6 to 14 Hz), whose patterns at rest are thought to play a role in neural coordination and communication between distributed brain regions. Figure 4 shows what the pre-processed data from the T8 electrode looks like for children who are at least 100 months old. Older children tend to have more noticeable differences between the ASD group and the TD group, however, we can still see that there is a lot of heterogeneity within the clinical cohorts.

As clinicians examine sample paths for the two cohorts, they are often interested in the location of a single prominent peak in the spectral density located within the alpha frequency band called the peak alpha frequency (PAF). This quantity has been previously linked to neural development in TD children (Rodríguez-Martínez et al., 2017). Scheffler

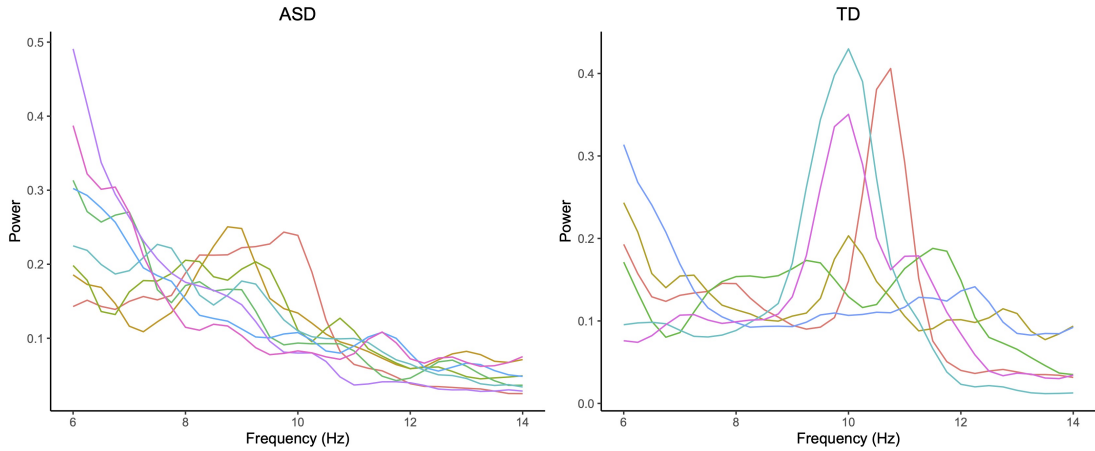


**Fig. 4.** Data from the T8 electrode stratified by clinical diagnosis, for children who are at least 100 months old.

et al. (2019) found that as TD children grow, the peak becomes more prominent and the PAF shifts to a higher frequency. Conversely, a discernible PAF pattern is attenuated for most children with ASD when compared to their TD counterpart.

In this case study, we will use a mixed membership model with 2 latent functional features ( $K = 2$ ). Mixed membership models with more features were considered. However, information criteria, such as AIC and BIC, indicated that a mixed membership model with 2 latent functional features was the optimal model. In this study, we assume that the underlying smooth random functions will lie in a space spanned by cubic b-spline basis functions with 4 equally spaced internal nodes ( $P = 8$ ) and that 3 eigenfunctions can sufficiently capture the covariance process ( $M = 3$ ). We ran the the MCMC chain for 500,000 iterations and used the Multiple Start Algorithm, described in section C.2 of the appendix, to get a good initial starting point.

Figure 5, reports the mean functions associated with the two latent functional features, with 95% pointwise and simultaneous credible bands. The mean function of the first feature can be interpreted as  $1/f$  noise, or *pink noise*. The  $1/f$  noise component can be described as noise that has spectral power that is inversely proportional to the frequency of the signal. This component noise is expected to be found in every individual to some extent, but we can see that the first feature has no discernible PAF pattern. The mean function of the second feature captures a distinct local PAF pattern, typically observed in EEGs of older neurotypical individuals.

In this context, a model of *uncertain membership* would be necessarily inadequate to describe the observed sample path heterogeneity, as we would not naturally think of subjects in our sample to belong to one or the other cluster. Instead, assuming *mixed membership* between the two feature processes is likely to represent a more realistic and interpretable data generating mechanism, as we conceptualize spectral patterns to mix continuously between  $1/f$  noise and distinct PAF patterns.

Figure 6, reports the posterior median estimate of the subject-level (feature 1)-membership, stratified by clinical cohort. We find that TD children are highly likely

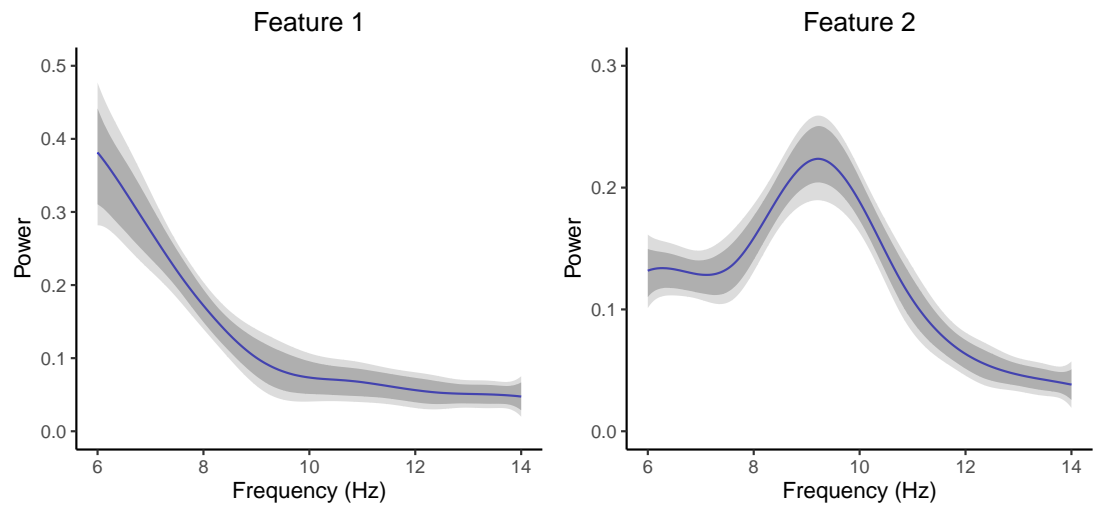


**Fig. 5.** Posterior median and 95% credible (pointwise credible interval in dark gray and simultaneous credible interval in light gray) of the mean function for each functional feature.

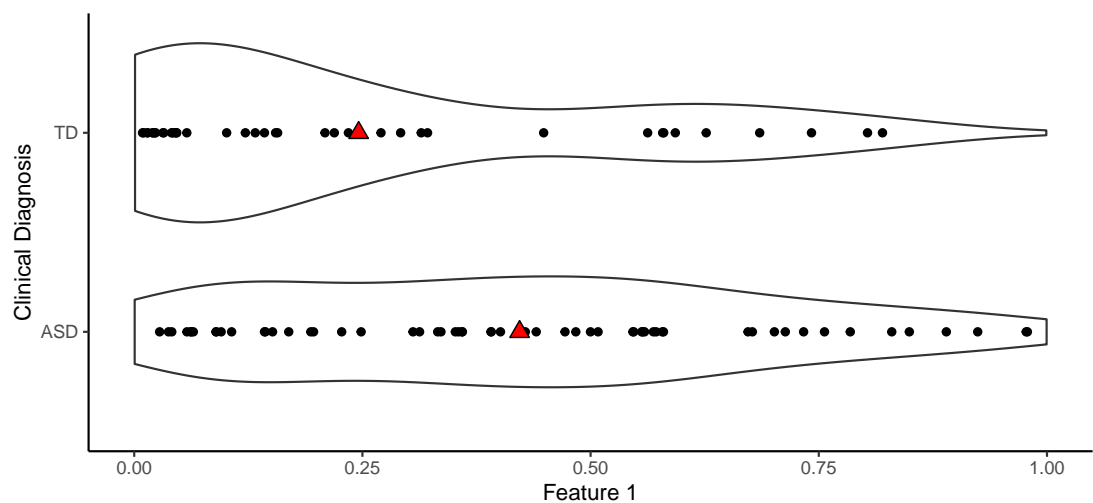


**Fig. 6.** Posterior median for the membership to feature 1, stratified by clinical cohort. The red triangles represent the mean (feature-1)-membership for each clinical group.

to load heavily on feature 2 (well defined PAF), whereas ASD children exhibit a higher level of heterogeneity, or a broader spectrum of mixed membership. Thus on average, children with ASD tend to have a less discernible PAF pattern when compared to their TD counterpart.

Overall, our findings confirm related evidence in the scientific literature on developmental neuroimaging, but offer a completely novel point of view in quantifying group membership as part of a spectrum. Posterior estimates of the covariance and cross-covariance functions are reported in section B.3 of the appendix. An extended analysis of multi-channel EEG for the same case study is reported in Section D of the web-based supporting materials.

## 5. Discussion

This manuscript introduces the concept of functional mixed membership to the broader field of functional data analysis. Mixed membership is defined as a natural generalization of the concept of *uncertain membership*, which underlies the many approaches to functional clustering discussed in the literature. Our discussion is carried out within the context of Bayesian analysis. In this paper, a coherent and flexible sampling model is introduced by defining a mixed membership Gaussian process through projections on the linear subspace spanned by a suitable set of basis functions. Within this context, we leverage the multivariate KL formulation (Happ and Greven, 2018), to define a model ensuring weak conditional posterior consistency. Inference is carried out through standard MCMC with the inclusion of tempered transitions to improve Markov chain exploration over differential modal configurations.

Our work is closely related to the approach introduced by Heller et al. (2008), who extended the theory of mixed membership models in the Bayesian framework for multivariate exponential family data. For Gaussian marginal distributions, their representation implies multivariate normal observations, with the natural parameters modeled as convex combinations of the individual cluster's natural parameters. While intuitively appealing, this idea has important drawbacks. Crucially, the differential entropy of observations in multiple clusters is constrained to be smaller than the minimum differential entropy across clusters, which may not be realistic in many sampling scenarios, e.g. figure 1.

The main computational challenge associated MCMC simulations from the posterior target has to do with the presence of multiple modal configurations for the model parameters, which is typical of mixture models. To ensure good mixing and irreducible exploration of the target, our implementation included tempered transitions (section C.3 of the web-based supporting materials) allowing the Markov chain to cross areas of low posterior density. We also recommend non-naïve chain initialization by using the Multiple Start Algorithm (section C.2 of the web-based supporting materials). As it is often the case for non-trivial posterior simulations, careful consideration is needed in tuning temperature ladders and the associated tuning parameters.

Information criteria are often used to aid the choice of  $K$  in the context of mixture models. However, in section 4.2, we saw that they often overestimated the number of features in our model. In simulations, we observed that using the “elbow-method”

could lead to the selection of the correct number of features with good frequency. The literature has discussed non-parametric approaches to feature allocation models by using, for example, the Indian Buffet Processes (Griffiths and Ghahramani, 2011), but little is known about operating characteristics of these proposed procedures and little has been discussed about the ensuing need to carry out statistical inference across changing-dimensions. Rousseau and Mengerson (2011), as well as Nguyen (2013), proved that under certain conditions, overfitted mixture model have a posterior distribution that converges to a set of parameters where the only components with positive weight will be the “true” parameters (the rest will be zero). Thus if a model fits their criteria, we could select a large  $K$ , and would still be able to recover the “true” model parameters. However, by allowing the membership parameters to be a continuous random variable we introduce a stronger type of non-identifiability, which led to the *rescaling problem* discussed in section 2.2. Therefore, more work on the posterior convergence of overfitted models is needed for mixed membership models.

To remove the interpretability problems caused by the *rescaling problem*, we recommend using the Membership Rescale Algorithm (algorithm 2 of the appendix) when using a model with only two latent features. The Membership Rescale Algorithm ensures that the entire range of the scale is used, guaranteeing that at least one observation completely lies within each latent feature. Ensuring that we use the entire range of the scale can be more challenging when we have more than 2 functional features, but it can be reformulated as solving an optimization problem (discussed in section C.4 of the appendix). In practice, we found that rescaling was seldomly needed when working with 3 or more functional features. An R package for fitting functional mixed membership models is available for download at <https://github.com/ndmarco/BayesFMM>.

## References

Akaike, H. (1974) A new look at the statistical model identification. *IEEE transactions on automatic control*, **19**, 716–723.

Azar, Y., Fiat, A., Karlin, A., McSherry, F. and Saia, J. (2001) Spectral analysis of data. In *Proceedings of the thirty-third annual ACM symposium on Theory of computing*, 619–626.

Behrens, G., Friel, N. and Hurn, M. (2012) Tuning tempered transitions. *Statistics and computing*, **22**, 65–78.

Bhattacharya, A. and Dunson, D. B. (2011) Sparse bayesian infinite factor models. *Biometrika*, 291–306.

Blei, D., Ng, A. and Jordan, M. (2003) Latent Dirichlet allocation. *JMLR*.

Broderick, T., Pitman, J. and Jordan, M. (2013) Feature allocations, probability functions, and paintboxes. *Bayesian Analysis*, **8**, 801–836.

Celeux, G., Forbes, F., Robert, C. P. and Titterington, D. M. (2006) Deviance information criteria for missing data models. *Bayesian analysis*, **1**, 651–673.

Chen, Y., He, S., Yang, Y. and Liang, F. (2022) Learning topic models: Identifiability and finite-sample analysis. *Journal of the American Statistical Association*, 1–16.

Chiou, J.-M. and Li, P.-L. (2007) Functional clustering and identifying substructures of longitudinal data. *Journal of the Royal Statistical Society: Series B (Statistical Methodology)*, **69**, 679–699.

Choi, T. and Schervish, M. J. (2007) On posterior consistency in nonparametric regression problems. *Journal of Multivariate Analysis*, **98**, 1969–1987.

Crainiceanu, C. M., Ruppert, D., Carroll, R. J., Joshi, A. and Goodner, B. (2007) Spatially adaptive bayesian penalized splines with heteroscedastic errors. *Journal of Computational and Graphical Statistics*, **16**, 265–288.

Dickinson, A., DiStefano, C., Senturk, D. and Jeste, S. S. (2018) Peak alpha frequency is a neural marker of cognitive function across the autism spectrum. *European Journal of Neuroscience*, **47**, 643–651.

Eddelbuettel, D. and Sanderson, C. (2014) Rcpparmadillo: Accelerating r with high-performance c++ linear algebra. *Computational Statistics & Data Analysis*, **71**, 1054–1063.

Erosheva, E., Fienberg, S. and Lafferty, J. (2004) Mixed membership models of scientific publications. *PNAS*.

Ghosal, S. and Van der Vaart, A. (2017) *Fundamentals of nonparametric Bayesian inference*, vol. 44. Cambridge University Press.

Ghosh, J. and Ramamoorthi, R. (2003) Bayesian nonparametrics. *Springer Series in Statistics*.

Golub, G. H. and Van Loan, C. F. (2013) *Matrix computations*. The Johns Hopkins University Press.

Griffiths, T. and Ghahramani, Z. (2011) The Indian buffet process: An introduction and review. *Journal of Machine Learning Research*, **12**, 1185–1224.

Grinvald, A. and Hildesheim, R. (2004) Vsd: a new era in functional imaging of cortical dynamics. *Nature Reviews Neuroscience*, **5**, 874–885.

Happ, C. and Greven, S. (2018) Multivariate functional principal component analysis for data observed on different (dimensional) domains. *Journal of the American Statistical Association*, **113**, 649–659.

Heller, K. A., Williamson, S. and Ghahramani, Z. (2008) Statistical models for partial membership. In *Proceedings of the 25th International Conference on Machine learning*, 392–399.

Helwig, N. E. (2018) *eegkit: Toolkit for Electroencephalography Data*. URL: <https://CRAN.R-project.org/package=eegkit>. R package version 1.0-4.

Hennig, C., Meila, M., Murtagh, F. and Rocci, r. (2015) *Handbook of Cluster Analysis*. CRC Press.

Huang, K., Fu, X. and Sidiropoulos, N. D. (2016) Anchor-free correlated topic modeling: Identifiability and algorithm. *Advances in Neural Information Processing Systems*, **29**.

Jacques, J. and Preda, C. (2014) Model-based clustering for multivariate functional data. *Computational Statistics & Data Analysis*, **71**, 92–106.

James, G. M. and Sugar, C. A. (2003) Clustering for sparsely sampled functional data. *Journal of the American Statistical Association*, **98**, 397–408.

Jang, B. and Hero, A. (2019) Minimum volume topic modeling. In *The 22nd International Conference on Artificial Intelligence and Statistics*, 3013–3021. PMLR.

Kowal, D. R., Matteson, D. S. and Ruppert, D. (2017) A bayesian multivariate functional dynamic linear model. *Journal of the American Statistical Association*, **112**, 733–744.

Lang, S. and Brezger, A. (2004) Bayesian p-splines. *Journal of computational and graphical statistics*, **13**, 183–212.

Lord, C., Elsabbagh, M., Baird, G. and Veenstra-Vanderweele, J. (2018) Autism spectrum disorder. *The Lancet*, **392**, 508–520.

McSherry, F. (2001) Spectral partitioning of random graphs. In *Proceedings 42nd IEEE Symposium on Foundations of Computer Science*, 529–537. IEEE.

Nguyen, X. (2013) Convergence of latent mixing measures in finite and infinite mixture models. *The Annals of Statistics*, **41**, 370–400.

Papadimitriou, C. H., Tamaki, H., Raghavan, P. and Vempala, S. (1998) Latent semantic indexing: A probabilistic analysis. In *Proceedings of the seventeenth ACM SIGACT-SIGMOD-SIGART symposium on Principles of database systems*, 159–168.

Petrone, S., Guindani, M. and Gelfand, A. E. (2009) Hybrid dirichlet mixture models for functional data. *Journal of the Royal Statistical Society: Series B (Statistical Methodology)*, **71**, 755–782.

Pritchard, J. K., Stephens, M. and Donnelly, P. (2000) Inference of population structure using multilocus genotype data. *Genetics*, **155**, 945–959.

Ramsay, J. and Silverman, B. (2005) Principal components analysis for functional data. *Functional data analysis*, 147–172.

Reed, M. and Simon, B. (1972) *Methods of modern mathematical physics*, vol. 1. Elsevier.

Roberts, G. O. and Rosenthal, J. S. (2007) Coupling and ergodicity of adaptive markov chain monte carlo algorithms. *Journal of applied probability*, **44**, 458–475.

Rodríguez-Martínez, E., Ruiz-Martínez, F., Paulino, C. B. and Gómez, C. M. (2017) Frequency shift in topography of spontaneous brain rhythms from childhood to adulthood. *Cognitive neurodynamics*, **11**, 23–33.

Roeder, K. and Wasserman, L. (1997) Practical bayesian density estimation using mixtures of normals. *Journal of the American Statistical Association*, **92**, 894–902.

Rousseau, J. and Mengersen, K. (2011) Asymptotic behaviour of the posterior distribution in overfitted mixture models. *Journal of the Royal Statistical Society: Series B (Statistical Methodology)*, **73**, 689–710.

Scheffler, A. W., Telesca, D., Sugar, C. A., Jeste, S., Dickinson, A., DiStefano, C. and Sentürk, D. (2019) Covariate-adjusted region-referenced generalized functional linear model for eeg data. *Statistics in medicine*, **38**, 5587–5602.

Schwarz, G. (1978) Estimating the dimension of a model. *The annals of statistics*, 461–464.

Shamshoian, J., Senturk, D., Jeste, S. and Telesca, D. (2022) Bayesian analysis of longitudinal and multidimensional functional data. *Biostatistics*, **23**, 558–573.

Spiegelhalter, D. J., Best, N. G., Carlin, B. P. and Van Der Linde, A. (2002) Bayesian measures of model complexity and fit. *Journal of the royal statistical society: Series B (statistical methodology)*, **64**, 583–639.

Stephens, M. (2000) Dealing with label switching in mixture models. *Journal of the Royal Statistical Society: Series B (Statistical Methodology)*, **62**, 795–809.

## A. Proofs

### A.1. Proof of Lemma 2.1

PROOF. We will first show that  $\mathcal{S}$  is a linear subspace of  $L^2(\mathcal{T})$ . Let  $w_1, w_2 \in \mathcal{S}$ , and let  $\alpha_1, \alpha_2 \in \mathbb{R}$ . Since  $\mathcal{S}$  is the space spanned by the square-integrable basis functions  $b_1, \dots, b_P$  ( $\mathcal{S} = \left\{ \sum_{p=1}^P a_p b_p : a_i \in \mathbb{R} \right\}$ ), we can write  $w_1 = \sum_{p=1}^P \delta_p b_p$  and  $w_2 = \sum_{p=1}^P \beta_p b_p$  for some  $\delta_p, \beta_p \in \mathbb{R}$ . Therefore we have that

$$\alpha_1 w_1 + \alpha_2 w_2 = \alpha_1 \left( \sum_{p=1}^P \delta_p b_p \right) + \alpha_2 \left( \sum_{p=1}^P \beta_p b_p \right).$$

Letting  $\gamma_p = \alpha_1 \delta_p + \alpha_2 \beta_p$ , we have that

$$\alpha_1 w_1 + \alpha_2 w_2 = \sum_{p=1}^P \gamma_p b_p \in \mathcal{S}.$$

Therefore, by definition, we know that  $\mathcal{S}$  is a linear subspace of  $L^2(\mathcal{T})$ . Next, we will show that  $\mathcal{S}$  is a closed linear subspace. Let  $f_n$  be a Cauchy sequence in  $\mathcal{S}$ . Thus by definition, for some  $\epsilon > 0$ , there exists a  $m \in \mathbb{N}$  such that for  $i, j > m$  we have

$$\|f_i - f_j\|_{\mathcal{S}} < \epsilon. \quad (20)$$

Since  $f_i, f_j \in \mathcal{S}$ , we know that  $f_i, f_j \in \text{span}\{b_1, \dots, b_P\}$ . Thus using the Gram–Schmidt process, we know that there exists an orthonormal set of functions such that  $\text{span}\{b_1, \dots, b_P\} = \text{span}\{\tilde{b}_1, \dots, \tilde{b}_P\}$ . Thus we can expand  $f_i$  and  $f_j$  such that  $f_i = \sum_{p=1}^P \alpha_{ip} \tilde{b}_p$  and  $f_j = \sum_{p=1}^P \alpha_{jp} \tilde{b}_p$ . Thus we can rewrite equation 20 as

$$\begin{aligned} \|f_i - f_j\|_{\mathcal{S}} &= \left( \left\langle \sum_{p=1}^P (\alpha_{ip} - \alpha_{jp}) \tilde{b}_p, \sum_{p=1}^P (\alpha_{ip} - \alpha_{jp}) \tilde{b}_p \right\rangle \right)^{1/2} \\ &= \left( \sum_{p=1}^P \left\langle (\alpha_{ip} - \alpha_{jp}) \tilde{b}_p, (\alpha_{ip} - \alpha_{jp}) \tilde{b}_p \right\rangle \right)^{1/2} \\ &= \left( \sum_{p=1}^P \left\| (\alpha_{ip} - \alpha_{jp}) \tilde{b}_p \right\|_{\mathcal{S}} \right)^{1/2} \\ &= \left( \sum_{p=1}^P \int_{\mathcal{T}} \left( (\alpha_{ip} - \alpha_{jp}) \tilde{b}_p(t) \right)^2 dt \right)^{1/2} \\ &= \left( \sum_{p=1}^P (\alpha_{ip} - \alpha_{jp})^2 \int_{\mathcal{T}} \tilde{b}_p(t)^2 dt \right)^{1/2}. \end{aligned} \quad (21)$$

Since  $\tilde{b}_p(t)$  are orthonormal, we know that  $\int_{\mathcal{T}} \tilde{b}_p(t)^2 dt = 1$ . Thus from equations 20 and 21, for  $i, j > m$ , we have that

$$\begin{aligned} \epsilon &> \|f_i - f_j\|_{\mathcal{S}} \\ &= \left( \sum_{p=1}^P (\alpha_{ip} - \alpha_{jp})^2 \int_{\mathcal{T}} \tilde{b}_p(t)^2 dt \right)^{1/2} \\ &= \left( \sum_{p=1}^P (\alpha_{ip} - \alpha_{jp})^2 \right)^{1/2}. \end{aligned} \tag{22}$$

Thus we can see that the sequence  $\alpha_{ip}$  is a Cauchy sequence. Since the Euclidean space is a complete metric space, there exists  $\alpha_p \in \mathbb{R}$  such that  $\alpha_{ip} \rightarrow \alpha_p$ . Letting  $f = \sum_{p=1}^P \alpha_p \tilde{b}_p(t)$ , we have

$$\begin{aligned} \|f_i - f\| &= \left( \sum_{p=1}^P (\alpha_{ip} - \alpha_p)^2 \int_{\mathcal{T}} \tilde{b}_p(t)^2 dt \right)^{1/2} \\ &= \left( \sum_{p=1}^P (\alpha_{ip} - \alpha_p)^2 \right)^{1/2} \\ &= \sum_{p=1}^P \|\alpha_{ip} - \alpha_p\|, \end{aligned} \tag{23}$$

for all  $i, j > m$ . By definition of  $\alpha_{ip} \rightarrow \alpha_p$ , we know that for  $\epsilon_2 = \frac{\epsilon_1}{P}$ , there exists a  $m_1 \in \mathbb{N}$ , such that for all  $i > m_1$  we have  $\|\alpha_{ip} - \alpha_p\| < \epsilon_1$  for  $p = 1, \dots, P$ . Thus from equation 23, we have that for all  $i > m_1$ , we have

$$\|f_i - f\| < \epsilon_2.$$

Thus by definition, we have that the Cauchy sequence is convergent, and that  $\mathcal{S}$  is a closed linear subspace.

### A.2. Proof of Lemma 2.2

PROOF. We will start by fixing  $\epsilon > 0$ . Notice that since  $b_j$  are uniformly continuous functions and  $\mathcal{T}$  is a closed and bounded domain, we know that  $b_j$  is bounded. Thus let  $R$  be such that  $|b_j(s)| < R$  for  $j = 1, \dots, P$  and any  $s \in \mathcal{T}$ . Let  $\tilde{\epsilon} := \frac{\epsilon}{P^2 R M}$ , where  $M$  is defined in (b) of lemma 2.2. Since  $b_1, \dots, b_k$  are uniformly continuous we have that there exists  $\delta_i > 0$  such that for all  $t, t_* \in \mathcal{T}$ , we have

$$\|t - t_*\| < \delta_i \implies |b_i(t) - b_i(t_*)| < \tilde{\epsilon}, \tag{24}$$

for  $i = 1, \dots, P$ . Define  $\tilde{\delta} = \min_i \delta_i$ . Thus from equation 9, if  $\|t - t_*\| < \tilde{\delta}$ , then we have

$$\begin{aligned}
|C^{(i,j)}(s, t) - C^{(i,j)}(s, t_*)| &= |\mathbf{B}'(s) \text{Cov}(\boldsymbol{\theta}_i, \boldsymbol{\theta}_j) [\mathbf{B}(t) - \mathbf{B}(t_*)]| \\
&= \left| \sum_{k=1}^P \sum_{l=1}^P b_k(s) \text{Cov}(\theta_{(i,k)}, \theta_{(j,l)}) [b_l(t) - b_l(t_*)] \right| \\
&\leq \left| \sum_{k=1}^P \sum_{l=1}^P b_k(s) M [b_l(t) - b_l(t_*)] \right| \\
&\leq \sum_{k=1}^P \sum_{l=1}^P |b_k(s) M [b_l(t) - b_l(t_*)]| \\
&= \sum_{k=1}^P \sum_{l=1}^P |b_k(s) M| |b_l(t) - b_l(t_*)|.
\end{aligned}$$

From equation 24, we have that

$$\begin{aligned}
|C^{(i,j)}(s, t) - C^{(i,j)}(s, t_*)| &< \sum_{k=1}^P \sum_{l=1}^P |b_k(s) M| \tilde{\epsilon} \\
&\leq \sum_{k=1}^P \sum_{l=1}^P R M \tilde{\epsilon} \\
&= \epsilon.
\end{aligned}$$

Thus we have that for any  $\epsilon > 0$ , there exists a  $\tilde{\delta} > 0$ , such that for any  $t, t_*, s \in \mathcal{T}$  and  $1 \leq i \leq j \leq K$ , we have

$$\|t - t_*\| < \tilde{\delta} \implies |C^{(i,j)}(s, t) - C^{(i,j)}(s, t_*)| < \epsilon. \quad (25)$$

Consider  $\mathcal{B}_Z := \{\mathbf{f} \in \mathcal{H} : \|\mathbf{f}\| < Z\}$  for some  $Z \in \mathbb{R}^+$ . We will show that the family of functions  $\mathcal{K}\mathbf{f}_{\mathcal{B}_Z} := \{\mathcal{K}\mathbf{f} : \mathbf{f} \in \mathcal{B}_Z\}$  is an equicontinuous set of functions. We will fix  $\epsilon_1 > 0$ . Letting  $\mathbf{f} \in \mathcal{B}_Z$  and  $t^{(i)}, t_*^{(i)} \in \mathcal{T}$  such that  $\|t^{(i)} - t_*^{(i)}\| < \tilde{\delta}$ , we have from equation 7 that

$$\begin{aligned}
|(\mathcal{K}\mathbf{f})^{(i)}(\mathbf{t}) - (\mathcal{K}\mathbf{f})^{(i)}(\mathbf{t}_*)| &= \left| \sum_{k=1}^K \int_{\mathcal{T}} C^{(k,i)}(s, t^{(i)}) f^{(k)}(s) - C^{(k,i)}(s, t_*^{(i)}) f^{(k)}(s) ds \right| \\
&\leq \sum_{k=1}^K \int_{\mathcal{T}} |C^{(k,i)}(s, t^{(i)}) f^{(k)}(s) - C^{(k,i)}(s, t_*^{(i)}) f^{(k)}(s)| ds \\
&= \sum_{k=1}^K \int_{\mathcal{T}} |C^{(k,i)}(s, t^{(i)}) - C^{(k,i)}(s, t_*^{(i)})| |f^{(k)}(s)| ds. \quad (26)
\end{aligned}$$

Thus from equation 25 we have that  $|C^{(k,i)}(s, t^{(i)}) - C^{(k,i)}(s, t_*^{(i)})| < \epsilon$ . Notice that since  $\mathbf{f} \in \mathcal{H}$ , we know that  $f^{(k)}(s)$  can be written as  $f^{(k)}(s) = \sum_{i=1}^P a_i b_i(s)$ . Since the

sum of uniformly continuous functions is also a uniformly continuous function, we know that  $f^{(k)}$  is uniformly continuous. Therefore, since  $\mathcal{T}$  is a closed and bounded domain, we know that  $f^{(k)}$  is bounded. Let  $M_1$  be such that  $|f^{(k)}| < M_1$ . Thus we can write equation 26 as

$$\begin{aligned} |(\mathcal{K}\mathbf{f})^{(i)}(\mathbf{t}) - (\mathcal{K}\mathbf{f})^{(i)}(\mathbf{t}_*)| &< \sum_{k=1}^K \int_{\mathcal{T}} \epsilon M_1 ds \\ &= \epsilon M_1 \sum_{k=1}^K \int_{\mathcal{T}} 1 ds. \end{aligned}$$

Since  $\mathcal{T}$  is compact subset of  $\mathbb{R}^d$ , by the Bolzano–Weierstrass theorem, we know that  $\mathcal{T}$  is closed and bounded. Therefore, let  $B$  be such that  $\int_{\mathcal{T}} 1 dt = B$ . Thus, for  $i = 1, \dots, K$ , we have

$$|(\mathcal{K}\mathbf{f})^{(i)}(\mathbf{t}) - (\mathcal{K}\mathbf{f})^{(i)}(\mathbf{t}_*)| < \epsilon M_1 K B.$$

Since

$$\|(\mathcal{K}\mathbf{f})(\mathbf{t}), (\mathcal{K}\mathbf{f})(\mathbf{t}_*)\| = \left( \sum_{i=1}^K |(\mathcal{K}\mathbf{f})^{(i)}(\mathbf{t}) - (\mathcal{K}\mathbf{f})^{(i)}(\mathbf{t}_*)|^2 \right)^{1/2},$$

we know that

$$\|(\mathcal{K}\mathbf{f})(\mathbf{t}), (\mathcal{K}\mathbf{f})(\mathbf{t}_*)\| < \epsilon M_1 K^{3/2} B.$$

If we let  $\epsilon = \frac{\epsilon_1}{M_1 K^{3/2} B}$  ( $\tilde{\epsilon} = \frac{\epsilon_1}{M_1 K^{3/2} B P^2 R M}$ ), then we have that  $\|(\mathcal{K}\mathbf{f})(\mathbf{t}), (\mathcal{K}\mathbf{f})(\mathbf{t}_*)\| < \epsilon_1$ . Thus, from the assumption that  $b_j$  are uniformly continuous (equation 24), we know there exists a  $\tilde{\delta}$  such that for  $j = 1, \dots, K$ , we have that

$$\|t - t_*\| < \tilde{\delta} \implies |b_j(t) - b_j(t_*)| < \frac{\epsilon_1}{M_1 K^{3/2} B P^2 R M} \implies \|(\mathcal{K}\mathbf{f})(\mathbf{t}), (\mathcal{K}\mathbf{f})(\mathbf{t}_*)\| < \epsilon_1. \quad (27)$$

Thus by definition, we have proved that  $\mathcal{K}\mathbf{f}_{\mathcal{B}_z}$  is an equicontinuous set of functions. Next, we will show that  $\mathcal{K}\mathbf{f}_{\mathcal{B}_z}$  is a family of uniformly bounded functions. If  $t \in \mathcal{T}$ , then

we have

$$\begin{aligned}
|(\mathcal{K}\mathbf{f})^{(i)}(\mathbf{t})| &= \left| \sum_{k=1}^K \int_{\mathcal{T}} \mathbf{B}'(s) \text{Cov}(\boldsymbol{\theta}_k, \boldsymbol{\theta}_i) \mathbf{B}\left(t^{(i)}\right) f^{(k)}(s) ds \right| \\
&= \left| \sum_{k=1}^K \int_{\mathcal{T}} \sum_{p=1}^P \sum_{l=1}^P b_p(s) \text{Cov}(\theta_{(k,l)}, \theta_{(i,p)}) b_l\left(t^{(i)}\right) f^{(k)}(s) ds \right| \\
&= \left| \sum_{k=1}^K \sum_{p=1}^P \sum_{l=1}^P b_l\left(t^{(i)}\right) \text{Cov}(\theta_{(k,l)}, \theta_{(i,p)}) \int_{\mathcal{T}} b_p(s) f^{(k)}(s) ds \right| \\
&\leq \left( \sum_{k=1}^K \sum_{p=1}^P \sum_{l=1}^P \left| b_l\left(t^{(i)}\right) \text{Cov}(\theta_{(k,l)}, \theta_{(i,p)}) \int_{\mathcal{T}} b_p(s) f^{(k)}(s) ds \right| \right) \\
&= \left( \sum_{k=1}^K \sum_{p=1}^P \sum_{l=1}^P \left| b_l\left(t^{(i)}\right) \right| \left| \text{Cov}(\theta_{(k,l)}, \theta_{(i,p)}) \right| \left| \int_{\mathcal{T}} b_p(s) f^{(k)}(s) ds \right| \right).
\end{aligned}$$

Using the  $R$  defined such that  $|b_j(s)| < R$  for all  $s \in \mathcal{T}$ , and condition (b), we have that

$$|(\mathcal{K}\mathbf{f})^{(i)}(\mathbf{t})| < \left( \sum_{k=1}^K \sum_{p=1}^P \sum_{l=1}^P R M \left| \int_{\mathcal{T}} b_p(s) f^{(k)}(s) ds \right| \right).$$

Using Hölder's Inequality, we have

$$\begin{aligned}
|(\mathcal{K}\mathbf{f})^{(i)}(\mathbf{t})| &< \left( \sum_{k=1}^K \sum_{p=1}^P \sum_{l=1}^P R M \left( \int_{\mathcal{T}} |b_p(s)|^2 ds \right)^{1/2} \left( \int_{\mathcal{T}} |f^{(k)}(s)|^2 ds \right)^{1/2} \right) \\
&< \left( \sum_{k=1}^K \sum_{p=1}^P \sum_{l=1}^P R M \left( \int_{\mathcal{T}} R^2 ds \right)^{1/2} \left( \int_{\mathcal{T}} |f^{(k)}(s)|^2 ds \right)^{1/2} \right).
\end{aligned}$$

Since  $\mathcal{K}$  is the direct sum of Hilbert spaces, we know that if  $\mathbf{f} \in \mathcal{B}_Z$ , then  $\|f^{(j)}\| < Z$  for all  $j$ , since  $\|\mathbf{f}\| = \sum_{j=1}^K \|f^{(j)}\|$ . Since  $\|f^{(j)}\| = \int_{\mathcal{T}} f^{(j)}(s)^2 ds = \int_{\mathcal{T}} |f^{(j)}(s)|^2 ds$ , we know that  $\int_{\mathcal{T}} |f^{(k)}(s)|^2 ds < Z$ . Thus, we have

$$\begin{aligned}
|(\mathcal{K}\mathbf{f})^{(i)}(\mathbf{t})| &< \left( \sum_{k=1}^K \sum_{p=1}^P \sum_{l=1}^P R M (R^2 B)^{1/2} (Z)^{1/2} \right) \\
&= K P^2 R^2 M B^{1/2} Z^{1/2} < \infty. \tag{28}
\end{aligned}$$

Since  $\|\mathcal{K}\mathbf{f}\|_{\mathcal{H}}^2 = \sum_{i=1}^K |(\mathcal{K}\mathbf{f})^{(i)}(\mathbf{t})|^2$ , we have that

$$\|\mathcal{K}\mathbf{f}\|_{\mathcal{H}}^2 < K^{3/2} P^2 R^2 M B^{1/2} Z^{1/2} < \infty.$$

Thus we know that  $\mathcal{K}\mathbf{f}_{\mathcal{B}_Z}$  is a bounded equicontinuous set of functions. Therefore, using Ascoli's Theorem (Reed and Simon (1972), page 30), we know that for every sequence  $\mathbf{f}_n \in \mathcal{B}_Z$ , the set  $\mathcal{K}\mathbf{f}_{\mathcal{B}_Z}$  has a subsequence that converges (Reed and Simon (1972), page 199). Therefore,  $\mathcal{K}\mathbf{f}_{\mathcal{B}_Z}$  is precompact, which implies that  $\mathcal{K}$  is compact.

We will now show that  $\mathcal{K}$  is a bounded operator. Let  $\mathbf{f} \in \mathcal{B}_Z$ . Thus, we have

$$\|\mathcal{K}\mathbf{f}\|_{\mathcal{H}}^2 = \sum_{i=1}^K \int_{\mathcal{T}} |(\mathcal{K}\mathbf{f})^{(i)}(\mathbf{t})|^2 dt.$$

From equation 28, we have that

$$\begin{aligned} \|\mathcal{K}\mathbf{f}\|_{\mathcal{H}}^2 &< \sum_{i=1}^K \int_{\mathcal{T}} \left( K P^2 R^2 M B^{1/2} Z^{1/2} \right)^2 dt \\ &= K^3 P^4 R^4 M^2 B Z \int_{\mathcal{T}} dt. \end{aligned}$$

Using the  $B$  defined above ( $\int_{\mathcal{T}} 1 dt < B$ ), we have that

$$\begin{aligned} \|\mathcal{K}\mathbf{f}\|_{\mathcal{H}}^2 &= K^3 P^4 R^4 M^2 B Z \int_{\mathcal{T}} 1 dt \\ &< K^3 P^4 R^4 M^2 B^2 Z < \infty \end{aligned}$$

Therefore we have that  $\mathcal{K}$  is a bounded linear operator. Therefore, if conditions (a) and (b) are met, then  $\mathcal{K}$  is a bounded and compact linear operator.

### A.3. Proof of Lemma 3.1

We will start by explicitly defining the functions  $\Lambda_i(\boldsymbol{\omega}_0, \boldsymbol{\omega})$ ,  $K_i(\boldsymbol{\omega}_0, \boldsymbol{\omega})$ , and  $V_i(\boldsymbol{\omega}_0, \boldsymbol{\omega})$ . Thus we have

$$\begin{aligned} \Lambda_i(\boldsymbol{\omega}_0, \boldsymbol{\omega}) &= \log \left( \frac{|(\boldsymbol{\Sigma}_i)_0|^{-1/2} \exp \left\{ -\frac{1}{2} (\mathbf{Y}_i - (\boldsymbol{\mu}_i)_0)' (\boldsymbol{\Sigma}_i)_0^{-1} (\mathbf{Y}_i - (\boldsymbol{\mu}_i)_0) \right\}}{|\boldsymbol{\Sigma}_i|^{-1/2} \exp \left\{ -\frac{1}{2} (\mathbf{Y}_i - \boldsymbol{\mu}_i)' (\boldsymbol{\Sigma}_i)^{-1} (\mathbf{Y}_i - \boldsymbol{\mu}_i) \right\}} \right) \\ &= -\frac{1}{2} [\log(|(\boldsymbol{\Sigma}_i)_0|) - \log(|\boldsymbol{\Sigma}_i|)] \\ &\quad - \frac{1}{2} \left[ (\mathbf{Y}_i - (\boldsymbol{\mu}_i)_0)' (\boldsymbol{\Sigma}_i)_0^{-1} (\mathbf{Y}_i - (\boldsymbol{\mu}_i)_0) - (\mathbf{Y}_i - \boldsymbol{\mu}_i)' (\boldsymbol{\Sigma}_i)^{-1} (\mathbf{Y}_i - \boldsymbol{\mu}_i) \right] \\ &= -\frac{1}{2} \left[ \sum_{l=1}^R \log((d_{il})_0 + \sigma_0^2) - \log(d_{il} + \sigma^2) \right] \\ &\quad - \frac{1}{2} \left[ (\mathbf{Y}_i - (\boldsymbol{\mu}_i)_0)' (\boldsymbol{\Sigma}_i)_0^{-1} (\mathbf{Y}_i - (\boldsymbol{\mu}_i)_0) - (\mathbf{Y}_i - \boldsymbol{\mu}_i)' (\boldsymbol{\Sigma}_i)^{-1} (\mathbf{Y}_i - \boldsymbol{\mu}_i) \right] \end{aligned} \tag{29}$$

$$\begin{aligned}
K_i(\boldsymbol{\omega}_0, \boldsymbol{\omega}) &= -\frac{1}{2} \left[ \sum_{l=1}^R \log \left( (d_{il})_0 + \sigma_0^2 \right) - \log \left( d_{il} + \sigma^2 \right) \right] \\
&\quad - \frac{1}{2} \mathbb{E}_{\boldsymbol{\omega}_0} \left[ (\mathbf{Y}_i - (\boldsymbol{\mu}_i)_0)' (\boldsymbol{\Sigma}_i)_0^{-1} (\mathbf{Y}_i - (\boldsymbol{\mu}_i)_0) - (\mathbf{Y}_i - \boldsymbol{\mu}_i)' (\boldsymbol{\Sigma}_i)^{-1} (\mathbf{Y}_i - \boldsymbol{\mu}_i) \right] \\
&= -\frac{1}{2} \left[ \sum_{l=1}^R \log \left( (d_{il})_0 + \sigma_0^2 \right) - \log \left( d_{il} + \sigma^2 \right) \right] \\
&\quad - \frac{1}{2} \left[ R - \left( \text{tr} (\boldsymbol{\Sigma}_i^{-1} (\boldsymbol{\Sigma}_i)_0) + ((\boldsymbol{\mu}_i)_0 - \boldsymbol{\mu}_i)' (\boldsymbol{\Sigma}_i)^{-1} ((\boldsymbol{\mu}_i)_0 - \boldsymbol{\mu}_i) \right) \right] \quad (30)
\end{aligned}$$

$$\begin{aligned}
V_i(\boldsymbol{\omega}_0, \boldsymbol{\omega}) &= \frac{1}{4} \text{Var}_{\boldsymbol{\omega}_0} \left[ (\mathbf{Y}_i - (\boldsymbol{\mu}_i)_0)' (\boldsymbol{\Sigma}_i)_0^{-1} (\mathbf{Y}_i - (\boldsymbol{\mu}_i)_0) - (\mathbf{Y}_i - \boldsymbol{\mu}_i)' (\boldsymbol{\Sigma}_i)^{-1} (\mathbf{Y}_i - \boldsymbol{\mu}_i) \right] \\
&= \frac{1}{4} \text{Var}_{\boldsymbol{\omega}_0} \left[ \mathbf{Y}_i' \left( (\boldsymbol{\Sigma}_i)_0^{-1} + \boldsymbol{\Sigma}_i^{-1} \right) \mathbf{Y}_i - 2 \mathbf{Y}_i' \left( (\boldsymbol{\Sigma}_i)_0^{-1} (\boldsymbol{\mu}_i)_0 + \boldsymbol{\Sigma}_i^{-1} \boldsymbol{\mu}_i \right) \right]
\end{aligned}$$

Letting  $\mathbf{M}_v = (\boldsymbol{\Sigma}_i)_0^{-1} + \boldsymbol{\Sigma}_i^{-1}$ , and  $\mathbf{m}_v = (\boldsymbol{\Sigma}_i)_0^{-1} (\boldsymbol{\mu}_i)_0 + \boldsymbol{\Sigma}_i^{-1} \boldsymbol{\mu}_i$ , we have

$$\begin{aligned}
V_i(\boldsymbol{\omega}_0, \boldsymbol{\omega}) &= \frac{1}{4} \text{Var}_{\boldsymbol{\omega}_0} \left[ (\mathbf{Y}_i - \mathbf{M}_v^{-1} \mathbf{m}_v)' \mathbf{M}_v (\mathbf{Y}_i - \mathbf{M}_v^{-1} \mathbf{m}_v) \right] \\
&= \frac{1}{4} \left[ 2 \text{tr} (\mathbf{M}_v (\boldsymbol{\Sigma}_i)_0 \mathbf{M}_v (\boldsymbol{\Sigma}_i)_0) + 4 ((\boldsymbol{\mu}_i)_0 - \mathbf{M}_v^{-1} \mathbf{m}_v)' (\boldsymbol{\Sigma}_i)_0 ((\boldsymbol{\mu}_i)_0 - \mathbf{M}_v^{-1} \mathbf{m}_v) \right] \\
&= \frac{1}{2} \left[ R + 2 \text{tr} (\boldsymbol{\Sigma}_i^{-1} (\boldsymbol{\Sigma}_i)_0) + \text{tr} (\boldsymbol{\Sigma}_i^{-1} (\boldsymbol{\Sigma}_i)_0 \boldsymbol{\Sigma}_i^{-1} (\boldsymbol{\Sigma}_i)_0) \right] \\
&\quad + ((\boldsymbol{\mu}_i)_0 - \boldsymbol{\mu}_i)' (\boldsymbol{\Sigma}_i^{-1} (\boldsymbol{\Sigma}_i)_0 \boldsymbol{\Sigma}_i^{-1}) ((\boldsymbol{\mu}_i)_0 - \boldsymbol{\mu}_i). \quad (31)
\end{aligned}$$

Let  $\boldsymbol{\Omega}_\epsilon(\boldsymbol{\omega}_0) = \{\boldsymbol{\omega} : K_i(\boldsymbol{\omega}_0, \boldsymbol{\omega}) < \epsilon \text{ for all } i\}$  for some  $\epsilon > 0$ . We will assume that  $\sigma_0^2 > 0$ . Consider the set  $\mathcal{B}(\boldsymbol{\omega}_0) = \{\boldsymbol{\omega} : \frac{1}{a}((d_{il})_0 + \sigma_0^2) \leq d_{il} + \sigma^2 \leq a((d_{il})_0 + \sigma_0^2), \|(\boldsymbol{\mu}_i)_0 - \boldsymbol{\mu}_i\| \leq b\}$  for some  $a, b \in \mathbb{R}$  such that  $a > 1$  and  $b > 0$ . Thus for a fixed  $\boldsymbol{\omega}_0 \in \boldsymbol{\Omega}$  and any  $\boldsymbol{\omega} \in \mathcal{C}(\boldsymbol{\omega}_0, \epsilon) := \mathcal{B}(\boldsymbol{\omega}_0) \cap \boldsymbol{\Omega}_\epsilon(\boldsymbol{\omega}_0)$ , we can bound  $V_i(\boldsymbol{\omega}_0, \boldsymbol{\omega})$ . We will let  $\lambda_r(\mathbf{A})$  denote the  $r^{th}$  eigenvalue of the matrix  $\mathbf{A}$ , and  $\lambda_{\max}(\mathbf{A})$  denote the largest eigenvalue of  $\mathbf{A}$ . Thus we have

$$\text{tr} (\boldsymbol{\Sigma}_i^{-1} (\boldsymbol{\Sigma}_i)_0) \leq R \lambda_{\max} (\boldsymbol{\Sigma}_i^{-1} (\boldsymbol{\Sigma}_i)_0) \leq \frac{Ra}{\sigma_0^2} \left( \max_l (d_{il} + \sigma_0^2) \right)$$

$$\text{tr} (\boldsymbol{\Sigma}_i^{-1} (\boldsymbol{\Sigma}_i)_0 \boldsymbol{\Sigma}_i^{-1} (\boldsymbol{\Sigma}_i)_0) \leq \text{tr} (\boldsymbol{\Sigma}_i^{-1} (\boldsymbol{\Sigma}_i)_0)^2 \leq \left( \frac{Ra}{\sigma_0^2} \left( \max_l (d_{il} + \sigma_0^2) \right) \right)^2$$

$$\begin{aligned}
((\boldsymbol{\mu}_i)_0 - \boldsymbol{\mu}_i)' (\boldsymbol{\Sigma}_i^{-1} (\boldsymbol{\Sigma}_i)_0 \boldsymbol{\Sigma}_i^{-1}) ((\boldsymbol{\mu}_i)_0 - \boldsymbol{\mu}_i) &\leq b^2 \lambda_{\max} (\boldsymbol{\Sigma}_i^{-1} (\boldsymbol{\Sigma}_i)_0 \boldsymbol{\Sigma}_i^{-1}) \\
&\leq \frac{a^2 b^2}{\sigma_0^4} \max_l (d_{il} + \sigma_0^2)
\end{aligned}$$

Thus we can see that for any  $\omega \in \mathcal{C}(\omega_0, \epsilon)$ ,

$$\begin{aligned} V_i(\omega_0, \omega) &\leq \frac{1}{2} \left[ R + 2 \left( \frac{Ra}{\sigma_0^2} \left( \max_l (d_{il} + \sigma_0^2) \right) \right) + \left( \frac{Ra}{\sigma_0^2} \left( \max_l (d_{il} + \sigma_0^2) \right) \right)^2 \right] \\ &\quad + \frac{a^2 b^2}{\sigma_0^4} \max_l (d_{il} + \sigma_0^2) \\ &= M_V. \end{aligned}$$

If we can bound  $\lambda_{\max}((d_{il})_0 + \sigma_0)$ , then we have that  $V_i(\omega_0, \omega)$  is bounded. Let  $\|\cdot\|_F$  be the Frobenius norm. Using the triangle inequality, we have

$$\begin{aligned} \|(\Sigma_i)_0\|_F &\leq \sum_{k=1}^K \sum_{j=1}^K \sum_{p=1}^{KP} Z_{ij} Z_{ik} \|\mathbf{S}'(\mathbf{t})(\phi_{kp})_0 (\phi_{jp})'_0 \mathbf{S}(\mathbf{t})\|_F + \sigma_0^2 \|\mathbf{I}_R\|_F \\ &\leq \sum_{k=1}^K \sum_{j=1}^K \sum_{p=1}^{KP} \|\mathbf{S}'(\mathbf{t})(\phi_{kp})_0 (\phi_{jp})'_0 \mathbf{S}(\mathbf{t})\|_F + \sigma_0^2 \|\mathbf{I}_R\|_F \\ &= \sum_{k=1}^K \sum_{j=1}^K \sum_{p=1}^{KP} \sqrt{\text{tr}(\mathbf{S}'(\mathbf{t})(\phi_{jp})_0 (\phi_{kp})'_0 \mathbf{S}(\mathbf{t}) \mathbf{S}'(\mathbf{t})(\phi_{kp})_0 (\phi_{jp})'_0 \mathbf{S}(\mathbf{t}))} + \sqrt{R} \sigma_0^2 \\ &= \sum_{k=1}^K \sum_{j=1}^K \sum_{p=1}^{KP} \sqrt{\text{tr}((\phi_{kp})'_0 \mathbf{S}(\mathbf{t}) \mathbf{S}'(\mathbf{t})(\phi_{kp})_0 (\phi_{jp})'_0 \mathbf{S}(\mathbf{t}) \mathbf{S}'(\mathbf{t})(\phi_{jp})_0)} + \sqrt{R} \sigma_0^2 \\ &= \sum_{k=1}^K \sum_{j=1}^K \sum_{p=1}^{KP} \|\mathbf{S}'(\mathbf{t})(\phi_{jp})_0\|_2 \|\mathbf{S}'(\mathbf{t})(\phi_{kp})_0\|_2 + \sqrt{R} \sigma_0^2 \\ &= M_{\Sigma_0} < \infty, \end{aligned}$$

for all  $i \in \mathbb{N}$ . Therefore, we know that  $\lambda_{\max}((d_{il})_0 + \sigma_0) \leq M_{\Sigma_0}$ , as the Frobenius is the squareroot of the sum of the squared eigenvalues for a square matrix. Therefore, we have for all  $i \in \mathbb{N}$  and  $\omega \in \mathcal{C}(\omega_0, \epsilon)$ , we have that

$$\frac{V_i(\omega_0, \omega)}{i^2} \leq \frac{M_V}{i^2}.$$

Since  $\sum_{i=1}^{\infty} \frac{1}{i^2} = \frac{\pi^2}{6}$ , we have that  $\sum_{i=1}^{\infty} \frac{M_V}{i^2} = \frac{M_V \pi^2}{6} < \infty$ . Thus we have

$$\sum_{i=1}^{\infty} \frac{V_i(\omega_0, \omega)}{i^2} < \infty. \quad (32)$$

We will next show that for  $\omega_0 \in \Omega$  and  $\epsilon > 0$ ,  $\Pi(\mathcal{C}(\omega_0), \epsilon) > 0$ . Fix  $\omega_0 \in \Omega$ . While the  $(\phi_{jp})_0$  may not be identifiable (for any orthogonal matrix  $\mathbf{H}$ ,  $(\phi_{jp})_0 \mathbf{H} \mathbf{H}' (\phi_{kp})_0 = (\phi_{jp})'_0 (\phi_{kp})_0$ ), let  $(\phi_{jp})_0$  be such that  $\sum_{p=1}^{KP} (\phi_{jp})'_0 (\phi_{kp})_0 = (\Sigma_{jk})_0$ . Thus we can define

the following sets:

$$\begin{aligned}\Omega_{\phi_{jp}} &= \{\phi_{jp} : (\phi_{jp})_0 \leq \phi_{jp} \leq (\phi_{jp})_0 + \epsilon_1 \mathbf{1}\} \\ \Omega_{\nu_k} &= \{\nu_k : (\nu_k)_0 \leq \nu_k \leq (\nu_k)_0 + \epsilon_2 \mathbf{1}\} \\ \Omega_{\sigma^2} &= \{\sigma^2 : \sigma_0^2 \leq \sigma^2 \leq (1 + \epsilon_1)\sigma_0^2\}.\end{aligned}$$

We define  $\epsilon_{1jp}$  and  $\epsilon_{2k}$  such that each element of  $\epsilon_{1jp}$  is between 0 and  $\epsilon_1$ , and each element of  $\epsilon_{2k}$  is between 0 and  $\epsilon_2$ . Therefore  $(\phi_{jp})_0 + \epsilon_{1jp} \in \Omega_{\phi_{jp}}$  and  $(\nu_k)_0 + \epsilon_{2k} \in \Omega_{\nu_k}$ . We will define

$$\Omega_{\Sigma_{jk}} := \left\{ \sum_{p=1}^{KP} \phi'_{jp} \phi_{kp} \mid \phi_{jp} \in \Omega_{\phi_{jp}}, \phi_{kp} \in \Omega_{\phi_{kp}} \right\}.$$

Thus for  $\Sigma_i$  such that  $\phi_{jp} \in \Omega_{\phi_{jp}}$  and  $\sigma^2 \in \Omega_{\sigma^2}$ , we have that

$$\begin{aligned}\Sigma_i &= \sum_{k=1}^K \sum_{j=1}^K Z_{ik} Z_{ij} \left( \mathbf{S}'(\mathbf{t}) \sum_{p=1}^{KP} \left( ((\phi_{kp})_0 + \epsilon_{1kp}) ((\phi_{jp})_0 + \epsilon_{1jp})' \right) \mathbf{S}(\mathbf{t}) \right) + (1 + \epsilon_\sigma) \sigma_0^2 \mathbf{I}_R \\ &= (\Sigma_i)_0 + \sum_{k=1}^K \sum_{j=1}^K \sum_{p=1}^{KP} Z_{ik} Z_{ij} (\mathbf{S}'(\mathbf{t}) ((\epsilon_{1kp}) (\phi_{jp})'_0) \mathbf{S}(\mathbf{t})) \\ &\quad + \sum_{k=1}^K \sum_{j=1}^K \sum_{p=1}^{KP} Z_{ik} Z_{ij} (\mathbf{S}'(\mathbf{t}) ((\phi_{kp})_0 (\epsilon_{1jp})') \mathbf{S}(\mathbf{t})) \\ &\quad + \sum_{k=1}^K \sum_{j=1}^K \sum_{p=1}^{KP} Z_{ik} Z_{ij} (\mathbf{S}'(\mathbf{t}) ((\epsilon_{1kp}) (\epsilon_{1jp})') \mathbf{S}(\mathbf{t})) + \epsilon_\sigma \sigma_0^2 \mathbf{I}_R \\ &= (\Sigma_i)_0 + \tilde{\Sigma}_i,\end{aligned}$$

for some  $\epsilon_{kp}$  and  $\epsilon_\sigma$  such that  $0 < \epsilon_\sigma \leq \epsilon_1$ . Thus, letting  $\zeta_{jkp} = (\mathbf{S}'(\mathbf{t}) ((\epsilon_{1kp}) (\phi_{jp})'_0) \mathbf{S}(\mathbf{t}) + \mathbf{S}'(\mathbf{t}) ((\phi_{kp})_0 (\epsilon_{1jp})') \mathbf{S}(\mathbf{t}))$ , we have

$$\begin{aligned}\|Z_{ik} Z_{ij} \zeta_{jkp}\|_F^2 &\leq \|\zeta_{jkp}\|_F^2 \\ &= \text{tr} (\mathbf{S}'(\mathbf{t}) ((\epsilon_{1kp}) (\phi_{jp})'_0) \mathbf{S}(\mathbf{t}) \mathbf{S}'(\mathbf{t}) ((\phi_{jp})_0 (\epsilon_{1kp})') \mathbf{S}(\mathbf{t})) \\ &\quad + \text{tr} (\mathbf{S}'(\mathbf{t}) ((\epsilon_{1kp}) (\phi_{jp})'_0) \mathbf{S}(\mathbf{t}) \mathbf{S}'(\mathbf{t}) ((\epsilon_{1jp}) (\phi_{kp})'_0) \mathbf{S}(\mathbf{t})) \\ &\quad + \text{tr} (\mathbf{S}'(\mathbf{t}) ((\phi_{kp})_0 (\epsilon_{1jp})') \mathbf{S}(\mathbf{t}) \mathbf{S}'(\mathbf{t}) ((\phi_{jp})_0 (\epsilon_{1kp})') \mathbf{S}(\mathbf{t})) \\ &\quad + \text{tr} (\mathbf{S}'(\mathbf{t}) ((\phi_{kp})_0 (\epsilon_{1jp})') \mathbf{S}(\mathbf{t}) \mathbf{S}'(\mathbf{t}) ((\epsilon_{1jp}) (\phi_{kp})'_0) \mathbf{S}(\mathbf{t})) \\ &\leq \epsilon_1^2 \text{tr} ((\phi_{jp})'_0 \mathbf{S}(\mathbf{t}) \mathbf{S}'(\mathbf{t}) (\phi_{jp})_0 (\mathbf{1})' \mathbf{S}(\mathbf{t}) \mathbf{S}'(\mathbf{t}) (\mathbf{1})) \\ &\quad + 2 \text{tr} ((\phi_{jp})'_0 \mathbf{S}(\mathbf{t}) \mathbf{S}'(\mathbf{t}) (\epsilon_{1jp}) (\phi_{kp})'_0 \mathbf{S}(\mathbf{t}) \mathbf{S}'(\mathbf{t}) (\epsilon_{1kp})) \\ &\quad + \epsilon_1^2 \text{tr} ((\mathbf{1})' \mathbf{S}(\mathbf{t}) \mathbf{S}'(\mathbf{t}) (\mathbf{1}) (\phi_{kp})'_0 \mathbf{S}(\mathbf{t}) \mathbf{S}'(\mathbf{t}) (\phi_{kp})_0).\end{aligned}\tag{33}$$

Using the Cauchy-Schwarz inequality, we can simplify equation 33, such that

$$\begin{aligned}
 (33) &= 2\langle \mathbf{S}'(\mathbf{t})(\phi_{jp})_0, \mathbf{S}'(\mathbf{t})\epsilon_{1jp} \rangle \langle \mathbf{S}'(\mathbf{t})(\phi_{kp})_0, \mathbf{S}'(\mathbf{t})\epsilon_{1kp} \rangle \\
 &\leq 2\|\mathbf{S}'(\mathbf{t})(\phi_{jp})_0\|_2\|\mathbf{S}'(\mathbf{t})\epsilon_{1jp}\|_2\|\mathbf{S}'(\mathbf{t})(\phi_{kp})_0\|_2\|\mathbf{S}'(\mathbf{t})\epsilon_{1kp}\|_2 \\
 &\leq 2\epsilon_1^2\|\mathbf{S}'(\mathbf{t})(\phi_{jp})_0\|_2\|\mathbf{S}'(\mathbf{t})\mathbf{1}\|_2\|\mathbf{S}'(\mathbf{t})(\phi_{kp})_0\|_2\|\mathbf{S}'(\mathbf{t})\mathbf{1}\|_2.
 \end{aligned}$$

Letting

$$\begin{aligned}
 \tilde{M}_{jkp} &= \|\mathbf{S}'(\mathbf{t})\mathbf{1}\|_2^2 [\|\mathbf{S}'(\mathbf{t})(\phi_{jp})_0\|_2^2 + \|\mathbf{S}'(\mathbf{t})(\phi_{kp})_0\|_2^2] \\
 &\quad + 2(\|\mathbf{S}'(\mathbf{t})(\phi_{jp})_0\|_2\|\mathbf{S}'(\mathbf{t})\mathbf{1}\|_2\|\mathbf{S}'(\mathbf{t})(\phi_{kp})_0\|_2\|\mathbf{S}'(\mathbf{t})\mathbf{1}\|_2),
 \end{aligned}$$

we have

$$\left\| Z_{ik}Z_{ij}\zeta_{jkp} \right\|_F^2 \leq \epsilon_1^2 \tilde{M}_{jkp}.$$

In a similar fashion, we can show that

$$\|Z_{ik}Z_{ij}(\mathbf{S}'(\mathbf{t})((\epsilon_{1kp})'(\epsilon_{1jp})')\mathbf{S}(\mathbf{t}))\|_F^2 \leq \epsilon_1^2\|\mathbf{S}'(\mathbf{t})\mathbf{1}\|_2^4$$

and

$$\|\epsilon_\sigma\sigma_0^2\mathbf{I}_R\|_F^2 \leq \epsilon_1^2\sigma_0^4R.$$

By using the triangle inequality we have

$$\|\tilde{\Sigma}_i\|_F \leq \epsilon_1 \left( \sum_{j=1}^K \sum_{k=1}^K \sum_{p=1}^{KP} \left( \sqrt{\tilde{M}_{jkp}} \right) + JK^2P\|\mathbf{S}'(\mathbf{t})\mathbf{1}\|_2^2 + \sigma_0^2\sqrt{R} \right) := \epsilon_1 M_{\Sigma} \quad (34)$$

for all  $i \in \mathbb{N}$ . By the Wielandt-Hoffman Theorem (Golub and Van Loan (2013) Theorem 8.1.4), we have that

$$\sum_{r=1}^R \left( \lambda_r \left( (\Sigma_i)_0 + \tilde{\Sigma}_i \right) - \lambda_r \left( (\Sigma_i)_0 \right) \right)^2 \leq \|\tilde{\Sigma}_i\|_F^2,$$

which implies that

$$\max_r \left| \lambda_r \left( (\Sigma_i)_0 + \tilde{\Sigma}_i \right) - \lambda_r \left( (\Sigma_i)_0 \right) \right| \leq \|\tilde{\Sigma}_i\|_F \quad (35)$$

where  $\lambda_r(\mathbf{A})$  are the eigenvalues of the matrix  $\mathbf{A}$ . By using equation 34, we can bound the log-determinant of the ratio of the two covariance matrices as follows

$$\begin{aligned}
 \log \left( \frac{|\Sigma_i|}{|(\Sigma_i)_0|} \right) &= \log \left( \frac{\prod_{r=1}^R \lambda_r \left( (\Sigma_i)_0 + \tilde{\Sigma}_i \right)}{\prod_{r=1}^R \lambda_r \left( (\Sigma_i)_0 \right)} \right) \\
 &\leq \log \left( \prod_{r=1}^R \frac{((d_{ir})_0 + \sigma_0^2) + \epsilon_1 M_{\Sigma}}{(d_{ir})_0 + \sigma_0^2} \right) \\
 &\leq R \log \left( 1 + \frac{\epsilon_1 M_{\Sigma}}{\sigma_0^2} \right).
 \end{aligned} \quad (36)$$

We can also bound  $\text{tr}(\Sigma_i^{-1}(\Sigma_i)_0)$ . To do this, we will first consider the spectral norm, defined as  $\|\mathbf{A}\|_2 = \sqrt{\mathbf{A}^*\mathbf{A}}$  for some matrix  $\mathbf{A}$ . In the case where  $\mathbf{A}$  is symmetric, we have that  $\|\mathbf{A}\|_2 = \max_r |\lambda_r(\mathbf{A})|$ . By the submultiplicative property of induced norms, we have that

$$\max_r |\lambda_r(\mathbf{AB})| = \|\mathbf{AB}\|_2 \leq \|\mathbf{A}\|_2 \|\mathbf{B}\|_2 = \max_r |\lambda_r(\mathbf{A})| \max_r |\lambda_r(\mathbf{B})|, \quad (37)$$

for two symmetric matrices  $\mathbf{A}$  and  $\mathbf{B}$ . By using the Sherman–Morrison–Woodbury formula, we can see that

$$\begin{aligned} \Sigma_i^{-1} &= \left( (\Sigma_i)_0 + \tilde{\Sigma}_i \right)^{-1} \\ &= (\Sigma_i)_0^{-1} - (\Sigma_i)_0^{-1} \tilde{\Sigma}_i \left( (\Sigma_i)_0 + \tilde{\Sigma}_i \right)^{-1}. \end{aligned}$$

Thus, we have that

$$\Sigma_i^{-1}(\Sigma_i)_0 = \mathbf{I}_R - (\Sigma_i)_0^{-1} \tilde{\Sigma}_i \left( (\Sigma_i)_0 + \tilde{\Sigma}_i \right)^{-1} (\Sigma_i)_0. \quad (38)$$

Using equation 37, we would like to bound the magnitude of the eigenvalues of  $(\Sigma_i)_0^{-1} \tilde{\Sigma}_i \left( (\Sigma_i)_0 + \tilde{\Sigma}_i \right)^{-1} (\Sigma_i)_0$ . We know that

$$\max_r \left| \lambda_r \left( \left( (\Sigma_i)_0 + \tilde{\Sigma}_i \right)^{-1} \right) \right| \leq \frac{1}{\sigma_0^2}$$

and

$$\max_r \left| \lambda_r(\tilde{\Sigma}_i) \right| \leq \epsilon_1 M_{\Sigma},$$

with the second inequality coming from equation 34. From equation 38 and basic properties of the trace, we have that

$$\begin{aligned} \text{tr}(\Sigma_i^{-1}(\Sigma_i)_0) &= \text{tr} \left( \mathbf{I}_R - (\Sigma_i)_0^{-1} \tilde{\Sigma}_i \left( (\Sigma_i)_0 + \tilde{\Sigma}_i \right)^{-1} (\Sigma_i)_0 \right) \\ &= \text{tr}(\mathbf{I}_R) - \text{tr} \left( \tilde{\Sigma}_i \left( (\Sigma_i)_0 + \tilde{\Sigma}_i \right)^{-1} (\Sigma_i)_0 (\Sigma_i)_0^{-1} \right) \\ &= \text{tr}(\mathbf{I}_R) - \text{tr} \left( \tilde{\Sigma}_i \left( (\Sigma_i)_0 + \tilde{\Sigma}_i \right)^{-1} \right) \end{aligned}$$

Thus, using the fact that the trace of a matrix is the sum of its eigenvalues, we have that

$$\text{tr}(\Sigma_i^{-1}(\Sigma_i)_0) \leq R + R \max_r \left| \lambda_r \left( \tilde{\Sigma}_i \left( (\Sigma_i)_0 + \tilde{\Sigma}_i \right)^{-1} \right) \right|.$$

Using the submultiplicative property stated in equation 37, we have

$$\text{tr}(\Sigma_i^{-1}(\Sigma_i)_0) \leq R + \frac{R \epsilon_1 M_{\Sigma}}{\sigma_0^2}. \quad (39)$$

Lastly, we can bound the quadratic term in  $K_i(\boldsymbol{\omega}_0, \boldsymbol{\omega})$  in the following way:

$$\begin{aligned}
((\boldsymbol{\mu}_i)_0 - \boldsymbol{\mu}_i)' (\boldsymbol{\Sigma}_i)^{-1} ((\boldsymbol{\mu}_i)_0 - \boldsymbol{\mu}_i) &\leq \|(\boldsymbol{\mu}_i)_0 - \boldsymbol{\mu}_i\|_2^2 \max_r \lambda_r((\boldsymbol{\Sigma}_i)^{-1}) \\
&\leq \frac{1}{\sigma^2} \sum_{k=1}^K \|\mathbf{S}'(\mathbf{t})(\boldsymbol{\nu}_k)_0 - \mathbf{S}'(\mathbf{t})\boldsymbol{\nu}_k\|_2^2 \\
&= \frac{1}{\sigma^2} \sum_{k=1}^K \boldsymbol{\epsilon}'_{2k} \mathbf{S}(\mathbf{t}) \mathbf{S}'(\mathbf{t}) \boldsymbol{\epsilon}_{2k} \\
&\leq \frac{KR\epsilon_2^2}{\sigma_0^2} \lambda_{\mathbf{S}(\mathbf{t})}^{\max}, \tag{40}
\end{aligned}$$

where  $\lambda_{\mathbf{S}(\mathbf{t})}^{\max}$  is the maximum eigenvalue of the matrix  $\mathbf{S}(\mathbf{t})\mathbf{S}'(\mathbf{t})$ . Thus letting

$$\epsilon_1 < \min \left\{ \frac{\sigma_0^2}{M_{\boldsymbol{\Sigma}}} \left( \exp \left( \frac{2\epsilon}{3R} \right) - 1 \right), \frac{2\epsilon\sigma_0^2}{3RM_{\boldsymbol{\Sigma}}} \right\} \tag{41}$$

and

$$\epsilon_2 < \sqrt{\frac{2\sigma_0^2\epsilon}{3KR\lambda_{\mathbf{S}(\mathbf{t})}^{\max}}}, \tag{42}$$

we have from equations 36, 39, and 40 that

$$K_i(\boldsymbol{\omega}_0, \boldsymbol{\omega}) < \epsilon \text{ for all } \boldsymbol{\omega} \in \boldsymbol{\Omega}_1$$

where  $\boldsymbol{\Omega}_1 := \left( \times_{j=1}^K \times_{k=1}^K \boldsymbol{\Omega}_{\boldsymbol{\Sigma}_{jk}} \right) \times \left( \times_{k=1}^K \boldsymbol{\Omega}_{\boldsymbol{\nu}_k} \right) \times \boldsymbol{\Omega}_{\sigma^2}$ . Letting  $a > \max \left\{ 1 + \frac{\epsilon_1 M_{\boldsymbol{\Sigma}}}{\sigma_0^2}, \left( 1 - \frac{\epsilon_1 M_{\boldsymbol{\Sigma}}}{\sigma_0^2} \right)^{-1} \right\}$

and  $b > \sqrt{KR\epsilon_2^2\lambda_{\mathbf{S}(\mathbf{t})}^{\max}}$  in the definition of  $\mathcal{C}(\boldsymbol{\omega}_0, \epsilon)$ , we have that  $\boldsymbol{\Omega}_1 \subset \mathcal{C}(\boldsymbol{\omega}_0, \epsilon)$ . Let  $H_{\boldsymbol{\phi}}$  be the set of hyper-parameters corresponding to the  $\boldsymbol{\phi}$  parameters, and let  $\boldsymbol{\Pi}(\boldsymbol{\eta}_{\boldsymbol{\phi}})$  be the prior distribution on  $\boldsymbol{\eta}_{\boldsymbol{\phi}} \in H_{\boldsymbol{\phi}}$ . Thus we have that

$$\begin{aligned}
\boldsymbol{\Pi}(\boldsymbol{\omega} \in \mathcal{C}(\boldsymbol{\omega}_0, \epsilon)) &\geq \int_{H_{\boldsymbol{\phi}}} \prod_{j=1}^K \prod_{p=1}^{KP} \prod_{r=1}^P \int_{(\phi_{jrp})_0}^{(\phi_{jrp})_0 + \epsilon_1} \sqrt{\frac{\gamma_{jrp}\tilde{\tau}_{pj}}{2\pi}} \exp \left\{ -\frac{\gamma_{jrp}\tilde{\tau}_{pj}}{2} \phi_{jrp}^2 \right\} d\phi_{jrp} d\boldsymbol{\Pi}(\boldsymbol{\eta}_{\boldsymbol{\phi}}) \\
&\times \prod_{k=1}^K \int_0^\infty \int_{(\boldsymbol{\nu}_k)_0}^{(\boldsymbol{\nu}_k)_0 + \epsilon_2 \mathbf{1}} \left( \frac{\tau_k}{2\pi} \right)^{P/2} |\mathbf{P}|^{-1/2} \exp \left\{ \frac{\tau_k}{2} \boldsymbol{\nu}'_k \mathbf{P} \boldsymbol{\nu}_k \right\} d\boldsymbol{\nu}_k d\boldsymbol{\Pi}(\tau_k) \\
&\times \int_{\sigma_0^2}^{(1+\epsilon_1)\sigma_0^2} \frac{\beta_0^{\alpha_0}}{\Gamma(\alpha_0)} (\sigma^2)^{-\alpha_0-1} \exp \left\{ -\frac{\beta_0}{\sigma^2} \right\} d\sigma^2.
\end{aligned}$$

Restricting the hyper-parameters of  $\boldsymbol{\phi}$  to only a subset of the support, say  $\tilde{H}_{\boldsymbol{\phi}}$ , where

$$\tilde{H}_{\boldsymbol{\phi}} = \left\{ \boldsymbol{\eta}_{\boldsymbol{\phi}} : \frac{1}{10} \leq \gamma_{jrp} \leq 10, 1 \leq \delta_{pj} \leq 2, 1 \leq a_{1j} \leq 10, 1 \leq a_{2j} \leq 10 \right\},$$

we can see that there exists a  $M_{\phi_{jrp}} > 0$  such that

$$\sqrt{\frac{\gamma_{jrp}\tilde{\tau}_{pj}}{2\pi}} \exp \left\{ -\frac{\gamma_{jrp}\tilde{\tau}_{pj}}{2} \phi_{jrp}^2 \right\} \geq M_{\phi_{jrp}},$$

for all  $\phi_{jrp} \in [(\phi_{jrp})_0, (\phi_{jrp})_0 + \epsilon_1]$ . Similarly, we can find a lower bound  $M_{\tilde{H}_\phi} > 0$ , such that

$$\int_{\tilde{H}_\phi} d(\boldsymbol{\eta}_\phi) \geq M_{\tilde{H}_\phi}.$$

Similarly, if we bound  $\tau_k$  such that  $\frac{1}{10} \leq \tau_k \leq 10$ , it is easy to see that there exists constants  $M_{\boldsymbol{\nu}_k}, M_{\tau_k}, M_{\sigma^2} > 0$  such that

$$\left(\frac{\tau_k}{2\pi}\right)^{P/2} |\mathbf{P}|^{-1/2} \exp\left\{\frac{\tau_k}{2} \boldsymbol{\nu}'_k \mathbf{P} \boldsymbol{\nu}_k\right\} \geq M_{\boldsymbol{\nu}_k},$$

for all  $\boldsymbol{\nu}_k \in [(\boldsymbol{\nu}_k)_0, (\boldsymbol{\nu}_k)_0 + \epsilon_2 \mathbf{1}]$ ,

$$\int_{\frac{1}{10}}^{10} \boldsymbol{\Pi}(\tau_k) \geq M_{\tau_k},$$

and

$$\frac{\beta_0^{\alpha_0}}{\Gamma(\alpha_0)} (\sigma^2)^{-\alpha_0-1} \exp\left\{-\frac{\beta_0}{\sigma^2}\right\} \geq M_{\sigma^2}$$

for all  $\sigma^2 \in [\sigma_0^2, (1 + \epsilon_1)\sigma_0^2]$ . Therefore we have that

$$\begin{aligned} \boldsymbol{\Pi}(\boldsymbol{\omega} \in \mathcal{C}(\boldsymbol{\omega}_0, \epsilon)) &\geq M_{\tilde{H}_\phi} \prod_{j=1}^K \prod_{p=1}^{KP} \prod_{r=1}^P \epsilon_1 M_{\phi_{jrp}} \\ &\times \prod_{k=1}^K M_{\tau_k} \epsilon_2^P M_{\boldsymbol{\nu}_k} \\ &\times \epsilon_1 \sigma_0^2 M_{\sigma_0^2} \\ &> 0. \end{aligned}$$

Therefore, for  $\epsilon > 0$ , there exists  $a$  and  $b$  such that  $\sum_{i=1}^{\infty} \frac{V_i(\boldsymbol{\omega}_0, \boldsymbol{\omega})}{i^2} < \infty$  for any  $\boldsymbol{\omega} \in \mathcal{C}(\boldsymbol{\omega}_0, \epsilon)$  and  $\boldsymbol{\Pi}(\boldsymbol{\omega} \in \mathcal{C}(\boldsymbol{\omega}_0, \epsilon)) > 0$ .

#### A.4. Proof of Lemma 3.2

Following the notation of Ghosal and Van der Vaart (2017), we will let  $P_{\boldsymbol{\omega}_0}^{(N)}$  denote the joint distribution of  $\mathbf{Y}_1, \dots, \mathbf{Y}_N$  at  $\boldsymbol{\omega}_0 \in \boldsymbol{\Omega}$ . In order to show that the posterior distribution,  $\boldsymbol{\Pi}_N(\cdot | \mathbf{Y}_1, \dots, \mathbf{Y}_N)$ , is weakly consistent at  $\boldsymbol{\omega}_0 \in \boldsymbol{\Omega}$ , we need to show that  $\boldsymbol{\Pi}_N(\mathcal{U}^c | \mathbf{Y}_1, \dots, \mathbf{Y}_N) \rightarrow 0$  a.s.  $[P_{\boldsymbol{\omega}_0}]$  for every weak neighborhood,  $\mathcal{U}$  of  $\boldsymbol{\omega}_0$ . Following a similar notation to Ghosal and Van der Vaart (2017), let  $\psi_N$  be measurable mappings,  $\psi_N : \mathcal{S}^N \times \mathcal{Z}^N \rightarrow [0, 1]$ , where  $\mathcal{Z}$  is the sample space of  $\{Z_{i1}, \dots, Z_{iK}\}$ . Let  $\psi_N(\mathbf{Y}_1, \dots, \mathbf{Y}_N, \mathbf{z}_1, \dots, \mathbf{z}_N)$  be the corresponding test function, and  $P_{\boldsymbol{\omega}}^N \psi_N = \mathbb{E}_{P_{\boldsymbol{\omega}}^N} \psi_N(\mathbf{Y}_1, \dots, \mathbf{Y}_N, \mathbf{z}_1, \dots, \mathbf{z}_N) = \int \psi_N dP_{\boldsymbol{\omega}}^N$ , where  $P_{\boldsymbol{\omega}}^N$  denotes the joint distribution on  $\mathbf{Y}_1, \dots, \mathbf{Y}_N$  with parameters  $\boldsymbol{\omega}$ . Suppose there exists tests  $\psi_N$  such that  $P_{\boldsymbol{\omega}_0}^N \psi_N \rightarrow 0$ , and  $\sup_{\boldsymbol{\omega} \in \mathcal{U}^c} P_{\boldsymbol{\omega}}^N (1 - \psi_N) \rightarrow 0$ . Since  $\psi_N(\mathbf{Y}_1, \dots, \mathbf{Y}_N, \mathbf{z}_1, \dots, \mathbf{z}_N) \in [0, 1]$ ,

we have that

$$\begin{aligned}\mathbf{\Pi}_n(U^c|\mathbf{Y}_1, \dots, \mathbf{Y}_N) &\leq \mathbf{\Pi}_n(U^c|\mathbf{Y}_1, \dots, \mathbf{Y}_N) + \psi_N(\mathbf{Y}_1, \dots, \mathbf{Y}_N)(1 - \mathbf{\Pi}_n(U^c|\mathbf{Y}_1, \dots, \mathbf{Y}_N)) \\ &= \psi_N(\mathbf{Y}_1, \dots, \mathbf{Y}_N) + \frac{(1 - \psi_N(\mathbf{Y}_1, \dots, \mathbf{Y}_N)) \int_{U^c} \prod_{i=1}^N \frac{f_i(\mathbf{Y}_i; \boldsymbol{\omega})}{f_i(\mathbf{Y}_i; \boldsymbol{\omega}_0)} d\mathbf{\Pi}(\boldsymbol{\omega})}{\int_{\Omega} \prod_{i=1}^N \frac{f_i(\mathbf{Y}_i; \boldsymbol{\omega})}{f_i(\mathbf{Y}_i; \boldsymbol{\omega}_0)} d\mathbf{\Pi}(\boldsymbol{\omega})}.\end{aligned}\quad (43)$$

To show that  $\mathbf{\Pi}_n(U^c|\mathbf{Y}_1, \dots, \mathbf{Y}_N) \rightarrow 0$ , it is sufficient to show the following three conditions:

- (a)  $\psi_N(\mathbf{Y}_1, \dots, \mathbf{Y}_N, \mathbf{z}_1, \dots, \mathbf{z}_N) \rightarrow 0$  a.s.  $[P_{\boldsymbol{\omega}_0}]$ ,
- (b)  $e^{\beta_1 N} (1 - \psi_N(\mathbf{Y}_1, \dots, \mathbf{Y}_N, \mathbf{z}_1, \dots, \mathbf{z}_N)) \int_{U^c} \prod_{i=1}^N \frac{f_i(\mathbf{Y}_i; \boldsymbol{\omega})}{f_i(\mathbf{Y}_i; \boldsymbol{\omega}_0)} d\mathbf{\Pi}(\boldsymbol{\omega}) \rightarrow 0$  a.s.  $[P_{\boldsymbol{\omega}_0}]$  for some  $\beta_1 > 0$ ,
- (c)  $e^{\beta N} \left( \int_{\Omega} \prod_{i=1}^N \frac{f_i(\mathbf{Y}_i; \boldsymbol{\omega})}{f_i(\mathbf{Y}_i; \boldsymbol{\omega}_0)} d\mathbf{\Pi}(\boldsymbol{\omega}) \right) \rightarrow \infty$  a.s.  $[P_{\boldsymbol{\omega}_0}]$  for all  $\beta > 0$ .

We will start by proving (c). Fix  $\beta > 0$ . Thus we have

$$e^{\beta N} \left( \int_{\Omega} \prod_{i=1}^N \frac{f_i(\mathbf{Y}_i; \boldsymbol{\omega})}{f_i(\mathbf{Y}_i; \boldsymbol{\omega}_0)} d\mathbf{\Pi}(\boldsymbol{\omega}) \right) = e^{\beta N} \left( \int_{\Omega} \exp \left[ - \sum_{i=1}^N \log \left( \frac{f_i(\mathbf{Y}_i; \boldsymbol{\omega}_0)}{f_i(\mathbf{Y}_i; \boldsymbol{\omega})} \right) \right] d\mathbf{\Pi}(\boldsymbol{\omega}) \right).$$

By Fatou's lemma, we have

$$\begin{aligned}\liminf_{N \rightarrow \infty} \int_{\Omega} \exp \left[ \beta N - \sum_{i=1}^N \log \left( \frac{f_i(\mathbf{Y}_i; \boldsymbol{\omega}_0)}{f_i(\mathbf{Y}_i; \boldsymbol{\omega})} \right) \right] d\mathbf{\Pi}(\boldsymbol{\omega}) \\ \geq \int_{\Omega} \liminf_{N \rightarrow \infty} \exp \left[ \beta N - \sum_{i=1}^N \log \left( \frac{f_i(\mathbf{Y}_i; \boldsymbol{\omega}_0)}{f_i(\mathbf{Y}_i; \boldsymbol{\omega})} \right) \right] d\mathbf{\Pi}(\boldsymbol{\omega})\end{aligned}$$

Let  $\beta > \epsilon > 0$  and  $a, b > 0$  be defined such that lemma 3.1 holds. Since  $\mathcal{C}(\boldsymbol{\omega}_0, \epsilon) \subset \Omega$ , we have that

$$\begin{aligned}\int_{\Omega} \liminf_{N \rightarrow \infty} \exp \left[ \beta N - \sum_{i=1}^N \log \left( \frac{f_i(\mathbf{Y}_i; \boldsymbol{\omega}_0)}{f_i(\mathbf{Y}_i; \boldsymbol{\omega})} \right) \right] d\mathbf{\Pi}(\boldsymbol{\omega}) \\ \geq \int_{\mathcal{C}(\boldsymbol{\omega}_0, \epsilon)} \liminf_{N \rightarrow \infty} \exp \left[ \beta N - \sum_{i=1}^N \log \left( \frac{f_i(\mathbf{Y}_i; \boldsymbol{\omega}_0)}{f_i(\mathbf{Y}_i; \boldsymbol{\omega})} \right) \right] d\mathbf{\Pi}(\boldsymbol{\omega})\end{aligned}$$

By Kolmogorov's strong law of large numbers for non-identically distributed random variables, we have that

$$\frac{1}{N} \sum_{i=1}^N (\Lambda_i(\boldsymbol{\omega}_0, \boldsymbol{\omega}) - K_i(\boldsymbol{\omega}_0, \boldsymbol{\omega})) \rightarrow 0$$

a.s.  $[P_{\boldsymbol{\omega}_0}]$ . Thus for each  $\boldsymbol{\omega} \in \mathcal{C}(\boldsymbol{\omega}_0, \epsilon)$ , with  $P_{\boldsymbol{\omega}_0}$ -probability 1,

$$\frac{1}{N} \sum_{i=1}^N \Lambda_i(\boldsymbol{\omega}_0, \boldsymbol{\omega}) \rightarrow \mathbb{E}(\overline{K_i(\boldsymbol{\omega}_0, \boldsymbol{\omega})}) < \epsilon < B,$$

since  $\omega \in \mathcal{C}(\omega_0, \epsilon)$ . Therefore, we have that

$$\int_{\mathcal{C}(\omega_0, \epsilon)} \liminf_{N \rightarrow \infty} \exp \left[ \beta N - \sum_{i=1}^N \log \left( \frac{f_i(\mathbf{Y}_i; \omega_0)}{f_i(\mathbf{Y}_i; \omega)} \right) \right] d\Pi(\omega) \geq \int_{\mathcal{C}(\omega_0, \epsilon)} \inf_{N \rightarrow \infty} \exp \{N(\beta - \epsilon)\} d\Pi(\omega).$$

Since  $\beta - \epsilon > 0$ , and  $\Pi(\theta \in \mathcal{C}(\omega_0, \epsilon)) > 0$  (lemma 3.1), we have that

$$e^{\beta N} \left( \int_{\Omega} \prod_{i=1}^N \frac{f_i(\mathbf{Y}_i; \omega)}{f_i(\mathbf{Y}_i; \omega_0)} d\Pi(\omega) \right) \rightarrow \infty \quad (44)$$

a.s.  $[P_{\omega_0}]$  for all  $\beta > 0$ . We will now show that exists measurable mappings such that  $P_{\omega_0}^N \psi_N \rightarrow 0$  and  $\sup_{\omega \in \mathcal{U}^c} P_{\omega}^N (1 - \psi_N) \rightarrow 0$ . Consider weak neighborhoods  $\mathcal{U}$  of  $\omega_0$  of the form

$$\mathcal{U} = \left\{ \omega : \left| \int f_i dP_{\omega} - \int f_i dP_{\omega_0} \right| < \epsilon_i, \quad i = 1, 2, \dots, r \right\}, \quad (45)$$

where  $r \in \mathbb{N}$ ,  $\epsilon_i > 0$ , and  $f_i$  are continuous functions such that  $f_i : \mathcal{S} \times \mathcal{Z} \rightarrow [0, 1]$ . As shown in Ghosh and Ramamoorthi (2003), for any particular  $f_i$  and  $\epsilon_i > 0$ ,  $|\int f_i dP_{\omega} - \int f_i dP_{\omega_0}| < \epsilon_i$  iff  $\int f_i dP_{\omega} - \int f_i dP_{\omega_0} < \epsilon_i$  and  $\int (1 - f_i) dP_{\omega} - \int (1 - f_i) dP_{\omega_0} < \epsilon_i$ . Since  $\tilde{f}_i := (1 - f_i)$  is still a continuous function such that  $\tilde{f}_i : \mathcal{S} \times \mathcal{Z} \rightarrow [0, 1]$ , we can rewrite equation 45 as

$$\mathcal{U} = \cap_{i=1}^{2r} \left\{ \omega : \int g_i dP_{\omega} - \int g_i dP_{\omega_0} < \epsilon_i \right\}, \quad (46)$$

where  $g_i$  are continuous functions such that  $g_i : \mathcal{S} \times \mathcal{Z} \rightarrow [0, 1]$  and  $\epsilon_i > 0$ . Following Ghosal and Van der Vaart (2017), it can be shown by Hoeffding's inequality that using the test function  $\tilde{\psi}$ , defined as

$$\tilde{\psi}_{iN}(\mathbf{Y}_1, \dots, \mathbf{Y}_N, \mathbf{z}_1, \dots, \mathbf{z}_N) := \mathbb{1} \left\{ \frac{1}{N} \sum_{j=1}^N g_i(\mathbf{Y}_j, \mathbf{z}_j) > \int g_i dP_{\omega_0} + \frac{\epsilon_i}{2} \right\}, \quad (47)$$

leads to

$$\int \tilde{\psi}_{iN}(\mathbf{Y}_1, \dots, \mathbf{Y}_N, \mathbf{z}_1, \dots, \mathbf{z}_N) dP_{\omega_0} \leq e^{-N\epsilon_i^2/2}$$

and

$$\int (1 - \tilde{\psi}_{iN}(\mathbf{Y}_1, \dots, \mathbf{Y}_N, \mathbf{z}_1, \dots, \mathbf{z}_N)) dP_{\omega} \leq e^{-N\epsilon_i^2/2}$$

for any  $\omega \in \mathcal{U}^c$ . Let  $\psi_n = \max_i \tilde{\psi}_{iN}$  be our test function and  $\epsilon = \min_i \epsilon_i$ . Using the fact that  $\mathbb{E}(\max_i \tilde{\psi}_{iN}) \leq \sum_i \mathbb{E}(\tilde{\psi}_{iN})$  and  $\mathbb{E}(1 - \max_i \tilde{\psi}_{iN}) \leq \mathbb{E}(1 - \tilde{\psi}_{iN})$ , we have

$$\int \psi_N(\mathbf{Y}_1, \dots, \mathbf{Y}_N, \mathbf{z}_1, \dots, \mathbf{z}_N) dP_{\omega_0} \leq (2r) e^{-N\epsilon^2/2} \quad (48)$$

and

$$\int (1 - \psi_N(\mathbf{Y}_1, \dots, \mathbf{Y}_N, \mathbf{z}_1, \dots, \mathbf{z}_N)) dP_{\omega} \leq e^{-N\epsilon^2/2}, \quad (49)$$

for any  $\omega \in \mathcal{U}^c$ . Using Markov's inequality on equation 48, we have that

$$\begin{aligned} P(\psi_N(\mathbf{Y}_1, \dots, \mathbf{Y}_N, \mathbf{z}_1, \dots, \mathbf{z}_N) \geq e^{-nC}) &\leq \frac{\mathbb{E}(\psi_N(\mathbf{Y}_1, \dots, \mathbf{Y}_N, \mathbf{z}_1, \dots, \mathbf{z}_N))}{e^{-nC}} \\ &\leq (2r)e^{-N(\epsilon^2/2-C)} \end{aligned}$$

Thus letting  $C < \epsilon^2/2$ , we have that  $\sum_{N=1}^{\infty} P(\psi_N(\mathbf{Y}_1, \dots, \mathbf{Y}_N, \mathbf{z}_1, \dots, \mathbf{z}_N) \geq e^{-nC}) < \infty$ . Thus by the Borel-Cantelli lemma, we know that

$$P\left(\limsup_{N \rightarrow \infty} P(\psi_N(\mathbf{Y}_1, \dots, \mathbf{Y}_N, \mathbf{z}_1, \dots, \mathbf{z}_N) \geq e^{-nC})\right) = 0$$

Thus we have that  $\psi_N(\mathbf{Y}_1, \dots, \mathbf{Y}_N, \mathbf{z}_1, \dots, \mathbf{z}_N) \rightarrow 0$  a.s.  $[P_{\omega_0}]$  (Condition (a)). To prove condition (b), we will first start by taking the expectation with respect to  $P_{\omega_0}$ :

$$\begin{aligned} &\mathbb{E}_{P_{\omega_0}^N} \left( e^{\beta N} (1 - \psi_N(\mathbf{Y}_1, \dots, \mathbf{Y}_N, \mathbf{z}_1, \dots, \mathbf{z}_N)) \int_{\mathcal{U}^c} \prod_{i=1}^N \frac{f_i(\mathbf{Y}_i; \omega)}{f_i(\mathbf{Y}_i; \omega_0)} d\Pi(\omega) \right) \\ &= \int_{\mathcal{S}^N} \left( e^{\beta N} (1 - \psi_N(\mathbf{Y}_1, \dots, \mathbf{Y}_N, \mathbf{z}_1, \dots, \mathbf{z}_N)) \int_{\mathcal{U}^c} \prod_{i=1}^N \frac{f_i(\mathbf{Y}_i; \omega)}{f_i(\mathbf{Y}_i; \omega_0)} d\Pi(\omega) \right) dP_{\omega_0}^N \\ &= \int_{\mathcal{U}^c} \left( \prod_{i=1}^N \int_{\mathcal{S}} e^{\beta N} (1 - \psi_N(\mathbf{Y}_1, \dots, \mathbf{Y}_N, \mathbf{z}_1, \dots, \mathbf{z}_N)) f_i(\mathbf{Y}_i; \omega) d\mathbf{Y}_i \right) d\Pi(\omega) \\ &= e^{\beta N} \int_{\mathcal{U}^c} \mathbb{E}_{P_{\omega}^N} (1 - \psi_N(\mathbf{Y}_1, \dots, \mathbf{Y}_N, \mathbf{z}_1, \dots, \mathbf{z}_N)) d\Pi(\omega) \\ &\leq e^{\beta_1 N} e^{-N\epsilon^2/2}, \end{aligned}$$

where the last inequality is from equation 49. Thus by Markov's inequality and letting  $\beta_1 < \epsilon^2/2$ , we have that

$$\begin{aligned} &P\left(e^{\beta N} (1 - \psi_N(\mathbf{Y}_1, \dots, \mathbf{Y}_N, \mathbf{z}_1, \dots, \mathbf{z}_N)) \int_{\mathcal{U}^c} \prod_{i=1}^N \frac{f_i(\mathbf{Y}_i; \omega)}{f_i(\mathbf{Y}_i; \omega_0)} d\Pi(\omega) \geq e^{-N((\epsilon^2/2-\beta_1)/2)}\right) \\ &\leq \frac{\mathbb{E}_{P_{\omega_0}^N} \left( e^{\beta N} (1 - \psi_N(\mathbf{Y}_1, \dots, \mathbf{Y}_N, \mathbf{z}_1, \dots, \mathbf{z}_N)) \int_{\mathcal{U}^c} \prod_{i=1}^N \frac{f_i(\mathbf{Y}_i; \omega)}{f_i(\mathbf{Y}_i; \omega_0)} d\Pi(\omega) \right)}{e^{-N((\epsilon^2/2-\beta_1)/2)}} \\ &\leq e^{-N((\epsilon^2/2-\beta_1)/2)} \end{aligned}$$

Letting  $E_N$  be the event that  $e^{\beta N} (1 - \psi_N(\mathbf{Y}_1, \dots, \mathbf{Y}_N, \mathbf{z}_1, \dots, \mathbf{z}_N)) \int_{\mathcal{U}^c} \prod_{i=1}^N \frac{f_i(\mathbf{Y}_i; \omega)}{f_i(\mathbf{Y}_i; \omega_0)} d\Pi(\omega) \geq e^{-N((\epsilon^2/2-\beta_1)/2)}$ , we have that  $\sum_{i=1}^{\infty} P(E_N) < \infty$ . Thus by the Borel-Cantelli lemma, we have that

$$e^{\beta N} (1 - \psi_N(\mathbf{Y}_1, \dots, \mathbf{Y}_N, \mathbf{z}_1, \dots, \mathbf{z}_N)) \int_{\mathcal{U}^c} \prod_{i=1}^N \frac{f_i(\mathbf{Y}_i; \omega)}{f_i(\mathbf{Y}_i; \omega_0)} d\Pi(\omega) \rightarrow 0$$

a.s.  $[P_{\omega_0}]$  for  $0 < \beta_1 < \epsilon^2/2$ . Therefore, we have proved conditions (a), (b), and (c). Thus by letting  $\beta$  in condition (c) be such that  $\beta = \beta_1$ , where  $0 < \beta_1 < \epsilon^2/2$ , we can see that  $\Pi_N(\mathcal{U}^c | \mathbf{Y}_1, \dots, \mathbf{Y}_N) \rightarrow 0$  a.s.  $[P_{\omega_0}]$  for every weak neighborhood,  $\mathcal{U}$  of  $\omega_0$ .

## B. Case Studies

### B.1. Simulation Study 1

In this simulation study, we looked at how well we could recover the mean, covariance, and cross-covariance functions at different numbers of functional observations. For this simulation, we used 3 different number of functional observations ( $N = 40, 80, 160$ ), and ran 50 MCMC chains for 500,000 iterations. To help the chain converge, we used the Multiple Start Algorithm (Algorithm 1) with  $n\_try1 = 50$ ,  $n\_try2 = 10$ ,  $n\_MCMC1 = 2000$ , and  $n\_MCMC2 = 20000$ . Due to our allocated computation budget, we did not use tempered transitions to help move around the space of parameters. In order to save on memory, we only saved every 100 iterations. We used 8 functions to form the basis of the observed functions, such that the observed smooth functions lie in a space spanned by cubic b-spline basis functions with 4 equally spaced internal nodes ( $P = 8$ ), and that 3 eigenfunctions can capture the entire covariance process ( $M = 3$ ). For this simulation, we used the two feature model ( $K = 2$ ). For each simulation, we used the same  $\nu$ ,  $\Phi$ , and  $\sigma^2$  parameters for each simulation. We specified that  $\sigma^2 = 0.001$ , while the  $\nu$  parameters were drawn according to the following distributions:

$$\nu_1 \sim \mathcal{N}((6, 4, \dots, -6, -8)', 4\mathbf{P}),$$

$$\nu_2 \sim \mathcal{N}((-8, -6, \dots, 4, 6)', 4\mathbf{P}),$$

where  $\mathbf{P}$  is the matrix corresponding with the first order random walk penalty. Due to the non-identifiability described in section 2.2, we drew the  $\Phi$  parameters from the subspace orthogonal to the space spanned by the  $\nu$  parameters. Thus let  $\text{colsp}(\mathbf{B}^\perp) := \text{span}\{b_1^\perp, \dots, b_6^\perp\} \subset \mathbb{R}^8$  be the subspace orthogonal to the  $\nu$  parameters, which can be described as the span of 6 vectors in  $\mathbb{R}^8$ . The  $\Phi$  parameters were drawn according to the following distributions:

$$\phi_{km} = \mathbf{q}_{km} \mathbf{B}^\perp \quad k = 1, 2 \quad m = 1, 2, 3,$$

where  $\mathbf{q}_{k1} \sim \mathcal{N}(\mathbf{0}_6, 2.25\mathbf{I}_6)$ ,  $\mathbf{q}_{k2} \sim \mathcal{N}(\mathbf{0}_6, \mathbf{I}_6)$ ,  $\mathbf{q}_{k3} \sim \mathcal{N}(\mathbf{0}_6, 0.49\mathbf{I}_6)$ . While this may not completely remove the effect of the non-identifiability mentioned in section 2.2, it should help minimize its impact on our recovery of the mean and covariance structures.

For the  $\mathbf{z}_i$  and  $\chi_{im}$  parameters, we would draw 3 different sets of parameters (corresponding to the various number of functional observations). The  $\chi_{im}$  parameters were drawn from a standard normal distribution. The  $\mathbf{z}_i$  parameters were drawn from a mixture of Dirichlet distributions. Roughly 30% of the  $\mathbf{z}_i$  parameters were drawn from a Dirichlet distribution with  $\alpha_1 = 10$  and  $\alpha_2 = 1$ . Another roughly 30% of the  $\mathbf{z}_i$  parameters were drawn from a Dirichlet distribution where  $\alpha_1 = 1$  and  $\alpha_2 = 10$ . The rest of the  $\mathbf{z}_i$  parameters were drawn from a Dirichlet distribution with  $\alpha_1 = \alpha_2 = 1$ . For each simulation, we used these parameters to simulate observed functions from our model.

Before getting the posterior median estimates of the functions of interest, we used the Membership Rescale Algorithm (algorithm 2) to help with interpretability and identifiability. From figure 7, we can see that that we do a good job in recovering the covariance and cross-covariance functions. The estimated functions are slightly conservative, as they tend to slightly underestimate the magnitude of the covariance functions. Figure 8 show the median posterior mean recovered from each of the 10 MCMC chains when

we have 250 functional observations. As we can see from the figure, there is very little variation in the estimates of the mean function between 10 MCMC chains.

### B.2. Simulation Study 2

Picking the number of features can be a challenging task for many practitioners, especially when there is little scientific knowledge on the data. Practitioners often rely on information criterion to help aid in picking the number of features. In this simulation, we simulate 10 different “true” data-sets from a 3 feature model to see if information criterion can help pick the correct number of features. For this simulation study, we considered testing the information criterion under the model when  $K = 2, 3, 4$ , and  $5$  (where  $K$  is the number of features in our model). For each  $K$  and each data-set, we ran a MCMC chain for 100,000 iterations each. To help the chain converge, we used the Multiple Start Algorithm (Algorithm 1) with  $n\_try1 = 50$ ,  $n\_try2 = 5$ ,  $n\_MCMC1 = 2000$ , and  $n\_MCMC2 = 4000$ . To save on memory, we only saved every 10 iterations.

For the 10 “true” data-sets with 3 functional features ( $K = 3$ ) and 200 functional observations ( $N = 200$ ,  $n_i = 100$ ), we assumed that the observed smooth functions lie in a space spanned by cubic b-spline basis functions with 4 equally spaced internal nodes ( $P = 8$ ), and that 3 eigenfunctions can capture the entire covariance process ( $M = 3$ ). In this simulation, we assumed that  $\sigma^2 = 0.001$ , and randomly drew the  $\boldsymbol{\nu}$  and  $\boldsymbol{\Phi}$  parameters for each data-set according to the following distributions:

$$\begin{aligned}\boldsymbol{\nu}_1 &\sim \mathcal{N}((6, 4, \dots, -6, -8)', 4\mathbf{P}), \\ \boldsymbol{\nu}_2 &\sim \mathcal{N}((-8, -6, \dots, 4, 6)', 4\mathbf{P}), \\ \boldsymbol{\nu}_3 &\sim \mathcal{N}(\mathbf{0}, 4\mathbf{P}), \\ \boldsymbol{\phi}_{k1} &\sim \mathcal{N}(\mathbf{0}, \mathbf{I}_8), \\ \boldsymbol{\phi}_{k2} &\sim \mathcal{N}(\mathbf{0}, 0.5\mathbf{I}_8), \\ \boldsymbol{\phi}_{k3} &\sim \mathcal{N}(\mathbf{0}, 0.2\mathbf{I}_8).\end{aligned}$$

The  $\chi_{im}$  parameters were drawn from a standard normal distribution, while the  $\mathbf{Z}$  parameters were drawn from a mixture of Dirichlet distributions. 20% of the  $\mathbf{z}_i$  parameters were drawn from a Dirichlet distribution with  $\alpha_1 = 10$ ,  $\alpha_2 = 1$ , and  $\alpha_3 = 1$ . Another 20% of the  $\mathbf{z}_i$  parameters were drawn from a Dirichlet distribution where  $\alpha_1 = 1$ ,  $\alpha_2 = 10$ , and  $\alpha_3 = 1$ . Another 20% of the  $\mathbf{z}_i$  parameters were drawn from a Dirichlet distribution where  $\alpha_1 = 1$ ,  $\alpha_2 = 1$ , and  $\alpha_3 = 10$ . The rest of the  $\mathbf{z}_i$  parameters were drawn from a Dirichlet distribution with  $\alpha_1 = \alpha_2 = 1$ . Once all of the parameters for the “true” data-set were specified, the observed data points were generated according to the model. MCMC was then conducted with various values of  $K$ , but with the correct number of eigenfunctions,  $M$ , and the correct basis functions.

### B.3. A Case Study of EEG in ASD

In this study, we grouped patients based off of their T8 electrode signal. We used a two functional feature model, and found that patients in the first feature could be

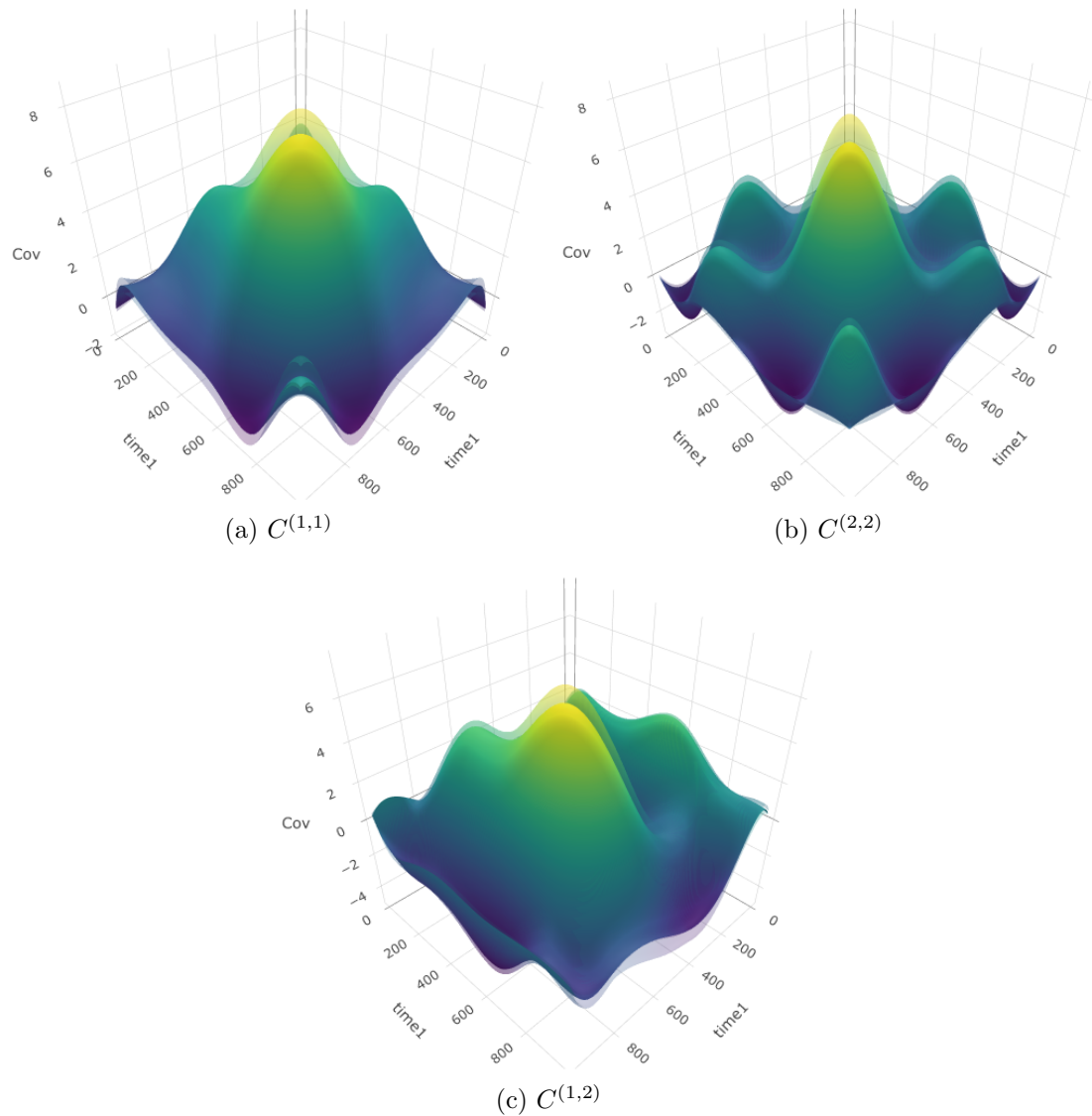


**Fig. 7.** Posterior median estimates of the covariance and cross-covariance functions (opaque) along with the true functions (transparent) for a simulated data set with 160 functional observations.

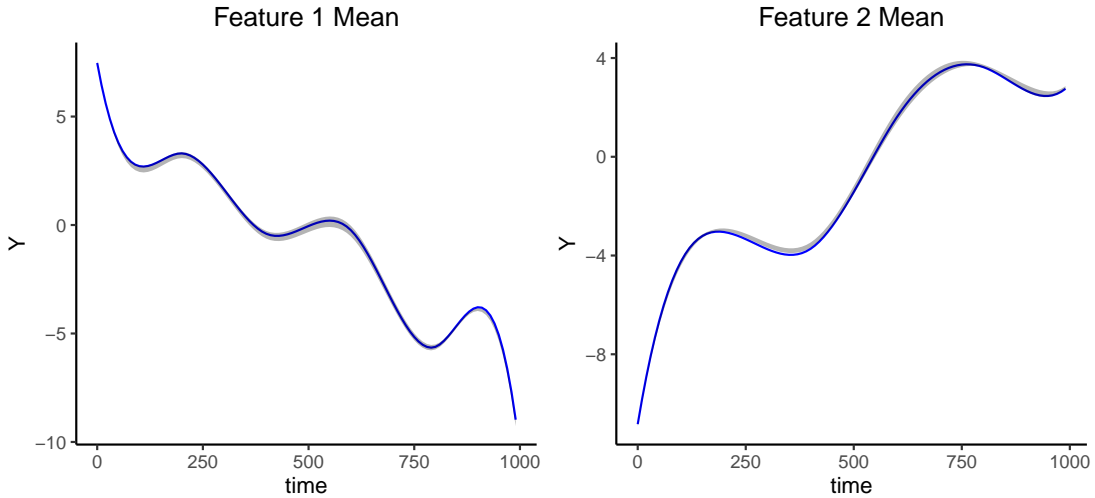


**Fig. 8.** 95% credible interval of the posterior mean functions for the case when we have 160 functional observations.

interpreted as  $1/f$  noise, while the second feature could be interpreted as a distinct PAF. We also fit a three functional feature mixed membership model, but found that the two feature mixed membership model (AIC = -13091.31, BIC = 9369.66, DIC = -13783.5) seemed to be optimal compared to the three feature paratial membership model (AIC = -12831.17, BIC = 8138.12, DIC = -13815.34). Figure 9 shows the median of the posterior posterior distribution of the covariance and cross-covariance functions. We can see that the covariance function associated with feature 1 ( $C^{(1,1)}$ ) has high covariance around 6 Hz, which is where we have the highest power of  $1/f$  noise.

When looking at the mean function for feature 2 (figure 5), we can see that the peak power occurs at around 9 Hz. However, for people who have a distinct PAF pattern, it is common for their peak power to occur anywhere between 9 Hz and 11 Hz. When looking at the covariance function associated with feature 2 ( $C^{(2,2)}$ ), we can see that this is being modeled by the high variance at 9 Hz and at 11 Hz. We can also see that people who only have high Alpha power typically tend to only have one peak in the alpha band, which is also accounted for in our model by the negative covariance between 9 Hz and 11 Hz. When looking at the cross-covariance function, we can see that there is high cross-covariance between 9 Hz in feature 1 and 6 Hz in feature 2, and negative cross-covariance between 11 Hz in feature 1 and 6 Hz in feature 2. This means that patients who are simultaneously in feature 1 and 2 that have moderate  $1/f$  noise are likely to have moderate alpha power around 9 Hz and are less likely to have a peak around 11 Hz. According to the scientific literature, this is likely to occur in younger TD individuals.

From figure 6, we can see that on average ASD children were tended to belong to feature 1 more than feature 2. Thus on average, ASD children tended to have a less distinct PAF when compared to TD children.

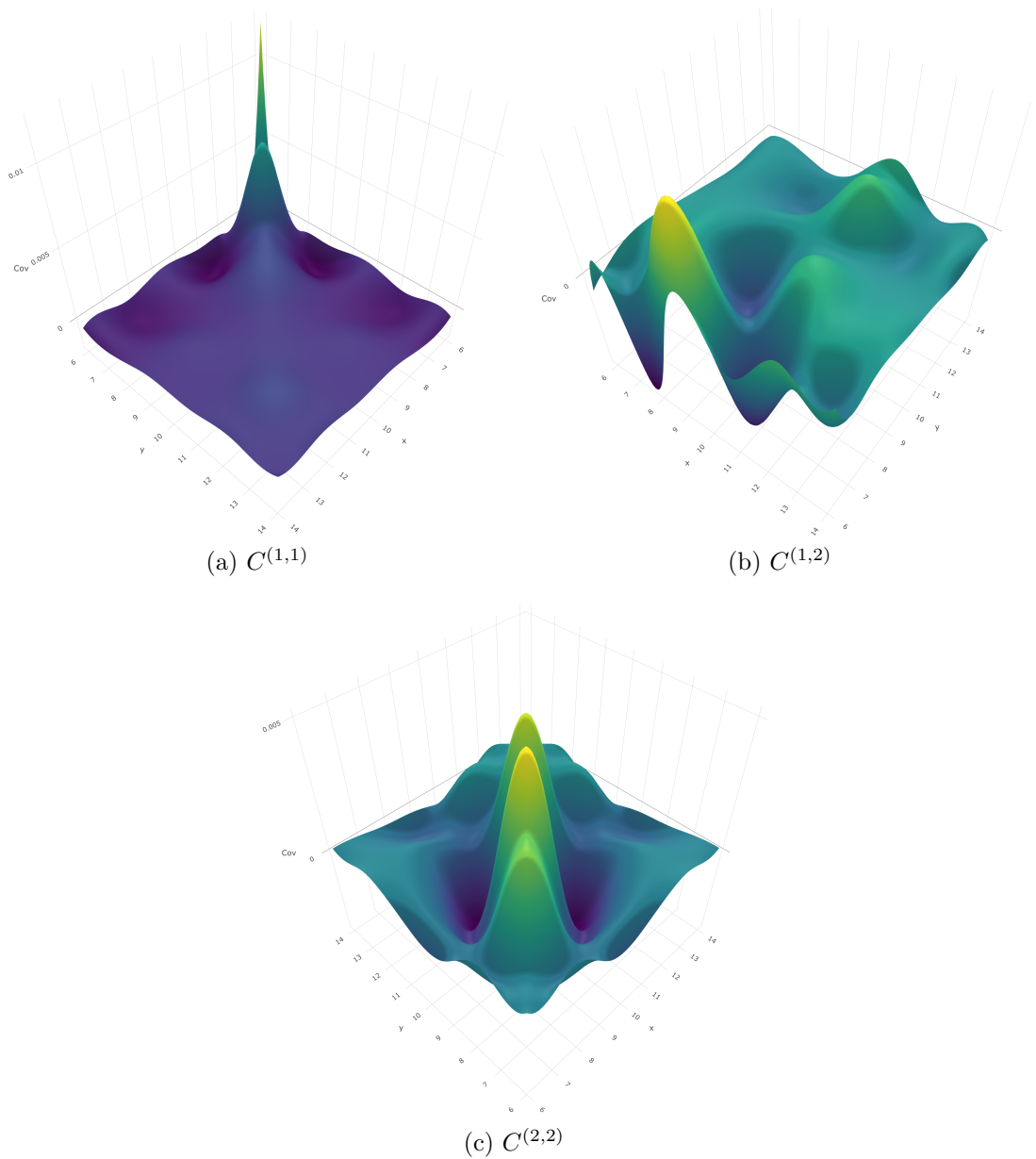


**Fig. 9.** Posterior estimates of the covariance and cross-covariance functions

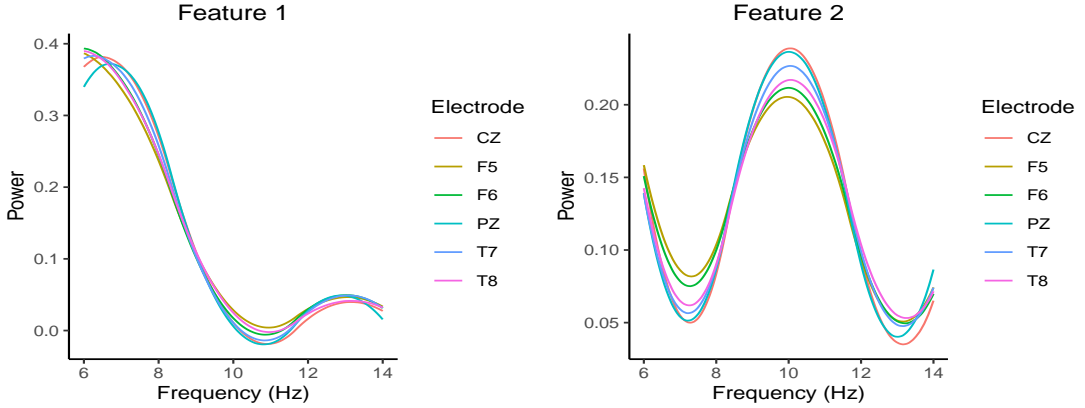


**Fig. 10.** Posterior estimates of the means of the two functional features viewed at specific electrodes.

#### B.4. Analysis of Multi-Channel EEG Data

The proposed modeling framework is suitable for the analysis of functional data evaluated over  $\mathcal{T} \subset \mathbb{R}^d$ . Therefore, we extend our analysis in the main manuscript to include EEG data measured on the entire cortex. Specifically, we will use a model with 2 latent functional features ( $K = 2$ ) where  $\mathcal{T} \subset \mathbb{R}^3$ . Two of the three indices denote the spatial position on the scalp, while the third index contains information on the frequency observed. Similarly, the value of the function at some point  $t \in \mathcal{T}$  represents the spectral power of the observed signal. For computational purposes, we project the true three-dimensional coordinates of the electrodes to a two-dimensional bird's eye view of electrodes using the 'eegkit' package developed by [Helwig \(2018\)](#). In this section, we used two eigenfunctions to capture the covariance process ( $M = 2$ ). We used a tensor product of B-splines to create a basis for our space of functions. For each dimension we used quadratic B-splines, with 3 internal nodes for each spatial index and 2 internal nodes for the frequency index ( $P = 180$ ). Since we are using functional data analysis techniques to model the EEG data, we assume that the smoothness over the spatial and frequency domains. Since EEG data has poor spatial resolution ([Grinvald and Hildesheim, 2004](#)) and we have relatively sparse sampling across the spatial domain (25 channels), the smoothness assumption can be thought of as a type of regularization over the domain of our function. Due to computational limitations, we ran the Multiple Start Algorithm (algorithm 1) with  $n\_try1 = 6$ ,  $n\_try2 = 1$ ,  $n\_MCMC1 = 3000$ , and  $n\_MCMC2 = 4000$ . We then ran the chain for 19,000 iterations, saving only every 10 iterations.

Figure 10 reports posterior mean estimates for the feature means over a sample of electrodes. Our findings are similar to our results on electrode T8, analyzed in the main manuscript; one latent feature corresponding to  $1/f$  noise, and the other exhibiting well defined PAF across electrodes. Figure 11, reports the electrode-specific variance at frequency 6 Hz and 10 Hz, corresponding respectively to the highest relative power in the first latent feature and the average peak alpha frequency in second latent feature.

The right-temporal region around electrode T8, is found to exhibit a high level of

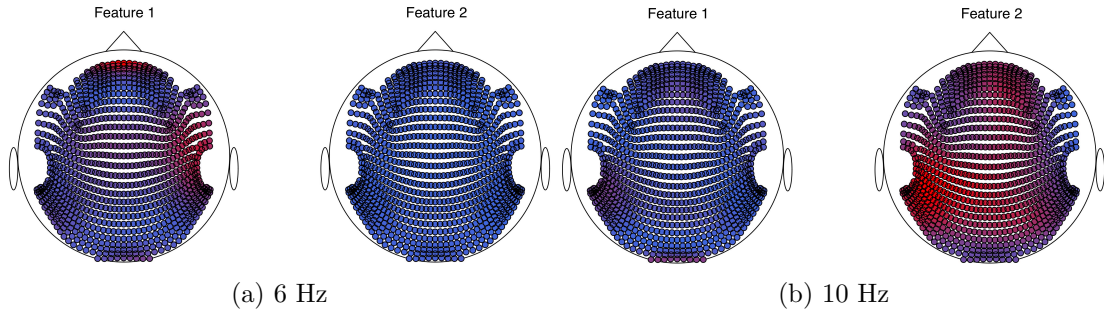


**Fig. 11.** Variance of the electrodes at 6 and 10 Hz for each functional feature. The relative magnitude of the variance of each electrode is indicated by the color of the electrode (red is relatively high variance, while blue is relatively low variance).

heterogeneity (high relative variance) at 6 Hz, within latent feature 1 (poorly defined PAF), which relates to the findings of Scheffler et al. (2019), who identified patterns of variation in the right-temporal region as the highest contributor to log-odds of ASD vs. TD discrimination. Contrastingly, feature 2 (well defined PAF) exhibits high levels of heterogeneity (relative variance) throughout the cortex at frequency 10 Hz, corresponding to the location of the PAF in feature 2. Overall, results for our analysis on the whole set of electrodes agree with our findings for electrode T8 in the main manuscript.

Figure 12 shows the posterior median estimates of the membership allocations for each individual. We can see from both the mean functions and membership allocations that these results seem to match the univariate results in section 4.3.

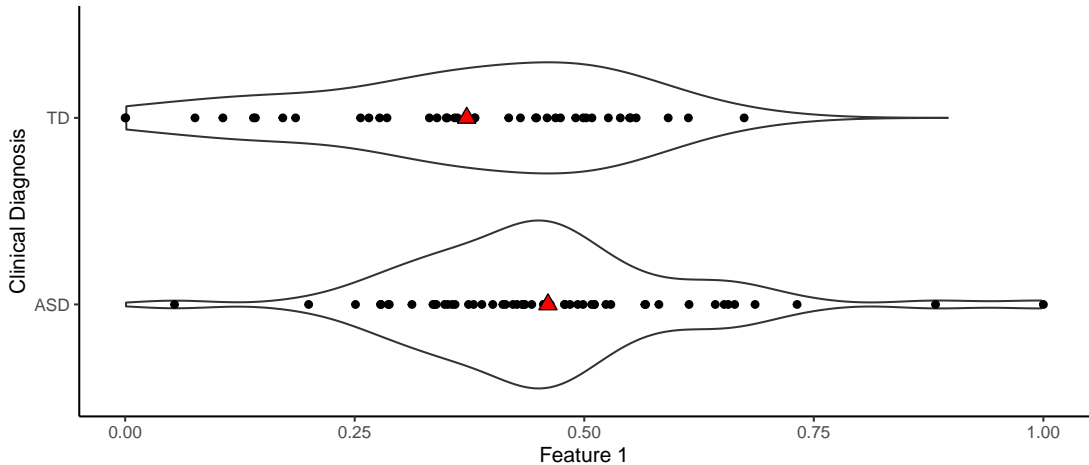


**Fig. 12.** Posterior estimates of the median membership to the first functional feature.

### C. Computation

#### C.1. Posterior Distributions and Computation

In this section, we will discuss the computational strategy used to perform Bayesian inference. In cases where the posterior distribution is a known distribution, a Gibbs update will be performed. We will let  $\Theta$  be the collection of all parameters, and  $\Theta_{-\zeta}$  be the collection of all parameters, excluding the  $\zeta$  parameter. We will first start with the  $\phi_{km}$  parameters, for  $j = 1, \dots, K$  and  $m = 1, \dots, M$ . Let  $\mathbf{D}_{jm} = \tilde{\tau}_{mj}^{-1} \text{diag}(\gamma_{j1m}^{-1}, \dots, \gamma_{jPm}^{-1})$ . By letting

$$\mathbf{m}_{jm} = \frac{1}{\sigma^2} \sum_{i=1}^N \sum_{l=1}^{n_i} \left( B(t_{il}) \chi_{im} \left( y_i(t_{il}) Z_{ij} - Z_{ij}^2 \boldsymbol{\nu}'_j B(t_{il}) - Z_{ij}^2 \sum_{n \neq m} [\chi_{in} \boldsymbol{\phi}'_{jn} B(t_{il})] \right) - \sum_{k \neq j} Z_{ij} Z_{ik} \left[ \boldsymbol{\nu}'_k B(t_{il}) + \sum_{n=1}^M \chi_{in} \boldsymbol{\phi}'_{kn} B(t_{il}) \right] \right),$$

and

$$\mathbf{M}_{jm}^{-1} = \frac{1}{\sigma^2} \sum_{i=1}^N \sum_{l=1}^{n_i} (Z_{ij}^2 \chi_{im}^2 B(t_{il}) B'(t_{il})) + \mathbf{D}_{jm}^{-1},$$

we have that

$$\boldsymbol{\phi}_{jm} | \Theta_{-\boldsymbol{\phi}_{jm}}, \mathbf{Y}_1, \dots, \mathbf{Y}_N \sim \mathcal{N}(\mathbf{M}_{jm} \mathbf{m}_{jm}, \mathbf{M}_{jm}).$$

The posterior distribution of  $\delta_{1k}$ , for  $k = 1, \dots, K$ , is

$$\delta_{1k} | \Theta_{-\delta_{1k}}, \mathbf{Y}_1, \dots, \mathbf{Y}_N \sim \Gamma \left( a_{1k} + (PM/2), 1 + \frac{1}{2} \sum_{r=1}^P \gamma_{k,r,1} \phi_{k,r,1}^2 + \frac{1}{2} \sum_{m=2}^M \sum_{r=1}^P \gamma_{k,r,m} \phi_{k,r,m}^2 \left( \prod_{j=2}^m \delta_{jk} \right) \right).$$

The posterior distribution for  $\delta_{ik}$ , for  $i = 2, \dots, M$  and  $k = 1, \dots, K$ , is

$$\delta_{ik} | \Theta_{-\delta_{ik}}, \mathbf{Y}_1, \dots, \mathbf{Y}_N \sim \Gamma \left( a_{2k} + (P(M-i+1)/2), 1 + \frac{1}{2} \sum_{m=i}^M \sum_{r=1}^P \gamma_{k,r,m} \phi_{k,r,m}^2 \left( \prod_{j=1; j \neq i}^m \delta_{jk} \right) \right).$$

The posterior distribution for  $a_{1k}$  is not a commonly known distribution, however we have that

$$P(a_{1k} | \Theta_{-a_{1k}}, \mathbf{Y}_1, \dots, \mathbf{Y}_N) \propto \frac{1}{\Gamma(a_{1k})} \delta_{1k}^{a_{1k}-1} a_{1k}^{\alpha_1-1} \exp\{-a_{1k}\beta_1\}.$$

Since this is not a known kernel of a distribution, we will have to use Metropolis-Hastings algorithm. Consider the proposal distribution  $Q(a'_{1k}|a_{1k}) = \mathcal{N}(a_{1k}, \epsilon_1 \beta_1^{-1}, 0, +\infty)$  (Truncated Normal) for some small  $\epsilon_1 > 0$ . Thus the probability of accepting any step is

$$A(a'_{1k}, a_{1k}) = \min \left\{ 1, \frac{P(a'_{1k}|\Theta_{-a'_{1k}}, \mathbf{Y}_1, \dots, \mathbf{Y}_N)}{P(a_{1k}|\Theta_{-a_{1k}}, \mathbf{Y}_1, \dots, \mathbf{Y}_N)} \frac{Q(a_{1k}|a'_{1k})}{Q(a'_{1k}|a_{1k})} \right\}.$$

Similarly for  $a_{2k}$ , we have

$$P(a_{2k}|\Theta_{-a_{2k}}, \mathbf{Y}_1, \dots, \mathbf{Y}_N) \propto \frac{1}{\Gamma(a_{2k})^{M-1}} \left( \prod_{i=2}^M \delta_{ik}^{a_{2k}-1} \right) a_{2k}^{\alpha_{2k}-1} \exp\{-a_{2k}\beta_2\}.$$

We will use a similar proposal distribution, such that  $Q(a'_{2k}|a_{2k}) = \mathcal{N}(a_{2k}, \epsilon_2 \beta_2^{-1}, 0, +\infty)$  for some small  $\epsilon_2 > 0$ . Thus the probability of accepting any step is

$$A(a'_{2k}, a_{2k}) = \min \left\{ 1, \frac{P(a'_{2k}|\Theta_{-a'_{2k}}, \mathbf{Y}_1, \dots, \mathbf{Y}_N)}{P(a_{2k}|\Theta_{-a_{2k}}, \mathbf{Y}_1, \dots, \mathbf{Y}_N)} \frac{Q(a_{2k}|a'_{2k})}{Q(a'_{2k}|a_{2k})} \right\}.$$

For the  $\gamma_{j,r,m}$  parameters, for  $j = 1, \dots, K$ ,  $r = 1, \dots, P$ , and  $m = 1, \dots, M$ , we have

$$\gamma_{j,r,m}|\Theta_{-\gamma_{j,r,m}}, \mathbf{Y}_1, \dots, \mathbf{Y}_N \sim \Gamma \left( \frac{\nu_\gamma + 1}{2}, \frac{\phi_{j,r,m}^2 \tilde{\tau}_{mj} + \nu_\gamma}{2} \right).$$

The posterior distribution for the  $\mathbf{z}_i$  parameters are not a commonly known distribution, so we will have to use the Metropolis-Hastings algorithm. We know that

$$\begin{aligned} p(\mathbf{z}_i|\Theta_{-\mathbf{z}_i}, \mathbf{Y}_1, \dots, \mathbf{Y}_N) &\propto \prod_{k=1}^K Z_{ik}^{\alpha_3 \pi_k - 1} \\ &\times \prod_{l=1}^{n_i} \exp \left\{ -\frac{1}{2\sigma^2} \left( y_i(t_{il}) - \sum_{k=1}^K Z_{ik} \left( \boldsymbol{\nu}'_k B(t_{il}) + \sum_{n=1}^M \chi_{in} \boldsymbol{\phi}'_{kn} B(t_{il}) \right) \right)^2 \right\}. \end{aligned}$$

We will use  $Q(\mathbf{z}'_i|\mathbf{z}_i) = \text{Dir}(a_{\mathbf{z}} \mathbf{z}_i)$  for some large  $a_{\mathbf{z}} \in \mathbb{R}^+$  as the proposal distribution. Thus the probability of accepting a proposed step is

$$A(\mathbf{z}'_i, \mathbf{z}_i) = \min \left\{ 1, \frac{P(\mathbf{z}'_i|\Theta_{-\mathbf{z}'_i}, \mathbf{Y}_1, \dots, \mathbf{Y}_N)}{P(\mathbf{z}_i|\Theta_{-\mathbf{z}_i}, \mathbf{Y}_1, \dots, \mathbf{Y}_N)} \frac{Q(\mathbf{z}_i|\mathbf{z}'_i)}{Q(\mathbf{z}'_i|\mathbf{z}_i)} \right\}.$$

Similarly, a Gibbs update is not available for an update of the  $\boldsymbol{\pi}$  parameters. We have that

$$\begin{aligned} p(\boldsymbol{\pi}|\Theta_{-\boldsymbol{\pi}}, \mathbf{Y}_1, \dots, \mathbf{Y}_N) &\propto \prod_{k=1}^K \pi_k^{c_k - 1} \\ &\times \prod_{i=1}^N \frac{1}{B(\alpha_3 \boldsymbol{\pi})} \prod_{k=1}^K Z_{ik}^{\alpha_3 \pi_k - 1}. \end{aligned}$$

Letting out proposal distribution be such that  $Q(\boldsymbol{\pi}'|\boldsymbol{\pi}) = Dir(a_{\boldsymbol{\pi}}\boldsymbol{\pi})$ , for some large  $a_{\boldsymbol{\pi}} \in \mathbb{R}^+$ , we have that our probability of accepting any proposal is

$$A(\boldsymbol{\pi}', \boldsymbol{\pi}) = \min \left\{ 1, \frac{P(\boldsymbol{\pi}'|\boldsymbol{\Theta}_{-\boldsymbol{\pi}'}, \mathbf{Y}_1, \dots, \mathbf{Y}_N)}{P(\boldsymbol{\pi}|\boldsymbol{\Theta}_{-\boldsymbol{\pi}}, \mathbf{Y}_1, \dots, \mathbf{Y}_N)} \frac{Q(\boldsymbol{\pi}|\boldsymbol{\pi}')}{Q(\boldsymbol{\pi}'|\boldsymbol{\pi})} \right\}.$$

The posterior distribution of  $\alpha_3$  is also not a commonly known distribution, so we will use the Metropolis-Hastings algorithm to sample from the posterior distribution. We have that

$$\begin{aligned} p(\alpha_3|\boldsymbol{\Theta}_{-\alpha_3}, \mathbf{Y}_1, \dots, \mathbf{Y}_N) &\propto e^{-b\alpha_3} \\ &\times \prod_{i=1}^N \frac{1}{B(\alpha_3|\boldsymbol{\pi})} \prod_{k=1}^K Z_{ik}^{\alpha_3\pi_k-1}. \end{aligned}$$

Using a proposal distribution such that  $Q(\alpha'_3|\alpha_3) = \mathcal{N}(\alpha_3, \sigma_{\alpha_3}^2, 0, +\infty)$  (Truncated Normal), we are left with the probability of accepting a proposed state as

$$A(\alpha'_3, \alpha_3) = \min \left\{ 1, \frac{P(\alpha'_3|\boldsymbol{\Theta}_{-\alpha'_3}, \mathbf{Y}_1, \dots, \mathbf{Y}_N)}{P(\alpha_3|\boldsymbol{\Theta}_{-\alpha_3}, \mathbf{Y}_1, \dots, \mathbf{Y}_N)} \frac{Q(\alpha_3|\alpha'_3)}{Q(\alpha'_3|\alpha_3)} \right\}.$$

Let  $\mathbf{P}$  be the following tridiagonal matrix:

$$\mathbf{P} = \begin{bmatrix} 1 & -1 & 0 \\ -1 & 2 & -1 \\ \ddots & \ddots & \ddots \\ & -1 & 2 & -1 \\ & 0 & -1 & 1 \end{bmatrix}.$$

Thus, letting

$$\mathbf{B}_j = \left( \tau_j \mathbf{P} + \frac{1}{\sigma^2} \sum_{i=1}^N \sum_{l=1}^{n_i} Z_{ij}^2 B(t_{il}) B'(t_{il}) \right)^{-1}$$

and

$$\mathbf{b}_j = \frac{1}{\sigma^2} \sum_{i=1}^N \sum_{l=1}^{n_i} Z_{ij} B(t_{il}) \left( y_i(t_{il}) - \left( \sum_{k \neq j} Z_{ik} \boldsymbol{\nu}'_k B(t_{il}) \right) - \left( \sum_{k=1}^K \sum_{m=1}^M Z_{ik} \chi_{im} \phi'_{km} B(t_{il}) \right) \right),$$

we have that

$$\boldsymbol{\nu}_j | \boldsymbol{\Theta}_{-\boldsymbol{\nu}_j}, \mathbf{Y}_1, \dots, \mathbf{Y}_N \sim \mathcal{N}(\mathbf{B}_j \mathbf{b}_j, \mathbf{B}_j),$$

for  $j = 1, \dots, K$ . Thus we can perform a Gibbs update to update our  $\boldsymbol{\nu}$  parameters. The  $\tau_l$  parameters, for  $l = 1, \dots, K$ , can also be updated by using a Gibbs update since the posterior distribution is:

$$\tau_l | \boldsymbol{\Theta}_{-\tau_l}, \mathbf{Y}_1, \dots, \mathbf{Y}_N \sim \Gamma \left( \alpha + P/2, \beta + \frac{1}{2} \boldsymbol{\nu}'_l \mathbf{P} \boldsymbol{\nu}_l \right).$$

The parameter  $\sigma^2$  can be updated by using a Gibbs update. If we let

$$\beta_\sigma = \frac{1}{2} \sum_{i=1}^N \sum_{l=1}^{n_i} \left( y_i(t_{il}) - \sum_{k=1}^K Z_{ik} \left( \boldsymbol{\nu}'_k B(t_{il}) + \sum_{n=1}^M \chi_{in} \boldsymbol{\phi}'_{kn} B(t_{il}) \right) \right)^2,$$

then we have

$$\sigma^2 | \boldsymbol{\Theta}_{-\sigma^2}, \mathbf{Y}_1, \dots, \mathbf{Y}_N \sim IG \left( \alpha_0 + \frac{\sum_{i=1}^N n_i}{2}, \beta_0 + \beta_\sigma \right),$$

where  $n_i$  are the number of time points observed for the  $i^{th}$  observed function. Lastly, we can update the  $\chi_{im}$  parameters, for  $i = 1, \dots, N$  and  $m = 1, \dots, M$ , using a Gibbs update. If we let

$$\mathbf{w}_{im} = \frac{1}{\sigma^2} \left( \sum_{l=1}^{n_i} \left( \sum_{k=1}^K Z_{ik} \boldsymbol{\phi}'_{km} B(t_{il}) \right) \left( y_i(t_{il}) - \sum_{k=1}^K Z_{ik} \left( \boldsymbol{\nu}'_k B(t_{il}) + \sum_{n \neq m} \chi_{in} \boldsymbol{\phi}'_{kn} B(t_{il}) \right) \right) \right)$$

and

$$\mathbf{W}_{im}^{-1} = 1 + \frac{1}{\sigma^2} \sum_{l=1}^{n_i} \left( \sum_{k=1}^K Z_{ik} \boldsymbol{\phi}'_{km} B(t_{il}) \right)^2,$$

then we have that

$$\chi_{im} | \boldsymbol{\zeta}_{-\chi_{im}}, \mathbf{Y}_1, \dots, \mathbf{Y}_N \sim \mathcal{N}(\mathbf{W}_{im} \mathbf{w}_{im}, \mathbf{W}_{im}).$$

In our model, we relax the assumption that the  $\boldsymbol{\Phi}$  parameters are orthogonal. Even though we relaxed the assumption, we proved that many of the desirable properties still hold. However, if users do not want to relax this assumption, Kowal et al. (2017) describes a framework that allows us to sample when orthogonality constraints are imposed. In our model, orthogonality is defined by the inner product in equation 6. Therefore, for  $p$  such that  $1 \leq p \leq KP$ , we must have that

$$\langle \boldsymbol{\Phi}_p, \boldsymbol{\Phi}_j \rangle_{\mathcal{H}} = 0 \quad \forall j \neq p.$$

By rearranging terms, we can see that we have

$$\begin{aligned} \langle \boldsymbol{\Phi}_p, \boldsymbol{\Phi}_j \rangle_{\mathcal{H}} &= \sum_{k=1}^K \int_{\mathcal{T}} \boldsymbol{\phi}'_{kp} \mathbf{B}(t) \boldsymbol{\phi}'_{kj} \mathbf{B}(t) dt \\ &= \sum_{k \neq i} \int_{\mathcal{T}} \boldsymbol{\phi}'_{kp} \mathbf{B}(t) \boldsymbol{\phi}'_{kj} \mathbf{B}(t) dt + \boldsymbol{\phi}'_{ip} \int_{\mathcal{T}} \mathbf{B}(t) \mathbf{B}(t)' dt \boldsymbol{\phi}_{ij}, \end{aligned}$$

where  $\int_{\mathcal{T}} \mathbf{B}(t) \mathbf{B}(t)' dt$  is the element-wise integration of the  $P \times P$  matrix. Letting

$$\mathbf{L}_{-ip} = \begin{bmatrix} \int_{\mathcal{T}} \mathbf{B}(t) \mathbf{B}(t)' dt \boldsymbol{\phi}_{i1} \\ \vdots \\ \int_{\mathcal{T}} \mathbf{B}(t) \mathbf{B}(t)' dt \boldsymbol{\phi}_{i(p-1)} \\ \int_{\mathcal{T}} \mathbf{B}(t) \mathbf{B}(t)' dt \boldsymbol{\phi}_{i(p+1)} \\ \vdots \\ \int_{\mathcal{T}} \mathbf{B}(t) \mathbf{B}(t)' dt \boldsymbol{\phi}_{i(KP)} \end{bmatrix} \quad \text{and} \quad \mathbf{c}_{-ip} = \begin{bmatrix} \sum_{k \neq i} \int_{\mathcal{T}} \boldsymbol{\phi}'_{kp} \mathbf{B}(t) \boldsymbol{\phi}'_{k1} \mathbf{B}(t) dt \\ \vdots \\ \sum_{k \neq i} \int_{\mathcal{T}} \boldsymbol{\phi}'_{kp} \mathbf{B}(t) \boldsymbol{\phi}'_{k(p-1)} \mathbf{B}(t) dt \\ \sum_{k \neq i} \int_{\mathcal{T}} \boldsymbol{\phi}'_{kp} \mathbf{B}(t) \boldsymbol{\phi}'_{k(p+1)} \mathbf{B}(t) dt \\ \vdots \\ \sum_{k \neq i} \int_{\mathcal{T}} \boldsymbol{\phi}'_{kp} \mathbf{B}(t) \boldsymbol{\phi}'_{k(KP)} \mathbf{B}(t) dt \end{bmatrix},$$

we can write our orthogonality constraint for  $\phi_{ip}$  given the other  $\phi$  parameters as

$$\phi'_{ip} \mathbf{L}_{-ip} = -\mathbf{c}_{-ip}.$$

Thus using the results in [Kowal et al. \(2017\)](#), we have that  $\phi_{ip} \sim \mathcal{N}(\tilde{\mathbf{M}}_{ip} \mathbf{m}_{ip}, \tilde{\mathbf{M}}_{ip})$ , where

$$\tilde{\mathbf{M}}_{ip} = \mathbf{M}_{ip} - \mathbf{M}_{ip} \mathbf{L}_{-ip} (\mathbf{L}'_{-ip} \mathbf{M}_{ip} \mathbf{L}_{-ip})^{-1} (\mathbf{L}'_{-ip} \mathbf{M}_{ip} + \mathbf{c}_{-ip}).$$

Like in [Kowal et al. \(2017\)](#),  $\mathbf{M}_{ip}$  and  $\mathbf{m}_{ip}$  are such that when we relax the orthogonal constraints, we have  $\phi_{ip} \sim \mathcal{N}(\mathbf{M}_{ip} \mathbf{m}_{ip}, \mathbf{M}_{ip})$  (defined in section [C.1](#)). Thus one can use the modified Gibbs update to ensure orthogonality. However, by using this alternative update, the mixing of the Markov chain will likely suffer.

### C.2. Multiple Start Algorithm

One of the main computational challenges that we encounter in this model is the multi-modal posterior distribution. Often times, the MCMC chain can get stuck in a mode, and it can have trouble moving through areas of low posterior density. One way to traverse through areas of low posterior density is to use tempered transitions. However, tempered transitions are computationally intensive and the hyperparameters can be somewhat difficult to tune. Thus, one of the best ways to converge to the correct mode is to have a good starting point. The Multiple Start Algorithm, found in [algorithm 1](#), is a way to pick an optimal starting point. To get optimal performance our of this algorithm, we recommend that the initial data is standardized before running this algorithm.

The function calls two other functions, `BFPMM_Nu_Z(Y, time, K, n_MCMC1, ...)` and `BFPMM_Theta(P, Y, time, K, n_MCMC2, ...)`. The first function, `BFPMM_Nu_Z(Y, time, K, n_MCMC1, ...)`, starts with random parameter values for  $\nu$ ,  $\mathbf{Z}$ ,  $\sigma^2$ , and other hyperparameters relating to these parameters. We then run an MCMC chain with the values of the  $\chi$  and  $\phi$  variables fixed as 0 (or as the matrix  $\mathbf{O}$ ). The function returns the mean likelihood for the last 20% of the MCMC chain as well as the entire MCMC chain. The variable `n_MCMC1` is assumed to be picked such that the chain converges in the first 80% of the MCMC iterations. Since the starting points are random, the MCMC chains are likely to explore different modes. Once we have a good initial starting point, we estimate the  $\chi$ ,  $\phi$ , and other parameters that have not already been estimated using the function `BFPMM_Theta(P, Y, time, K, n_MCMC2, ...)`. In this function, we run an MCMC chain while fixing the values of  $\nu$  and  $\mathbf{Z}$  to their optimal values found previously. We will use the outputs of [algorithm 1](#) as a starting point for our final MCMC chain.

### C.3. Tempered Transitions

Tempered transitions are used to help traverse areas of low posterior probability density when running MCMC chains. In problems that have multi-modal posterior distributions, traditional methods often have difficulty moving from one mode to another, which can cause the chain to not explore the entire state-space and therefore not converge to the true posterior distribution. Thus by using tempered transitions, we are potentially able to traverse the state-space to explore multiple modes. In simulations, we found that the

---

**Algorithm 1** Multiple Start Algorithm

---

**Require:**  $n\_try1, n\_try2, Y, time, K, n\_MCMC1, n\_MCMC2, \dots$

$P \leftarrow \text{BFPMM\_Nu\_Z}(Y, time, K, n\_MCMC1, \dots)$   $\triangleright$  Returns the likelihood and estimates for  $\nu$  and  $Z$

$\text{max\_likelihood} \leftarrow P[\text{"likelihood"}]$

$i \leftarrow 1$

**while**  $i \leq n\_try1$  **do**

$P_i \leftarrow \text{BFPMM\_Nu\_Z}(Y, time, K, n\_MCMC1, \dots)$

**if**  $\text{max\_likelihood} < P_i[\text{"likelihood"}]$  **then**

$\text{max\_likelihood} \leftarrow P_i[\text{"likelihood"}]$

$P \leftarrow P_i$

**end if**

$i \leftarrow i + 1$

**end while**

$\theta \leftarrow \text{BFPMM\_Theta}(P, Y, time, K, n\_MCMC2, \dots)$   $\triangleright$  Returns estimates for the rest of the parameters

$\text{max\_likelihood} \leftarrow \theta[\text{"likelihood"}]$

$i \leftarrow 1$

**while**  $i \leq n\_try2$  **do**

$\theta_i \leftarrow \text{BFPMM\_Theta}(P, Y, time, K, n\_MCMC2, \dots)$

**if**  $\text{max\_likelihood} < \theta_i[\text{"likelihood"}]$  **then**

$\text{max\_likelihood} \leftarrow \theta_i[\text{"likelihood"}]$

$\theta \leftarrow \theta_i$

**end if**

$i \leftarrow i + 1$

**end while**

**return**  $(\theta, P)$   $\triangleright$  Returns estimates for all model parameters

---

tuning parameters can be difficult to tune to get acceptable acceptance probabilities, however in this section we will outline a way to use tempered transitions with our model.

We will be following the works of [Behrens et al. \(2012\)](#) and [Pritchard et al. \(2000\)](#) and only temper the likelihood. The target distribution that we want to temper is usually assumed to be written as

$$p(x) \propto \pi(x) \exp(-\beta_h h(x)),$$

where  $\beta_h$  controls how much the distribution is tempered. We will assume  $1 = \beta_0 < \dots < \beta_h < \dots < \beta_{N_t}$ . The hyperparameters  $N_t$  and  $\beta_{N_t}$  are user specified, and will depend on the complexity of the model. For more complex models, we will most likely need a larger  $N_t$ . We will also assume that the parameters  $\beta_h$  follow a geometric scheme. We can rewrite our likelihood to fit the above form:

$$\begin{aligned} p_h(y_i(t)|\Theta) &\propto \exp \left\{ -\beta_h \left( \frac{1}{2} \log(\sigma^2) + \frac{1}{2\sigma^2} \left( y_i(t) - \sum_{k=1}^K Z_{ik} \left( \boldsymbol{\nu}'_k B(t) + \sum_{n=1}^M \chi_{in} \boldsymbol{\phi}'_{kn} B(t) \right) \right)^2 \right) \right\} \\ &= (\sigma^2)^{-\beta_h/2} \exp \left\{ -\frac{\beta_h}{2\sigma^2} \left( y_i(t) - \sum_{k=1}^K Z_{ik} \left( \boldsymbol{\nu}'_k B(t) + \sum_{n=1}^M \chi_{in} \boldsymbol{\phi}'_{kn} B(t) \right) \right)^2 \right\}. \end{aligned}$$

Let  $\Theta_h$  be the set of parameters generated from the model using the tempered likelihood associated with  $\beta_h$ . The tempered transition algorithm can be summarized by the following steps:

- (a) Start with initial state  $\Theta_0$ .
- (b) Transition from  $\Theta_0$  to  $\Theta_1$  using the tempered likelihood associated with  $\beta_1$ .
- (c) Continue in this manner until we transition from  $\Theta_{N_t-1}$  to  $\Theta_{N_t}$  using the tempered likelihood associated with  $\beta_{N_t}$ .
- (d) Transition from  $\Theta_{N_t}$  to  $\Theta_{N_t+1}$  using the tempered likelihood associated with  $\beta_{N_t}$ .
- (e) Continue in this manner until we transition from  $\Theta_{2N_t-1}$  to  $\Theta_{2N_t}$  using  $\beta_1$ .
- (f) Accept transition from  $\Theta_0$  to  $\Theta_{2N_t}$  with probability

$$\min \left\{ 1, \prod_{h=0}^{N_t-1} \frac{\prod_{i=1}^N \prod_{l=1}^{n_i} p_{h+1}(y_i(t_{il})|\Theta_h)}{\prod_{i=1}^N \prod_{l=1}^{n_i} p_h(y_i(t_{il})|\Theta_h)} \prod_{h=N_t+1}^{2N_t} \frac{\prod_{i=1}^N \prod_{l=1}^{n_i} p_h(y_i(t_{il})|\Theta_h)}{\prod_{i=1}^N \prod_{l=1}^{n_i} p_{h+1}(y_i(t_{il})|\Theta_h)} \right\}.$$

Since we only temper the likelihood, we can use many of updates in section [C.1](#). However, we will have to modify how we update the  $\boldsymbol{\nu}$ ,  $\boldsymbol{\phi}$ ,  $\sigma^2$ ,  $\mathbf{Z}$ , and  $\chi$  parameters. By letting

$$\begin{aligned} (\mathbf{m}_{jm})_h &= \frac{\beta_h}{(\sigma^2)_h} \sum_{i=1}^N \sum_{l=1}^{n_i} \left( B(t_{il})(\chi_{im})_h \left( y_i(t_{il})(Z_{ij})_h - (Z_{ij})_h^2 (\boldsymbol{\nu}_j)'_h B(t_{il}) \right. \right. \\ &\quad \left. \left. - (Z_{ij})_h^2 \sum_{n \neq m} [(\chi_{in})_h (\boldsymbol{\phi}_{jn})'_h B(t_{il})] \right. \right. \\ &\quad \left. \left. - \sum_{k \neq j} (Z_{ij})_h (Z_{ik})_h \left[ (\boldsymbol{\nu}_k)'_h B(t_{il}) + \sum_{n=1}^M (\chi_{in})_h (\boldsymbol{\phi}_{kn})'_h B(t_{il}) \right] \right) \right), \end{aligned}$$

and

$$(\mathbf{M}_{jm})_h^{-1} = \frac{\beta_h}{(\sigma^2)_h} \sum_{i=1}^N \sum_{l=1}^{n_i} ((Z_{ij})_h^2 (\chi_{im})_h^2 B(t_{il}) B'(t_{il})) + (\mathbf{D}_{jm})_h^{-1},$$

we have that

$$(\phi_{jm})_h | \Theta_{-(\phi_{jm})_h}, \mathbf{Y}_1, \dots, \mathbf{Y}_N \sim \mathcal{N}((\mathbf{M}_{jm})_h (\mathbf{m}_{jm})_h, (\mathbf{M}_{jm})_h).$$

The posterior distribution for  $(\mathbf{z}_i)_h$  is still not a commonly known distribution, so we will still have to use the Metropolis-Hastings algorithm. The new posterior distribution when using tempered transitions changes into

$$\begin{aligned} p((\mathbf{z}_i)_h | (\Theta_{-(\mathbf{z}_i)_h})_h, \mathbf{Y}_1, \dots, \mathbf{Y}_N) &\propto \prod_{k=1}^K (Z_{ik})_h^{(\alpha_3)_h (\pi_k)_h - 1} \\ &\times \prod_{l=1}^{n_i} \exp \left\{ -\frac{\beta_h}{2(\sigma^2)_h} \left( y_i(t_{il}) \right. \right. \\ &\quad \left. \left. - \sum_{k=1}^K (Z_{ik})_h \left( (\boldsymbol{\nu}_k)'_h B(t_{il}) + \sum_{n=1}^M (\chi_{in})_h (\boldsymbol{\phi}_{kn})'_h B(t_{il}) \right) \right)^2 \right\}. \end{aligned}$$

We will use  $Q((\mathbf{z}_i)'_h | (\mathbf{z}_i)_{h-1}) = \text{Dir}(a_{\mathbf{z}} | (\mathbf{z}_i)_{h-1})$  for some large  $a_{\mathbf{z}} \in \mathbb{R}^+$  as the proposal distribution. Thus the probability of accepting a proposed step is

$$A((\mathbf{z}_i)'_h, (\mathbf{z}_i)_{h-1}) = \min \left\{ 1, \frac{P((\mathbf{z}_i)'_h | (\Theta_{-(\mathbf{z}_i)'_h})_h, \mathbf{Y}_1, \dots, \mathbf{Y}_N)}{P((\mathbf{z}_i)_{h-1} | \Theta_{-(\mathbf{z}_i)_{h-1}}, \mathbf{Y}_1, \dots, \mathbf{Y}_N)} \frac{Q((\mathbf{z}_i)_{h-1} | (\mathbf{z}_i)'_h)}{Q((\mathbf{z}_i)'_h | (\mathbf{z}_i)_{h-1})} \right\}.$$

Letting

$$(\mathbf{B}_j)_h = \left( (\tau_j)_h \mathbf{P} + \frac{\beta_h}{(\sigma^2)_h} \sum_{i=1}^N \sum_{l=1}^{n_i} (Z_{ij})_h^2 B(t_{il}) B'(t_{il}) \right)^{-1}$$

and

$$\begin{aligned} (\mathbf{b}_j)_h &= \frac{\beta_h}{(\sigma^2)_h} \sum_{i=1}^N \sum_{l=1}^{n_i} (Z_{ij})_h B(t_{il}) \left( y_i(t_{il}) - \left( \sum_{k \neq j} (Z_{ik})_h (\boldsymbol{\nu}'_k)_h B(t_{il}) \right. \right. \\ &\quad \left. \left. - \left( \sum_{k=1}^K \sum_{n=1}^M (Z_{ik})_h (\chi_{in})_h (\boldsymbol{\phi}_{kn})'_h B(t_{il}) \right) \right) \right), \end{aligned}$$

we have that

$$(\boldsymbol{\nu}_j)_h | \Theta_{-(\boldsymbol{\nu}_j)_h}, \mathbf{Y}_1, \dots, \mathbf{Y}_N \sim \mathcal{N}((\mathbf{B}_j)_h (\mathbf{b}_j)_h, (\mathbf{B}_j)_h).$$

The parameter  $(\sigma^2)_h$  can be updated by using a Gibbs update. If we let

$$(\beta_\sigma)_h = \frac{\beta_h}{2} \sum_{i=1}^N \sum_{l=1}^{n_i} \left( y_i(t_{il}) - \sum_{k=1}^K (Z_{ik})_h \left( (\boldsymbol{\nu}_k)'_h B(t_{il}) + \sum_{n=1}^M (\chi_{in})_h (\boldsymbol{\phi}_{kn})'_h B(t_{il}) \right) \right)^2,$$

then we have

$$(\sigma^2)_h | \Theta_{-(\sigma^2)_h}, \mathbf{Y}_1, \dots, \mathbf{Y}_N \sim IG \left( \alpha_0 + \frac{\beta_h \sum_{i=1}^N n_i}{2}, \beta_0 + (\beta_\sigma)_h \right).$$

Lastly, letting let

$$\begin{aligned} (\mathbf{w}_{im})_h = & \frac{\beta_h}{(\sigma^2)_h} \left( \sum_{l=1}^{n_i} \left( \sum_{k=1}^K (Z_{ik})_h (\phi_{km})'_h B(t_{il}) \right) \left( y_i(t_{il}) \right. \right. \\ & \left. \left. - \sum_{k=1}^K (Z_{ik})_h \left( (\nu_k)'_h B(t_{il}) + \sum_{n \neq m} (\chi_{in})_h (\phi_{kn})'_h B(t_{il}) \right) \right) \right) \end{aligned}$$

and

$$(\mathbf{W}_{im}^{-1})_h = 1 + \frac{\beta_h}{(\sigma^2)_h} \sum_{l=1}^{n_i} \left( \sum_{k=1}^K (Z_{ik})_h (\phi_{km})'_h B(t_{il}) \right)^2,$$

then we have that

$$(\chi_{im})_h | \zeta_{-(\chi_{im})_h}, \mathbf{Y}_1, \dots, \mathbf{Y}_N \sim \mathcal{N}((\mathbf{W}_{im})_h (\mathbf{w}_{im})_h, (\mathbf{W}_{im})_h).$$

One of the biggest drawbacks to using tempered transition is the computational cost of just one iteration. It is common for  $N_t$  to be in the thousands, especially when dealing with a complex model, so each tempered transition will take thousands of times longer than an untempered transition. Thus we recommend using a mixture of tempered transition and untempered transitions to speed up computation. From proposition 1 in [Roberts and Rosenthal \(2007\)](#), we know that an independent mixture of tempered transitions and untempered transitions will still preserve our stationary distribution of our Markov chain.

#### C.4. Membership Rescale Algorithm

As discussed in section 2.2, our model is unidentifiable. To help with interpretability, we will apply a linear transformation to the  $\mathbf{Z}$  matrix to ensure that we use as much of the unit simplex as possible. In the case when  $K = 2$ , this will correspond to rescaling the observations such that at least one observation is entirely in each feature. This specific assumption that one observation belongs entirely in each feature is known as the *seperability* condition ([Papadimitriou et al., 1998](#); [McSherry, 2001](#); [Azar et al., 2001](#); [Chen et al., 2022](#)). Thus in order to ensure identifiability, algorithm 2 can be used when we only have two features. In the case of a two feature model, the seperability condition is a very weak assumption, however as we move to models with more features, it can be a relatively strong assumption. Weaker geometric assumptions such as the *sufficiently scattered* condition ([Huang et al., 2016](#); [Jang and Hero, 2019](#); [Chen et al., 2022](#)). In cases when we have more than two features, we can use the idea of the sufficiently scattered condition to help with identifiability. From [Chen et al. \(2022\)](#), we have that an allocation matrix  $\mathbf{Z}$  is sufficiently scattered if:

- (a)  $\text{cone}(\mathbf{Z}')^* \subseteq \mathcal{K}$
- (b)  $\text{cone}(\mathbf{Z}')^* \cap \text{bd}\mathcal{K} \subseteq \{\lambda \mathbf{e}_f, f = 1, \dots, k, \lambda \geq 0\}$

where  $\mathcal{K} := \{\mathbf{x} \in \mathbb{R}^K | \|\mathbf{x}\|_2 \leq \mathbf{x}'\mathbf{1}_K\}$ ,  $\text{bd}\mathcal{K} := \{\mathbf{x} \in \mathbb{R}^K | \|\mathbf{x}\|_2 = \mathbf{x}'\mathbf{1}_K\}$ ,  $\text{cone}(\mathbf{Z}')^* := \{\mathbf{x} \in \mathbb{R}^K | \mathbf{x}\mathbf{Z}' \geq 0\}$ , and  $\mathbf{e}_f$  is a vector with the  $i^{th}$  element equal to 1 and zero elsewhere. The first condition can be interpreted as the allocation parameters should from a convex polytope that contains the dual cone  $\mathcal{K}^*$ . Thus we have that

$$\text{Conv}(\mathbf{Z}') \subseteq \mathcal{K}^*,$$

where  $\mathcal{K}^* := \{\mathbf{x} \in \mathbb{R}^K | \mathbf{x}'\mathbf{1}_K \geq \sqrt{k-1}\|\mathbf{x}\|_2\}$  and  $\text{Conv}(\mathbf{Z}') := \{\mathbf{x} \in \mathbb{R}^K | \mathbf{x} = \mathbf{Z}'\lambda, \lambda \in \Delta^N\}$ , where  $\Delta^k$  denotes the  $N$ -dimensional simplex. Ensuring that these two conditions are met is not trivial in our setting. Therefore, we will focus on trying to promote allocation structures such that the first condition is satisfied. Similarly to the case of two functional features, we aim to find a linear transformation such that the convex polytope of our transformed allocation parameters covers the most area. Thus letting  $\mathbf{T} \in \mathbb{R}^K \times \mathbb{R}^K$  be our transformation matrix, we aim to solve the following optimization problem:

$$\begin{aligned} \max_{\mathbf{T}} \quad & |\text{Conv}(\mathbf{T}\mathbf{Z}')| \\ \text{s.t.} \quad & \mathbf{z}_i \mathbf{T} \in \mathcal{C} \quad \forall i, \end{aligned}$$

where  $|\text{Conv}(\mathbf{T}\mathbf{Z}')|$  denotes the volume of the convex polytope constructed by the allocation parameters. While this will not ensure that the first condition is met, it will promote an allocation structure that uses the entire simplex. While this algorithm does not ensure identifiability in the case when we have more than 2 functional features, it does make inference on the model more interpretable. Once the memberships are rescaled, we can conduct posterior inference on the mean function and covariance functions using the rescaled parameters.

---

**Algorithm 2** Membership Rescale Algorithm

---

**Require:**  $\mathbf{Z}, \boldsymbol{\nu}, \boldsymbol{\Phi}, M$ 

```

 $T \leftarrow \text{matrix}(0, 2, 2)$             $\triangleright$  Initialize inverse transformation matrix (2 x 2)
 $i \leftarrow 1$ 
while  $i \leq 2$  do
     $\text{max\_ind} \leftarrow \text{max\_ind}(\mathbf{Z}[:, i])$             $\triangleright$  Find index of max entry in  $i^{th}$  column
     $T[i, :] \leftarrow (\mathbf{Z}[\text{max\_ind}, :])$ 
     $i \leftarrow i + 1$ 
end while
 $\mathbf{Z\_t} \leftarrow \mathbf{Z} * \text{inv}(T)$             $\triangleright$  Transform the  $\mathbf{Z}$  parameters
 $\boldsymbol{\nu\_t} \leftarrow T * \boldsymbol{\nu}$             $\triangleright$  Transform the  $\boldsymbol{\nu}$  parameters
 $i \leftarrow 1$ 
while  $i \leq M$  do
     $\boldsymbol{\Phi\_t}[:, i] \leftarrow T * \boldsymbol{\Phi}[:, i]$             $\triangleright$  Transform the  $\boldsymbol{\Phi}$  parameters
     $i \leftarrow i + 1$ 
end while
return  $(\mathbf{Z\_t}, \boldsymbol{\nu\_t}, \boldsymbol{\Phi\_t})$ 

```

---